

**TR diss  
2815**

667422

3191079

TR diss 2815

**Theory of Carrier Adjusted DGPS Positioning Approach  
and Some Experimental Results**



# **Theory of Carrier Adjusted DGPS Positioning Approach and Some Experimental Results**

Proefschrift

ter verkrijging van de graad van doctor  
aan de Technische Universiteit Delft,  
op gezag van de Rector Magnificus Prof.ir. K.F. Wakker,  
in het openbaar te verdedigen ten overstaan van een commissie,  
door het College van Dekanen aangewezen,  
op maandag 14 oktober 1996 te 10.30 uur

door

Xin-Xiang JIN

Master of Science in Geodesy,  
Wuhan Technical University of Surveying and Mapping  
geboren te Wuhan, China



Dit proefschrift is goedgekeurd door de promotoren:

Prof.dr.bsc. P.A. Cross

Prof.dr.ing. R.A.P. Klees

Prof.dr.ir. M.G. Vosselman

Samenstelling promotiecommissie:

Rector Magnificus, voorzitter

Prof.dr.bsc. P.A. Cross, University of Newcastle upon Tyne, promotor

Prof.dr.ing. R.A.P. Klees, TU Delft, promotor

Prof.dr.ir. M.G. Vosselman, TU Delft, promotor

Prof.dr.ir. D. van Willigen, TU Delft

Prof.ir. J.A. Spaans, Koninklijk Instituut van de Marine

Ir. C.D. de Jong, Philips Electronics N.V.

Prof.dr.ir. P.J.G. Teunissen heeft als begeleider in belangrijke mate aan het totstandkomen van het proefschrift bijgedragen.

**Published and distributed by:**

Delft University Press

Stevinweg 1

2628 CN Delft

The Netherlands

Telephone +31 15 2783254

Fax +31 15 2781661

**CIP-DATA KONINKLIJKE BIBLIOTHEEK, DEN HAAG**

Jin, Xin-Xiang

Theory of Carrier Adjusted DGPS Positioning Approach and Some Experimental Results / Xin-Xiang Jin. - Delft : Delft University Press. - Ill.

Thesis Delft University of Technology. - With ref. - With summary in Dutch.

ISBN 90-407-1379-0

NUGI 816

Subject headings: GPS / DGPS positioning / Kalman filter

Copyright c 1996 by Xin-Xiang Jin

All rights reserved. No part of the material protected by this copyright notice may be reproduced or utilized in any form or by any means, electronic or mechanical, including photocopying, recording or by any information storage and retrieval system, without permission from the publisher: Delft University Press, Stevinweg 1, 2628 CN Delft, The Netherlands.

# Abstract

## Theory of Carrier Adjusted DGPS Positioning Approach and Some Experimental Results

The DGPS technique can greatly reduce or even eliminate biases in GPS observations and consequently provide quite precise relative positioning accuracy. It has been, therefore, paid more and more attention in many real-time positioning applications. The performance of DGPS positioning is a function of three elements: 1) generation of differential GPS corrections at a known DGPS reference station; 2) transmission of the corrections to mobile stations; and 3) computation of the mobile position.

This research derives a new algorithm for generating differential corrections, which has some distinct features. First, it directly uses code and carrier observations in the measurement model of a Kalman filter, so that the input measurements of the filter are not correlated in time if code and carrier observations can be assumed to have no time correlation. This makes it possible to use a simple stochastic observation model and to use the standard algorithm of the Kalman filter. Second, the algorithm accounts for biases like multipath errors and instrumental delays in code observations. It explicitly shows how code biases affect differential corrections when dual or single frequency data is used. Third, the algorithm can be easily integrated with a quality control procedure, so that the quality of the estimated states can be guaranteed with a certain probability. Fourth, in addition to generation of differential corrections, it also produces the change of ionospheric delays and that of code biases with time. It can, therefore, be used to investigate properties of ionospheric delays and code biases. Finally, all state estimates including differential correction are not affected by the opposite influence of ionospheric delay on code and carrier observations.

On the basis of data collected by TurboRogue SNR-8000, Trimble 4000 SSE and Trimble 4000 SST receivers, this research also investigates the relationship between satellite elevation and the precision of code observations. It turns out that the deterioration of code precision with decreasing elevation is very obvious at low elevation. When satellite elevation increases, the precision becomes more and more stable. The change of the code precision with satellite elevation can quite well be modelled by an exponential function of the form  $y = a_0 + a_1 \exp(-x/x_0)$ , where  $y$  (the RMS error),  $a_0$  and  $a_1$  have units of metres, and  $x$  (elevation) and  $x_0$  are in degrees. For different types of receivers and different types of code observables, the parameters  $a_0$ ,  $a_1$  and  $x_0$  may be different.

By using code and carrier data with a sampling interval of one second, the dynamic behaviour of SA clock errors and that of ionospheric delays can well be modelled by quadratic and linear functions, respectively. The modelling accuracy is within a few millimetres.

An alternative algorithm for computation of mobile positions is developed. This algorithm can

be applied at a mobile site when code and carrier observations are available. The algorithm directly uses code and carrier observations, rather than carrier filtered code observations, as inputs, therefore the stochastic model of observations can be easily specified. The algorithm can be applied in the case that the dynamic behaviour of mobile positions and receiver clock biases can or cannot be modelled. In the former case, the algorithm provides recursive estimates of mobile positions. Whereas in the latter case, it provides instantaneous estimates of mobile positions. In addition, the algorithm can also be integrated with a real time quality control procedure so as to ensure the quality of position estimates with a certain probability. Since in the use of the algorithm there always exist redundant observations unless the position parameters are inestimable, the quality control can even be performed when only four satellites are tracked.

By the use of data collected at a 100-km baseline, DGPS positioning experiments show that when dual-frequency data is used in both reference and mobile stations, half-metre instantaneous positioning accuracy can be achieved. While the data used in the mobile station is replaced by single-frequency data (L1 code and carrier), the accuracy can be still better than 7.5 decimeters. In addition, the use of an elevation-dependent standard deviation for code observations can improve DGPS positioning accuracies and it is more important to use dual-frequency data at a reference station than at a mobile station.

When ephemeris errors, vertical ionospheric delays, and vertical tropospheric delays are less than 10, 4.5, and 2.6 metres, respectively, using three reference stations in a 500×500 km<sup>2</sup> area can reduce the effect of ephemeris errors to one decimeter, ionospheric delays to less than two decimeters, and tropospheric delays to less than 2.5 decimeters. If a tropospheric delay model is used, the tropospheric delays can be further reduced to less than one decimeter.

GPS observation equations can be expanded into Taylor series which contain only up to first-order derivative quantities. Since the Taylor expansion does not contain the travel time of a GPS signal, solving it does not need iterations or code observations for the determination of the transmission time of the GPS signal. As a result, the use of the Taylor expansion can save computing time and can avoid the impact of any gross errors in code observations on determining satellite positions and satellite-clock biases, and consequently on computed observations.

# Contents

<b>Abstract</b>	<b>v</b>
<b>1. Introduction</b>	<b>1</b>
1.1 Overview of the Global Positioning System	1
1.2 Differential GPS	2
1.3 Outline of this dissertation	3
<b>2. Kalman filter and model testing procedure</b>	<b>5</b>
2.1 Linear Kalman filter	5
2.2 Recursive model testing procedure	7
2.2.1 Detection of model errors	8
2.2.2 Identification of model errors	9
2.2.3 Adaptation of the recursive filter	10
2.3 Internal and external reliability	11
2.3.1 Internal reliability	11
2.3.2 External reliability	12
<b>3. Discussion of existing algorithms for generating differential corrections</b>	<b>15</b>
3.1 Algorithm based on code observations	15
3.2 Algorithms based on carrier filtered code observations	18
3.2.1 Carrier filtered code observations without an ionosphere model	18
3.2.2 Carrier filtered code observations with an ionosphere model	21
3.3 Algorithm based on code observations and sequential differences of carrier observations	24
<b>4. Algorithm for generating carrier adjusted differential corrections and implementation of quality control</b>	<b>29</b>
4.1 Dynamic model and measurement model	29
4.2 Implementation of quality control	38
4.3 Effect of input parameters on estimated precision and reliability	40
<b>5. Some numerical results and discussion</b>	<b>47</b>
5.1 Description of data sets	47
5.1.1 TurboRogue SNR-8000 data	47
5.1.2 Trimble 4000 SSE data	47
5.1.3 Trimble 4000 SSE data under AS conditions	48
5.2 Validation of dynamic models	48
5.3 Dynamic behaviour of code biases	49
5.4 Performance of real time model testing	53
5.5 Accuracy of differential-correction prediction	56

<b>6. Relationship between satellite elevation and precision of code observations</b>	<b>59</b>
6.1 Introduction	59
6.2 Analytic approach of the precision of code observations	59
6.3 Numerical results and discussion	60
<b>7. Algorithm for carrier adjusted DGPS positioning and numerical results</b>	<b>67</b>
7.1 Introduction	67
7.2 Carrier adjusted DGPS positioning models	67
7.2.1 Positioning models	68
7.2.2 Discussion	75
7.3 DGPS positioning experiments	77
7.3.1 Data description and choices of a priori parameters	77
7.3.2 Numerical results and discussion	79
7.4 Concluding remarks	85
<b>8. Reduction of GPS observation biases by using a local DGPS network</b>	<b>87</b>
8.1 Introduction	87
8.2 Computation of differential correction vectors	88
8.3 Reduction of effect of ephemeris errors in a local DGPS network	89
8.4 Reduction of ionospheric delays in a local DGPS network	93
8.5 Reduction of tropospheric delays in a local DGPS network	96
8.5.1 The use of a differential correction vector	96
8.5.2 The use of a tropospheric model	98
8.6 Concluding remarks	100
<b>9. Taylor expansion of GPS observation equations</b>	<b>101</b>
9.1 Introduction	101
9.2 GPS observation equations	101
9.2.1 GPS code observation equations	101
9.2.2 GPS carrier observation equations	103
9.3 Discussion on some existing approaches to compute the travel time of GPS signals	108
9.4 Taylor expansion of observation equations	109
9.4.1 Expansion of satellite-receiver distances	111
9.4.2 Expansion of satellite clock biases	117
9.4.3 Expansion of observation equations	120
9.5 A simplified expression for the partial derivative of satellite-receiver distances	121
9.6 Concluding remarks	124
<b>10. Conclusions</b>	<b>127</b>
<b>References</b>	<b>131</b>
<b>A. Dynamic model with a constant acceleration or velocity</b>	<b>139</b>



---

<b>B. Zero correlations between dynamic noises and estimate errors of differential corrections</b>	<b>145</b>
<b>C. Carrier adjusted DGPS positioning models based on dual frequency data</b>	<b>147</b>
<b>D. Four identities and variation of <math>\frac{\Delta p}{\cos z'}</math> with zenith distances</b>	<b>155</b>
<b>Samenvatting</b>	<b>161</b>
<b>Acknowledgements</b>	<b>163</b>
<b>Curriculum Vitae</b>	<b>163</b>



# Chapter 1

## Introduction

### 1.1 Overview of the Global Positioning System

The Global Positioning System (GPS) is a satellite-based, all-weather radio navigation system developed by the US Department of Defense to enable unlimited number of users with the proper equipments to determine their position, velocity, and time in a common reference system, anywhere on or near the Earth. Simply speaking, GPS can be divided into three major segments: space segment, control segment and user segment [NATO 1991a].

The space segment consists of a nominal constellation of 21 operational satellites plus 3 active on-orbit spares which are used to ensure system availability. The 21+3 satellites are placed in six orbital planes with inclination relative to the equator of  $55^\circ$  and the orbit heights are 20,200 km. The satellites complete an orbit in approximately 12 hours and the same satellite becomes visible at the same location on the ground 4 minutes earlier each day because of a 4 minutes per day difference between the satellite orbit time and the rotation of the earth [NATO 1991a]. Each satellite transmits unique navigational signals.

The control segment includes a master control station located at the Consolidated Space Operations Centre in Colorado Springs and 5 worldwide monitor stations at Hawaii, Colorado Springs, Ascension Island in the South Atlantic Ocean, Diego Garcia in the Indian Ocean, and Kwajalein in the North Pacific Ocean [Gouldman et al. 1989]. The main tasks of the control segment are to track the GPS satellites and provide them with periodic updates of corrections to their ephemeris and their clock-bias errors.

The user segment consists of a variety of military and civilian GPS receivers located on the ground, in the air, in space, and aboard ships, which are capable of receiving, decoding, and processing the GPS satellite signals. They include stand-alone receiver sets, as well as equipment integrated with or embedded into other systems. Since there are various user applications including navigation, positioning, time transfer, and surveying etc., GPS receivers for different applications can vary significantly in design and function [NATO 1991a].

The navigational signals transmitted by each GPS satellite consist of two types of codes, that is, the P code (Precision code) for military users and the C/A code (Coarse/Acquisition code) for civilian users. The P code is transmitted on two frequencies, which are the L1 at 1575.42 MHz ( $=154 \times 10.23$  MHz, equivalent to a wavelength of about 19 cm) and the L2 at 1227.60 MHz ( $=120 \times 10.23$  MHz, equivalent to a wavelength of

about 24 cm). The C/A code is transmitted only on the L1 frequency and its fundamental purpose is to allow a rapid acquisition of the P code. Both L1 and L2 carriers are modulated with the navigation message, which is a data stream of 30 seconds long, broadcast continuously, containing satellite ephemerides, clock parameters, and general system status.

## **1.2 Differential GPS**

Like many types of observations, GPS observations include systematic errors and random noises, for example, satellite clock biases, effect of ephemeris errors, atmospheric delays. In addition, for reasons of U.S. security, a program called Selective Availability (SA) is implemented in GPS so that unauthorized (civilian) users can only obtain 100 m horizontal positioning accuracy with a probability of 95% [NATO 1991a].

For many real-time positioning applications, such as maritime navigation in inland waterways and constricted harbours, the GPS absolute positioning accuracy of about 100 metres is not sufficient [Alsip et al. 1992]. Most of the positioning errors are caused by biases in the observations, due to SA as well as orbital and atmospheric errors. These biases can be reduced or even eliminated when relative, rather than absolute, positions are determined. Real-time relative positioning with GPS is usually referred to as DGPS (Differential GPS) [Beser and Parkinson 1982], [Blackwell 1985].

Basically, the DGPS principle is as follows: a GPS reference receiver located at a station, of which the coordinates are known, continuously collects range measurements from all visible satellites. The biases in the observations can be determined by taking the difference between the measured distance and the computed distance from the known station and satellite positions. The observations of mobile GPS receivers (i.e., receivers at unknown locations) in the vicinity of the reference receiver will be contaminated by biases similar to those computed at the reference station. Therefore, if the biases computed at the reference station are transmitted to the mobile receivers, they can subtract these from their measurements, thus allowing them to considerably improve their positioning accuracy. The biases, computed and transmitted for these purposes, are known as differential corrections (DCs). They can be applied within a radius of a few hundred kilometres from the reference station [NATO 1991a]. Depending upon the distance to the reference station, DGPS positioning accuracies of 1-10 metres are possible [Pietraszewski et al. 1988], [Forbes et al. 1994].

The very simple procedure for computing DCs, as indicated above, has however some drawbacks. Firstly, the precision of the DCs is not better than that of the GPS code observations itself. Therefore the mobile user cannot profit by using carrier observations in order to get better precision. Secondly, gross errors in the measurements at the reference station will be included in the DCs, thereby affecting all DGPS users of these corrections. Thirdly, there will always be some latency in the transmission of DCs. Thus, the user is always using "old" corrections. Several procedures have been suggested in the literature to overcome all or some of these problems, which will be discussed later. But it can be seen

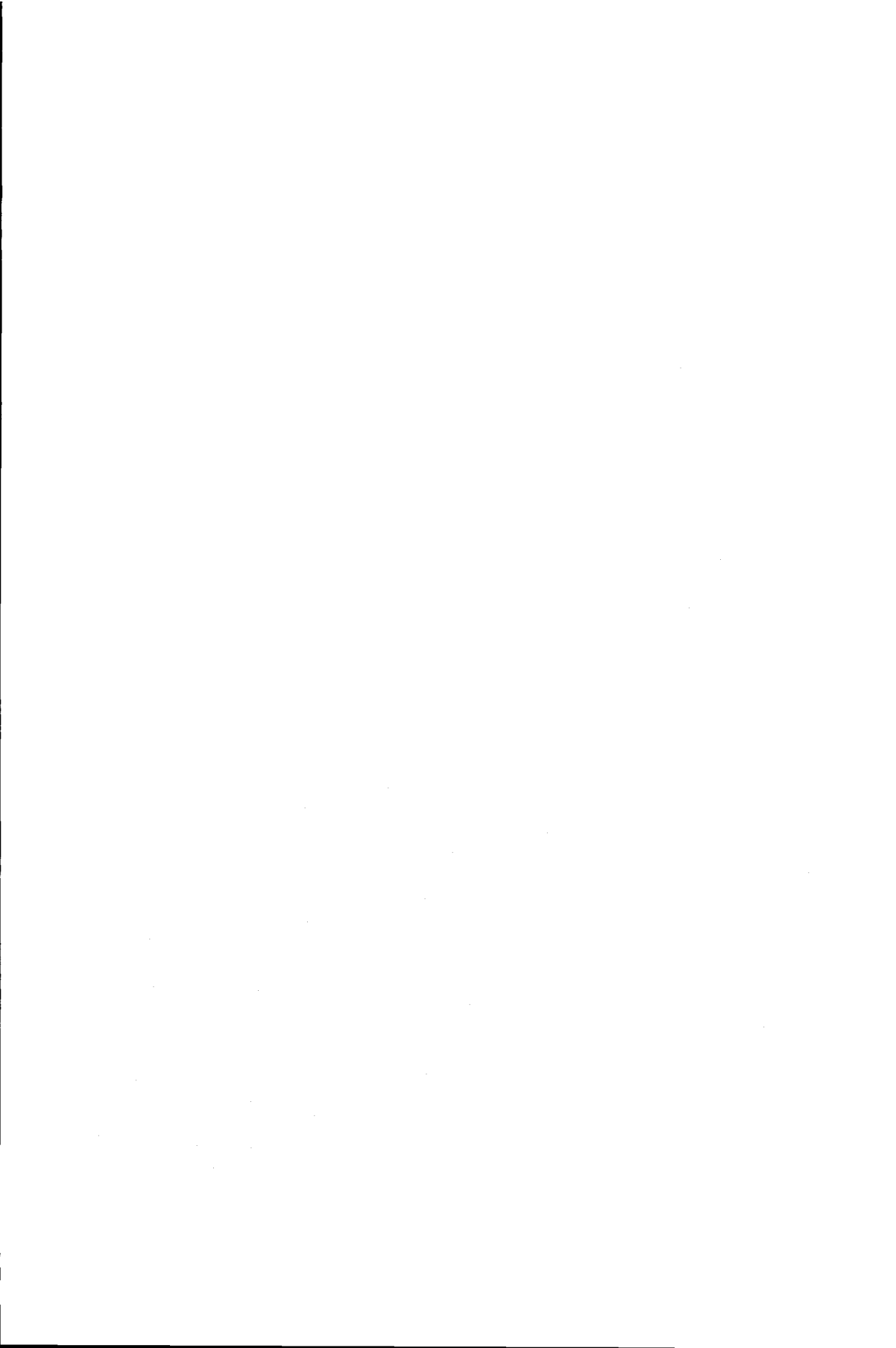
from the discussion that how to correctly generate DCs still needs to be further investigated.

With increasing the distance, the positioning accuracy will deteriorate, because the effect of ephemeris errors and atmospheric (ionospheric and tropospheric) delays at a user site cannot be sufficiently reduced by using the DCs computed at the reference station. Investigations and field tests have shown that using a network of DGPS reference stations is an economic and efficient way to overcome the spatial decorrelation of DCs [Bakker and Lapucha 1994].

### 1.3 Outline of this dissertation

The primary objective of this dissertation is to develop a new approach for real time DGPS positioning. This approach consists of a new algorithm for generating DCs at a reference station and an algorithm for determining mobile positions at a mobile site. In addition, the dissertation also quantitatively discusses the reduction of three main biases in GPS observations by the use of a network of reference stations. Furthermore, it presents the Taylor expansion of GPS observation equations. It could be worthwhile to mention that part of the work presented herein has been reported in [Jin 1995a, 1995b, 1995c], [Jin et al. 1995], [Jin and de Jong 1995, 1996a, 1996b] and [Jin 1996a, 1996b].

The dissertation will start in Chapter 2 with a review of the Kalman filter theory and the procedure of real-time model testing, followed by the concepts of internal and external reliability. In the next chapter, some existing algorithms for generation of DCs will be discussed. By using the Kalman filter theory, Chapter 4 will first derive an alternative algorithm for generation of DCs and next integrate the algorithm with a real-time quality control procedure. It will successively analyse how a priori input parameters of the filter affect the estimated precision of DCs and the performance of the quality control procedure in terms of reliability measures. By using real data and the algorithm presented in Chapter 4, Chapter 5 will investigate the validation of dynamic models chosen for DCs and for ionospheric delays, the dynamic behaviour of code biases, the performance of the real-time model testing, and the accuracy of DC prediction. Since in data processing the stochastic model of observations plays an important role, Chapter 6 will investigate the relationship between satellite elevation and the precision of GPS code observations. Chapter 7 will derive an alternative algorithm for DGPS positioning at a mobile station and show how positioning accuracies vary with the number of GPS observables used at reference and user stations and how the accuracy can be improved by choosing an elevation-dependent, instead of constant, standard deviation for code observations. Chapter 8 will extend the DGPS positioning research from the situation based on only one reference station to that based on a local DGPS network. It will individually show the reduction of the effects of ephemeris errors, ionospheric delays, and tropospheric delays by using multiple reference stations. Chapter 9, of which the topic is somewhat basic and independent, will show why and how we expand GPS observation equations into Taylor series which include only up to first-order derivative quantities. Finally, Chapter 10 summarizes some main conclusions of this research.



## Chapter 2

# Kalman filter and model testing procedure

The Kalman filter is a recursive data-processing procedure based on the well known least squares principle. Since in GPS positioning applications real-time solutions are required, the Kalman filter is a natural choice and is now widely used in GPS data processing. Like the least squares algorithm, the Kalman filter is not very robust against unspecified model errors. Therefore it is necessary to augment the Kalman filter with a procedure for the detection, identification, and adaptation of model errors. This chapter first reviews the Kalman filter. Next, it reviews the recursive procedure for the Detection, Identification, and Adaptation of model errors, known as the DIA procedure and introduced by Teunissen (1990a, 1990b). Finally the measures of internal and external reliability, which are related to the DIA procedure, are given.

### 2.1 Linear Kalman filter

In many time-dependent applications, the dynamics of a system, such as the positions of a vehicle, can be modelled. In the Kalman filter this information can be used along with measurements of the system. The Kalman filter consists of a dynamic model and a measurement model. For reasons of GPS applications, we restrict our discussion here on the discrete time linear(ized) dynamic and measurement models. One can refer to [Gelb 1974] for a more general case. The dynamic model is of the form

$$x_k = \Phi_{k,k-1} x_{k-1} + d_k, \quad k = 1, 2, \dots \quad (2.1)$$

where

- $x_k$ :  $n$ -dimensional state vector at time  $k$
- $\Phi_{k,k-1}$ :  $n \times n$  state transition matrix from time  $k-1$  to  $k$
- $d_k$ :  $n$ -dimensional vector of system dynamic noises

The measurement model is of the form

$$y_k = A_k x_k + e_k \quad (2.2)$$

where

- $y_k$ :  $m_k$ -dimensional vector of measurements  
 $A_k$ :  $m_k \times n$  design matrix  
 $e_k$ :  $m_k$ -dimensional vector of measurement noises

Assume that the initial state  $x_0$  is distributed as  $N(x_{0|0}, Q_{0|0})$  and is uncorrelated with  $d_k$  and  $e_k$  for all  $k$ .  $d_k$  is distributed as  $N(0, Q_{d_k})$  and  $d_k$  is uncorrelated with  $d_l$  for  $k \neq l$ ;  $e_k$  is distributed as  $N(0, Q_{y_k})$  and  $e_k$  is uncorrelated with  $e_l$  for  $k \neq l$ ; and  $d_k$  is uncorrelated with  $e_l$  for all  $k, l$ .

The problem we are faced with is to estimate the state vector at time  $k$  using a linear estimator based on all observations up to and including time  $k$ . Furthermore, the estimator must be 'best' in a certain sense. Kalman (1960) was the first who solved the problem based on the principle of minimum mean square error. It can be shown, however, (see, e.g., [Koch 1982], [Teunissen and Salzmann 1988]) that under certain assumptions, criterions like maximum likelihood and least squares lead to identical results.

The estimation procedure of the Kalman filter basically consists of two steps: the time update and the measurement update. The time update of the state estimator and its error covariance matrix are given by

$$\hat{x}_{k|k-1} = \Phi_{k,k-1} \hat{x}_{k-1|k-1} \quad (2.3)$$

$$Q_{k|k-1} = \Phi_{k,k-1} Q_{k-1|k-1} \Phi_{k,k-1}^* + Q_{d_k} \quad (2.4)$$

where

$\hat{x}_{k|k}$ : measurement update of the state estimator at time  $k$

$Q_{k|k}$ : error covariance matrix of  $\hat{x}_{k|k}$

Equation (2.3) gives the best unbiased estimator of the state at time  $k$  using all observations prior to time  $k$  in the sense of minimum mean square error of the estimation. The time update equation is also known as the one-step prediction equation.

Now, by using the predicted state, the so-called predicted residuals can be computed from the vector of observations, i.e.

$$v_k = y_k - A_k \hat{x}_{k|k-1} \quad (2.5)$$

with, if the model is valid

$$E\{v_k\} = 0 \quad \text{and} \quad E\{v_k v_l^*\} = \delta_{kl} Q_{v_k} \quad (2.6)$$

where



$$Q_{v_k} = Q_{y_k} + A_k Q_{k|k-1} A_k^* \quad (2.7)$$

The measurement update of the state estimator and its error covariance matrix are then given by

$$\hat{x}_{k|k} = \hat{x}_{k|k-1} + K_k v_k \quad (2.8)$$

$$Q_{k|k} = (I - K_k A_k) Q_{k|k-1} \quad (2.9)$$

where

$$K_k = Q_{k|k-1} A_k^* Q_{v_k}^{-1} \quad (2.10)$$

is the so-called Kalman gain matrix.

Equation (2.8) gives the best estimator of the state at time  $k$  using both  $\hat{x}_{k|k-1}$  and  $y_k$ . The measurement update equation is also known as the filter equation.

## 2.2 Recursive model testing procedure

The Kalman filter produces recursively optimal estimators of the state vector with well defined statistical properties. The state estimators are unbiased, are Gaussian distributed, and have minimum variances within the class of linear unbiased estimators. It is important to realize, however, that the optimality is only guaranteed as long as the assumptions underlying the mathematical model hold. Misspecifications in the model will invalidate the results of the estimation and thus also any conclusions based on them. It is therefore of importance to have some tools to verify the validity of the working hypothesis, denoted by  $H_0$ , made for the dynamic model and the measurement model.

An important role in the process of model testing can be played by predicted residuals. The knowledge of their distribution under  $H_0$  enables us to test the validity of the assumed mathematical model.

The DIA testing procedure consists of three steps:

- i) Detection: an overall model test is carried out to detect if an unspecified model error has occurred.
- ii) Identification: in the case that an unspecified model error is detected, various alternative hypotheses are evaluated to identify the most likely error source.
- iii) Adaptation: after identification of the most likely error source, the filter is adapted and the adverse effects of a model error are removed from the state vector estimate.

### 2.2.1 Detection of model errors

The objective of the detection step is to test the overall validity of the mathematical model under  $H_0$ . For practical reasons a distinction is made between local and global overall model tests. The local overall model test tests the validity of the model at a single epoch  $k$ , whereas the global overall model test tests the validity of the model in the time interval  $[k, l]$ . In the following, only the local overall model test, which will be used later, is addressed, for the global overall model test one can refer to [Teunissen 1990a, 1990b].

Assume that the validation of the null hypothesis  $H_0$  has been verified up to time  $k-1$ . What we need to detect at time  $k$  is whether an unspecified model error has occurred at the present time. Therefore, the null and alternative hypotheses are

$$\left. \begin{aligned} H_0^k: E\{y_k\} &= A_k x_k & \text{and} & E\{d_k\} = x_k - \Phi_{k|k-1} x_{k-1} \\ H_a^k: E\{y_k\} &= A_k x_k + \nabla y_k & \text{and} & E\{d_k\} = x_k - \Phi_{k|k-1} x_{k-1} + \nabla d_k \end{aligned} \right\} \quad (2.11)$$

or, when expressed in terms of predicted residuals

$$H_0^k: v_k \sim N(0, Q_{v_k}) \quad \text{and} \quad H_a^k: v_k \sim N(\nabla v_k, Q_{v_k}) \quad (2.12)$$

with  $\nabla v_k = \nabla y_k$  in the case of the model error in the measurement model or  $\nabla v_k = A_k \nabla d_k$  in the case of the model error in the dynamic model.

Assume that the  $m_k$ -dimension vector  $\nabla v_k$  can be written as

$$\nabla v_k = C_{v_k} \nabla \quad (2.13)$$

where  $C_{v_k}$  is a known  $m_k \times b$  matrix of full rank  $b$  and  $\nabla$  is an unknown model error vector of dimension  $b$ . The appropriate test statistic for testing  $H_0$  against  $H_a$  reads then [Teunissen and Salzmann 1989]

$$T^k = v_k^* Q_{v_k}^{-1} C_{v_k} (C_{v_k}^* Q_{v_k}^{-1} C_{v_k})^{-1} C_{v_k}^* Q_{v_k}^{-1} v_k \quad (2.14)$$

which is distributed under  $H_0$  and  $H_a$  as

$$H_0: T^k \sim \chi^2(b, 0) \quad \text{and} \quad H_a: T^k \sim \chi^2(b, \lambda) \quad (2.15)$$

with non-centrality parameter

$$\lambda = \nabla^* C_{v_k}^* Q_{v_k}^{-1} C_{v_k} \nabla \quad (2.16)$$

In most cases, it is impossible to be sure if the class of the alternative hypotheses specified by  $C_{v_k}$  indeed contains the true hypothesis. In order to test the overall validity of the local hypothesis  $H_0^k$ , the mean  $\nabla v_k = C_{v_k} \nabla$  of  $v_k$  under  $H_a^k$  should remain completely unspecified. This implies mathematically that the matrix  $C_{v_k}$  should be chosen to be a

square and regular matrix. Thus  $C_{v_k}$  can be eliminated from (2.14), which results in the local overall model test statistic

$$T^k = v_k^* Q_{v_k}^{-1} v_k \quad (2.17)$$

Since the mean of  $T^k$  under  $H_0$  equals the redundancy  $m_k$  (i.e., the number of observables at time  $k$ ), the dependency of the mean of  $T^k$  under  $H_0$  on the possibly time varying number of observables can be eliminated by normalizing (2.17) as

$$T_{LOM}^k = \frac{T^k}{m_k} \quad (2.18)$$

which is the normalized form of the local overall model (LOM) test statistic.

In the case of

$$T^k \geq \chi_{\alpha}^2(m_k, 0) \quad (2.19)$$

or

$$T_{LOM}^k \geq F_{\alpha}(m_k, \infty, 0) \quad (2.20)$$

we may at the confidence level of  $1-\alpha$  reject the null hypothesis  $H_0$  of (2.11) and consider that an unspecified local model error is present at time  $k$ .

### 2.2.2 Identification of model errors

The next step after detection is the identification of the most likely alternative hypothesis. As with detection, identification is based on the test statistic (2.14). For identification, however, candidate alternative hypotheses need to be specified explicitly. This specification is non-trivial and probably the most difficult task in the process of quality control. It depends to a great extent on the experience and one's knowledge of the dynamic and measurement models. In the following the discussion is restricted to model errors in the measurement model. The theory is, however, applicable for the case of model errors in the dynamic model as well. For the case that the local alternative hypothesis  $H_a^k$  of (2.11) is restricted to the measurement model, we denote  $C_{v_k}$  by  $C_k$ . It follows from (2.11) that the local alternative hypotheses read

$$H_a^k: E\{y_k\} = A_k x_k + C_k \nabla \quad (2.21)$$

This class of alternative hypotheses can be seen to model a slip in the mean of the vector of observables at time  $k$ . The dimension  $b$  of the vector  $\nabla$  in (2.21) depends on the alternative hypotheses considered and can range from 1 to  $m_k$  for identification purposes. Here we mainly consider the case  $b = 1$ , that is, the case of a single model error. But the theory is also applicable to the case of multiple model errors [Teunissen 1990b].

With  $b = 1$ , the model error vector  $\nabla$  reduces to a scalar and the matrix  $C_k$  reduces to an  $m_k$ -dimensional vector, which is denoted by  $c_k$ . It follows from taking the square-root of (2.14) that

$$t^k = \frac{c_k^* Q_{v_k}^{-1} v_k}{(c_k^* Q_{v_k}^{-1} c_k)^{1/2}} \quad (2.22)$$

This is the local slippage test statistic for the identification of a single local model error. The identification procedure works as follows: the test statistic  $t^k$  is computed for each of the candidate one-dimensional alternative hypotheses. The alternative hypothesis for which  $|t^k|$  is at a maximum, is then considered the one that contains the most likely model error. Since  $t^k$  is distributed under  $H_0^k$  and  $H_a^k$  as

$$t^k \sim \begin{cases} N(0, 1) & \text{under } H_0^k \\ N(\nabla \cdot (c_k^* Q_{v_k}^{-1} c_k)^{\frac{1}{2}}, 1) & \text{under } H_a^k \end{cases} \quad (2.23)$$

the likelihood of the most likely model error can be tested by comparing  $|t^k|$  with the critical value  $N_{\frac{\alpha}{2}}(0, 1)$  (i.e., the upper  $\frac{\alpha}{2}$ -percentage point of the standard normal distribution). If  $|t^k| \geq N_{\frac{\alpha}{2}}(0, 1)$ , the corresponding most likely model error can be considered at confidence level of  $1-\alpha$  to have occurred.

In most cases, one does not know in advance if only one or more unspecified model errors are present at time  $k$ . Therefore, the case of multiple model errors should also be considered. This can be handled as follows: first, all one dimensional test statistics are computed and the most likely hypothesis is identified. After this model error has been removed, the remaining test statistics are computed again, and the new most likely model error can be identified. It continues until the local overall model test is accepted.

### 2.2.3 Adaptation of the recursive filter

After identification of the most likely alternative hypothesis, adaptation of the recursive filter is required to eliminate the presence of biases in the filtered states. In order to be able to adapt the filter, we first need an estimate of the model error  $\nabla$ . The best linear unbiased estimator of the  $b$ -dimensional vector  $\nabla$  under  $H_a^k$  can be computed directly from predicted residuals and reads

$$\hat{\nabla}^k = (C_k^* Q_{v_k}^{-1} C_k)^{-1} C_k^* Q_{v_k}^{-1} v_k \quad (2.24)$$

$$Q_{\hat{v}^k} = (C_k^* Q_{v_k}^{-1} C_k)^{-1} \quad (2.25)$$

Note that when only a single error is identified, its estimator can be computed directly from the local slippage test statistic as

$$\hat{v}^k = \frac{t^k}{(C_k^* Q_{v_k}^{-1} C_k)^{1/2}} \quad (2.26)$$

The adapted filtered state at time  $k$  reads

$$\hat{x}_{k|k}^a = \hat{x}_{k|k}^0 - K_k C_k \hat{v}^k \quad (2.27)$$

and its error variance and covariance are given by

$$\left. \begin{aligned} Q_{k|k}^a &= Q_{k|k}^0 + K_k C_k Q_{\hat{v}^k} C_k^* K_k^* \\ Q_{\hat{x}_{k|k}^a, \hat{v}^k} &= -K_k C_k Q_{\hat{v}^k} \end{aligned} \right\} \quad (2.28)$$

where

$\hat{x}_{k|k}^a$ : filtered state estimator corresponding to  $H_a^k$

$\hat{x}_{k|k}^0$ : filtered state estimator corresponding to  $H_0^k$

## 2.3 Internal and external reliability

Besides testing for possible model errors, one is usually also interested in the size of the biases which can be detected with the tests described in the previous section. Also the influence of undetected errors on the estimation results is of interest.

### 2.3.1 Internal reliability

Internal reliability is a measure of the model error that can be detected by the test statistic  $t^k$  of (2.22) with a certain probability [Baarda 1968], [Teunissen 1989]. In order to design a statistical testing procedure that gives a reasonable protection against both type I (false alarm) and type II (missed detection) errors, one needs to specify not only the level of significance of the statistical test but also the power of it, which are denoted by  $\alpha_0$  and  $\gamma_0$  respectively.  $\alpha_0$  is actually equal to the probability of false alarm, whereas the testing power  $\gamma_0$  is the probability of rejecting the null hypothesis  $H_0$  when an alternative hypothesis  $H_a$  is true.

Suppose at time  $k$ , there is an unspecified model error  $\nabla$  in the measurement vector  $y_k$ , i.e.

$$E\{y_k\} = Ax_k + c_k \nabla \quad (2.29)$$

thus from (2.5) we arrive at

$$E\{v_k\} = c_k \nabla \quad (2.30)$$

It follows from (2.16) that the non-centrality parameter  $\lambda_0$  reads

$$\lambda_0 = (c_k \nabla)^* Q_{v_k}^{-1} c_k \nabla \quad (2.31)$$

Based on the given significance level  $\alpha_0$  and the power  $\gamma_0$  of the statistical test, the non-centrality parameter can be computed by the inverse power function [Baarda 1968], [Teunissen 1990a] as

$$\lambda_0 = \lambda(\alpha = \alpha_0, b = 1, \gamma = \gamma_0) \quad (2.32)$$

where  $b$  is the number of degrees of freedom.

Since  $c_k$  is a vector, it follows from (2.31) that the size of the unspecified model error that can be detected by the one-dimensional test statistic  $t^k$  for a certain level of significance  $\alpha_0$  and with power  $\gamma_0$  is equal to

$$\nabla = \left( \frac{\lambda_0}{c_k^* Q_{v_k}^{-1} c_k} \right)^{\frac{1}{2}} \quad (2.33)$$

This is called the minimum detectable bias (MDB) [Teunissen 1990a] and is a measure for the internal reliability.

### 2.3.2 External reliability

External reliability is the influence of an undetected model error on state estimates [Baarda 1968], [Teunissen 1989]. Obviously there is a probability that an unspecified model error can not be successfully identified by the test statistic  $t^k$  with a certain probability. Different undetected model errors have different impacts on state estimates. It is, therefore, important to know how large the effect of a particular model error is on the state vector or functions thereof.

As can be seen from state estimation equation (2.8), the biases in state estimates caused by a slip with the size of the MDB  $\nabla$  in an observation read

$$\nabla \hat{x}_{k|k} = K_k c_k \nabla \quad (2.34)$$

Often not the bias vector  $\nabla \hat{x}_{k|k}$  itself but its significance is analysed, because the analysis of the bias vector  $\nabla \hat{x}_{k|k}$  is complicated by the large amount of numbers involved. A measure of the significance of the bias in the state vector is the Bias to Noise Ratio (BNR) [Salzmann 1993], i.e.

$$\lambda_{\hat{x}} = \nabla \hat{x}_{k|k}^* Q_{k|k}^{-1} \nabla \hat{x}_{k|k} \quad (2.35)$$

Usually one is only concerned with the impact of an unspecified model error on a particular function of states. In this case, one can represent these linear(ized) functions of interest by a matrix  $F^*$ . The BNR pertaining to these functions follows from (2.34) as

$$\lambda_{F^* \hat{x}} = (F^* \nabla \hat{x}_{k|k})^* (F^* Q_{k|k} F)^{-1} F^* \nabla \hat{x}_{k|k} \quad (2.36)$$

Obviously, (2.35) is a special case of (2.36) with  $F$  equal to the unit matrix.

In practice one usually analyses the square root of the BNR ( $\lambda_{\hat{x}}^{1/2}$  or  $\lambda_{F^* \hat{x}}^{1/2}$ ) to facilitate a direct comparison with the ratio between the biases  $\nabla \hat{x}$  and the standard deviations of the (filtered) states [Salzmann 1993].





## Chapter 3

# Discussion of existing algorithms for generating differential corrections

Currently, based on the type(s) of observations used in the measurement model, there are three types of algorithms for the generation of DCs, which can be classified into

- algorithm based on code observations
- algorithms based on carrier-filtered code observations
- algorithm based on code observations and sequential differences of carrier observations

This chapter individually reviews and discusses these algorithms

### 3.1 Algorithm based on code observations

This algorithm is fundamental for the generation of DCs, though no literature explicitly discussed it.

Let us write the L1 GPS code observation in unit of length at time  $t_k$  as

$$P(t_k) = \rho(t_k) + c(dT(t_k) - dt(t_k)) + \nabla^{eph}(t_k) + I(t_k) + \nabla^{pro}(t_k) + e(t_k) \quad (3.1)$$

For the sake of simplicity, we replace  $t_k$  by the subscript  $k$  and thus (3.1) becomes

$$P_k = \rho_k + c(dT_k - dt_k) + \nabla_k^{eph} + I_k + \nabla_k^{pro} + e_k \quad (3.2)$$

where

- $P_k$ : L1 code observation (m)
- $\rho_k$ : satellite-receiver range computed from ephemeris data and station coordinates (m)
- $c$ : speed of light (m/s)
- $dT_k$ : receiver clock bias (s)
- $dt_k$ : satellite clock bias (including SA clock error) (s)
- $\nabla_k^{eph}$ : effect of ephemeris error (including SA orbit error) plus a priori coordinate error of station (m)
- $I_k$ : ionospheric delay (m)

$\nabla_k^{tro}$ : tropospheric delay (m)  
 $\epsilon_k$ : code observation noise (m)

By using the broadcast navigation data, the approximate value  $dt_k^0$  for  $dt_k$  can be computed. The DC is defined as (cf. [Loomis et al. 1989] and [RTCM SC-104 1994])

$$\nabla_k = c(dt_k - \delta t_k) + \nabla_k^{eph} + I_k + \nabla_k^{tro} \quad (3.3)$$

where

$\delta t_k$ : correction to  $dt_k^0$

Thus it follows from (3.2) and (3.3) that

$$P_k - \rho_k + c \cdot dt_k^0 = \nabla_k + \epsilon_k \quad (3.4)$$

Actually, this equation can already be used to compute DCs but the precision of this DC is not better than that of code observations itself. If the DC estimate is filtered, the precision and reliability can be improved.

As confirmed in Section 5.2, since all the quantities contained in  $\nabla_k$  are quite stable within a period of a few seconds, the third order time derivative of DCs, denoted by  $\ddot{\nabla}_k$ , can be modeled as a zero-mean white noise process with constant spectral density  $q_{\ddot{\nabla}}$  (having the unit of  $m^2/s^5$ ), i.e., [Brown and Hwang 1992]

$$E\{\ddot{\nabla}_k\} = 0 \quad (3.5)$$

$$\sigma_{\ddot{\nabla}\ddot{\nabla}}(\tau) = q_{\ddot{\nabla}}\delta(\tau) \quad (3.6)$$

where  $\delta(\tau)$  is the delta function [Gelb 1974].

Now we arrive at the following dynamic model for DCs (see Appendix A)<sup>1</sup>

$$\underbrace{\begin{bmatrix} \nabla_k \\ \dot{\nabla}_k \\ \ddot{\nabla}_k \end{bmatrix}}_{x_k} = \underbrace{\begin{bmatrix} 1 & \Delta t_k & \frac{1}{2}\Delta t_k^2 \\ & 1 & \Delta t_k \\ & & 1 \end{bmatrix}}_{\Phi_{k,k-1}} \underbrace{\begin{bmatrix} \nabla_{k-1} \\ \dot{\nabla}_{k-1} \\ \ddot{\nabla}_{k-1} \end{bmatrix}}_{x_{k-1}} + \underbrace{\begin{bmatrix} d_{\nabla_k} \\ d_{\dot{\nabla}_k} \\ d_{\ddot{\nabla}_k} \end{bmatrix}}_{d_k} \quad (3.7)$$

with

<sup>1</sup> Whenever a matrix appears with missing elements, then the elements are zero.

$$E\{d_k\} = 0 \quad (3.8)$$

$$E\{d_k d_l^*\} = \delta_{kl} Q_{d_k}, \quad Q_{d_k} = q_{\bar{v}} \begin{bmatrix} \frac{1}{20} \Delta t_k^5 & & \text{SYM.} \\ \frac{1}{8} \Delta t_k^4 & \frac{1}{3} \Delta t_k^3 & \\ \frac{1}{6} \Delta t_k^3 & \frac{1}{2} \Delta t_k^2 & \Delta t_k \end{bmatrix} \quad (3.9)$$

where

$\Delta$ : backwards differencing operator (e.g.  $\Delta t_k = t_k - t_{k-1}$ )

SYM.: indication of a symmetric matrix

In the case that the observation noise  $\epsilon_k$  is a time independent random error with standard deviation  $\sigma_\epsilon$ , then the measurement model reads

$$\underbrace{P_k - \rho_k + c \cdot dt_k^0}_{y_k} = \underbrace{[1 \ 0 \ 0]}_{A_k} x_k + \underbrace{\epsilon_k}_{e_k} \quad (3.10)$$

with

$$E\{e_k\} = 0 \quad (3.11)$$

$$E\{e_k e_l^*\} = \delta_{kl} Q_y, \quad Q_y = \sigma_\epsilon^2 \quad (3.12)$$

Based on the above dynamic and measurement models, the optimal solutions can be recursively obtained by using the Kalman filter algorithm. The initial values of the state vector and its corresponding error covariance matrix can be obtained from a batch least squares solution using three epochs of data.

One of the properties of this algorithm is that it only needs code observations. Therefore it is very simple but on the other hand the DC estimate is still quite noisy. In addition, because of using a dynamic model for DCs, the DC can be predicted, although the prediction is not that accurate. Finally, this algorithm can be combined with the DIA quality control procedure reviewed in Chapter 2.

It should be pointed out that although it is widely assumed in GPS data reduction that GPS observation noises are time independent random errors, the assumption may not be realistic in practice. It was reported in [van Dierendonck 1995] that the technique of carrier-aided code tracking has been widely used in GPS receivers, therefore the code

observations provided by most receivers are probably carrier filtered code observations, rather than the raw code observations we expect. Since the goal of this dissertation is not to challenge the assumption and instead is to discuss under this assumption what is the proper way to perform DGPS positioning, the assumption will be accepted here and afterwards. In addition, it will be shown later that to reduce the effect of code observation noises by using carrier observations, one does not need to use carrier-filtered code observations and can do better if the raw code and carrier observations are used. Therefore, GPS receivers should in fact provide users with raw code and carrier observations.

### 3.2 Algorithms based on carrier filtered code observations

This algorithm is widely found in the literature, for instance [van Dierendonck 1993], [Landau 1993], [Breeuwer et al. 1993] and [Casewell et al. 1994]. It consists of two steps. In the first step, code observations are filtered by carrier observations. Next, the carrier filtered code observations are used to generate DCs. Since the second step is identical to the algorithm based on code observations, the discussion on this algorithm will focus on the aspect of filtering code observations by carrier observations.

A carrier observation has much smaller noise than a code observation. It has been shown in the literature, for example [Hatch 1982], [Goad 1990], [Ashjaee 1990], and [Teunissen 1991], that filtering code observations by carrier observations is an efficient way to reduce code observation noises. In the following, some widely discussed approaches of filtering code observations by carrier observations for the generation of DCs will be addressed individually.

#### 3.2.1 Carrier filtered code observations without an ionosphere model

This approach was introduced by Hatch (1982). Let us write the L1 and L2 carrier observation equations in units of length as

$$\lambda_1 \phi_k = \rho_k + c(dT_k - dt_k) + \nabla_k^{eph} - I_k + \nabla_k^{tro} - \lambda_1 N + \eta_k \quad (3.13)$$

$$\lambda_2 \tilde{\phi}_k = \rho_k + c(dT_k - dt_k) + \nabla_k^{eph} - r I_k + \nabla_k^{tro} - \lambda_2 \tilde{N} + \tilde{\eta}_k \quad (3.14)$$

where

- $\lambda_1, \lambda_2$ : wave lengths corresponding to the L1 and L2 frequencies (m)
- $\phi_k, \tilde{\phi}_k$ : L1 and L2 carrier observations (cycles)
- $r$ : squared ratio of the L1 and L2 frequencies
- $N, \tilde{N}$ : L1 and L2 carrier ambiguities (cycles), which are real numbers
- $\eta_k, \tilde{\eta}_k$ : L1 and L2 carrier observation noises (m)

Usually when the difference of carrier phases at two epochs is taken, it is referred to as a delta range. Denoting L1 and L2 delta ranges over the interval  $(t_{k-1}, t_k)$  by  $D_{k-1,k}$  and  $\tilde{D}_{k-1,k}$ , we have

$$D_{k-1,k} = \lambda_1 \Delta \phi_k = \Delta \rho_k + c(\Delta dT_k - \Delta dt_k) + \Delta \nabla_k^{eph} - \Delta I_k + \Delta \nabla_k^{tro} + \Delta \eta_k \quad (3.15)$$

$$\tilde{D}_{k-1,k} = \lambda_2 \Delta \tilde{\phi}_k = \Delta \rho_k + c(\Delta dT_k - \Delta dt_k) + \Delta \nabla_k^{eph} - r \cdot \Delta I_k + \Delta \nabla_k^{tro} + \Delta \tilde{\eta}_k \quad (3.16)$$

From  $D_{k-1,k}$  and  $\tilde{D}_{k-1,k}$ , the ionosphere-free delta range, denoted by  $D_{k-1,k}^c$ , reads

$$\begin{aligned} D_{k-1,k}^c &= \frac{r}{r-1} D_{k-1,k} - \frac{1}{r-1} \tilde{D}_{k-1,k} \\ &= \Delta \rho_k + c(\Delta dT_k - \Delta dt_k) + \Delta \nabla_k^{eph} + \Delta \nabla_k^{tro} + \frac{r}{r-1} \Delta \eta_k - \frac{1}{r-1} \Delta \tilde{\eta}_k \end{aligned} \quad (3.17)$$

Making use of the L1 delta range and the ionosphere-free delta range, we can map the carrier range differences into equivalent code range differences as follows

$$\begin{aligned} M_{k-1,k} &= 2D_{k-1,k}^c - D_{k-1,k} \\ &= \Delta \rho_k + c(\Delta dT_k - \Delta dt_k) + \Delta \nabla_k^{eph} + \Delta I_k + \Delta \nabla_k^{tro} - \frac{r+1}{r-1} \Delta \eta_k - \frac{2}{r-1} \Delta \tilde{\eta}_k \end{aligned} \quad (3.18)$$

The quantity  $M_{k-1,k}$  has the important property that it contains the same information as  $P_k - P_{k-1}$  but with much smaller noise.

At the initial epoch, the carrier filtered code observation can be chosen to be the raw code observation, i.e.,  $\hat{P}_{0|0} = P_0$ . From then on, the predicted code observation  $\hat{P}_{k|k-1}$  can be computed by

$$\hat{P}_{k|k-1} = \hat{P}_{k-1|k-1} + M_{k-1,k}, \quad k=1, 2, \dots \quad (3.19)$$

where

$\hat{P}_{k-1|k-1}$ : carrier filtered code observation at epoch  $k-1$

Then the carrier filtered code observation at epoch  $k$  is given by

$$\hat{P}_{k|k} = \hat{P}_{k|k-1} + \frac{1}{k+1} (P_k - \hat{P}_{k|k-1}) \quad (3.20)$$

Since the carrier observation is only limitedly more accurate than the code observation while the epoch number  $k$  can be infinite, it makes sense to replace the coefficient of  $P_k - \hat{P}_{k|k-1}$  in the above equation by the variance ratio of carrier and code observations and that of  $\hat{P}_{k|k-1}$  by 1 minus the variance ratio in case processing epoch  $k$  is over the variance ratio of code and carrier observations [Hatch 1982].

It should be pointed out that the estimator given by (3.20) is not a strict recursive least-squares estimator, since the assumption that the variance of carrier observations is zero is implicitly made. The theoretical strict expression for L1 carrier filtered code should be

$$\hat{P}_{k|k} = \hat{P}_{k|k-1} + \frac{\sigma_e^2 + k\sigma_\eta^2}{k(\sigma_e^2 + \sigma_\eta^2)} (P_k - \hat{P}_{k|k-1}) \quad (3.21)$$

where  $\sigma_\eta$  is the standard deviation of L1 carrier observations. For more details one can refer to [Teunissen 1991].

Based on the above discussion, it can be seen that the precision of the carrier filtered code observation  $\hat{P}_{k|k}$  will become better and better with increasing epoch  $k$  and both code and carrier filtered code observations contain the same information. The most essential difference between the L1 and L2 carrier filtered observation  $\hat{P}_{k|k}$  and the raw code observation  $P_k$  is that the former has a lower noise than the latter. It should be noted that the assumption of cycle-slip free L1 and L2 carrier observations underlies the above filtering procedure. When cycle slips occur, the filtering procedure needs to be re-initialized. Apparently the above discussion is based on the case that L1 code and L1 as well as L2 carrier observations are available. When L2 code observations are available they can also be filtered by using a similar procedure. But then correlations are introduced, not only between the L1 or L2 filtered code observations at different epochs, but also between the L1 and L2 filtered code observations.

This approach has the property of simplicity, and moreover the L1 and L2 carrier filtered code observation produced by this filtering approach is not affected by the opposite influence of ionosphere on code and carrier observations. But on the other hand, making use of this approach to filter code observations needs dual-frequency carrier observations.

Since some receivers can only provide single frequency data, some authors have discussed the filtering of L1 code observations by L1 carrier observations only (e.g. [Goad 1990], [Ashjaee 1990]). When only single frequency code and carrier observations are available, the ionosphere-free delta range  $D_{k-1|k}^c$  cannot be obtained any more. In this case, replacing  $M_{k-1,k}$  in (3.19) by  $D_{k-1,k}$  gives the predicted code observation

$$\hat{P}_{k|k-1} = \hat{P}_{k-1|k-1} + D_{k-1,k} \quad (3.22)$$

and the single-frequency carrier filtered code observation can be obtained by (3.20) and (3.22) (cf. [Loomis et al. 1989] and [Landau 1993]).

Note that since the ionosphere has opposite effects (delay and advance) on code and carrier observations, the L1 carrier filtered code observation is affected differently by ionospheric delays than the raw L1 code observation, which is the major problem of the L1 carrier filtered code observations [Loomis et al. 1989], [Landau 1993]. It was shown in [Loomis et al. 1989] that after about 30-minute filtering, biases in single-frequency carrier filtered code observations resulting from the opposite effect of ionosphere on code and

carrier may be greater than code noises themselves. In [de Jong 1990] the following expression for L1 carrier filtered code observations can be found, which shows explicitly the ionospheric delay

$$\hat{P}_{k|k} = \rho_k + c(dt_k - dT_k) + \nabla_k^{eph} + \nabla_k^{tro} - \frac{k-2}{k}I_k + \frac{2}{k} \sum_{j=1}^{k-1} I_j + \text{noise} \quad (3.23)$$

To reduce the opposite effect of ionosphere, one can restart the filtering periodically, but each restart causes carrier filtered code noises to go back to the original code noise level. To make a compromise between these, Ashjaee (1990) introduced a technique called "Dual Ramp smoothing" for filtering code observations by the use of carrier observations. For each satellite in view, two ramps (or filters) are used (see Figure 3.1) and they have the same input code and carrier observations at each epoch. Initially and also after each loss of lock, both ramps restart at the same time. After  $N$  epochs ramp 2 resets and the filtering continues with ramp 1. After  $2N$  filtering epochs ramp 1 restarts and the filtering continues with ramp 2 that has already filtered  $N$  epochs. There is a jump when switching between ramps. Except for the first  $N$  epochs, the ramp having filtered at least  $N$  epochs is used to produce carrier filtered code observations. In [Ashjaee 1990], a value for  $N$  of 100 is proposed, and in this case the jump, due to switching between ramps, may cause a change of about a few centimetres in range.

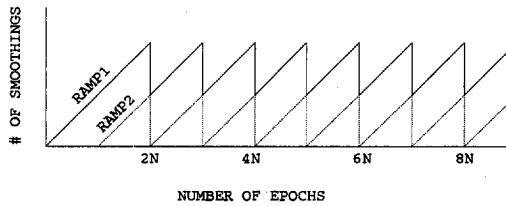


**Figure 3.1:** Illustration of "Dual Ramp" smoothing, after [Ashjaee 1990].

### 3.2.2 Carrier filtered code observations with an ionosphere model

This approach can be applied to both single-frequency data [Goad 1990] and dual-frequency data [Euler and Goad 1991]. The main property of this approach is that a simple exponential decay dynamic model, which is shown below, is used to model ionospheric delays. Since there is no fundamental difference between the applications of this approach to single-frequency data and dual-frequency data, the following discussion will be based on the single-frequency case.

In general, by using the ionosphere model parameters broadcast by a GPS satellite, the ionospheric delay can be corrected for at least 50% [Klobuchar 1987], [Feess and Stephens 1987]. Let

$$I_k = I_k^0 + \delta I_k \quad (3.24)$$

$$B_k = \rho_k + c(dT_k - dt_k) + \nabla_k^{eph} + \nabla_k^{tro} \quad (3.25)$$

where

$I_k^0$ : approximation of  $I_k$  computed from the broadcast information (m)

$\delta I_k$ : correction to  $I_k^0$  (m)

Then it follows with (3.2), (3.13), (3.24) and (3.25) that L1 code and carrier observations corrected for ionospheric delay, denoted by  $P_k^c$  and  $\phi_k^c$ , read

$$P_k^c = B_k + \delta I_k + e_k \quad (3.26)$$

$$\lambda_1 \phi_k^c = B_k - \delta I_k - \lambda_1 N + \eta_k \quad (3.27)$$

where  $P_k^c = P_k - I_k^0$  and  $\phi_k^c = \phi_k + I_k^0 / \lambda_1$ .

Since  $B_k$ ,  $\delta I_k$ , and  $\lambda_1 N$  are not individually estimable with only L1 code and carrier observations, (3.26) and (3.27) are rewritten into

$$P_k^c = (B_k + \delta I_1) + (\delta I_k - \delta I_1) + e_k \quad (3.28)$$

$$\lambda_1 \phi_k^c = (B_k + \delta I_1) - (\delta I_k - \delta I_1) - (\lambda_1 N + 2\delta I_1) + \eta_k \quad (3.29)$$

In matrix notation the above two equations can be written as

$$\underbrace{\begin{bmatrix} P_k^c \\ \lambda_1 \phi_k^c \end{bmatrix}}_{y_k} = \underbrace{\begin{bmatrix} 1 & 1 & 0 \\ 1 & -1 & -1 \end{bmatrix}}_{A_k} \underbrace{\begin{bmatrix} B_k + \delta I_1 \\ \delta I_k - \delta I_1 \\ \lambda_1 N + 2\delta I_1 \end{bmatrix}}_{x_k} + \underbrace{\begin{bmatrix} e_k \\ \eta_k \end{bmatrix}}_{e_k} \quad (3.30)$$

Since  $B_k$  is usually hard to predict and both  $\lambda_1 N$  and  $\delta I_1$  are constants as long as tracking of the satellite signals is maintained and since to a certain period the uncertainty in the broadcast ionospheric delay prediction model can be assumed to linearly increase with prediction time, the following dynamic model is built up

$$x_k = \Phi_{k,k-1} x_{k-1} + d_k \quad (3.31)$$

with



$$\Phi_{k,k-1} = \begin{bmatrix} 1 & & \\ & e^{-\frac{\Delta t_k}{\tau}} & \\ & & 1 \end{bmatrix} \quad (3.32)$$

$$E\{d_k\} = 0 \quad (3.33)$$

$$Q_{d_k} = \begin{bmatrix} \infty & & \\ & (Q_s \Delta t_k)^2 & \\ & & 0 \end{bmatrix} \quad (3.34)$$

where  $\tau$  and  $Q_s$  are constants. It is indicated in [Goad 1990] that the above model is rather insensitive to the value of  $\tau$  since the dynamic noise component will dominate, but no specific choice for it is given. With respect to  $Q_s$ , it is suggested to be chosen as 0.25 m/min for very quiet periods or 1.0 m/min for periods of moderate to high solar activity.

At each epoch a carrier filtered code observation can be computed by adding the first two states in  $x_k$ , i.e.  $\hat{P}_k^c = B_k + \delta I_k$ . Obviously, it will not be affected by the opposite effects of the ionosphere on code and carrier observations. Numerical results show that by using this method the noise of the code observations can be reduced by about 50% [Goad 1990].

It should be pointed out that the dynamic model used for the ionospheric delay, i.e.,

$$\delta I_k = e^{-\frac{\Delta t_k}{\tau}} \delta I_{k-1} + w_k \quad (3.35)$$

with

$$Q_{w_k} = (Q_s \Delta t_k)^2 \quad (3.36)$$

is not consistent because it is proved below that the variance of system dynamic noises from epoch  $l$  to  $k$  in one step does not lead to the same result as that in several steps.

Consider the variances of system dynamic noises from  $k-2$  to  $k$  in one and two steps. It follows from (3.35) that the state transition equation from epochs  $k-2$  to  $k-1$  reads

$$\delta I_{k-1} = e^{-\frac{\Delta t_{k-1}}{\tau}} \delta I_{k-2} + w_{k-1} \quad (3.37)$$

Inserting (3.37) into (3.35) gives the state transition equation from epochs  $k-2$  to  $k$

$$\delta I_k = e^{-\frac{\Delta t_k + \Delta t_{k-1}}{\tau}} \delta I_{k-2} + e^{-\frac{\Delta t_k}{\tau}} w_{k-1} + w_k \quad (3.38)$$

from which it can be seen that the dynamic noise from epochs  $k-2$  to  $k$  in two steps, denoted by  $w^{two}$ , reads

$$w^{two} = e^{-\frac{\Delta t_k}{\tau}} w_{k-1} + w_k \quad (3.39)$$

Thus its variance is

$$\begin{aligned} Q_{w^{two}} &= e^{-\frac{2\Delta t_k}{\tau}} Q_{w_{k-1}} + Q_{w_k} \\ &= e^{-\frac{2\Delta t_k}{\tau}} (Q_s \Delta t_{k-1})^2 + (Q_s \Delta t_k)^2 \end{aligned} \quad (3.40)$$

As is easy to see, the variance of system dynamic noises from epochs  $k-2$  to  $k$  in one step, denoted by  $w^{one}$ , reads

$$Q_{w^{one}} = (Q_s (\Delta t_{k-1} + \Delta t_k))^2 \quad (3.41)$$

which is not equal to  $Q_{w^{two}}$ . Therefore, the dynamic model specified by (3.35) and (3.36) is not consistent.

As can be seen from the above discussion, when dual-frequency data is available, one can obtain carrier filtered code observations which are not affected by the opposite effect of ionosphere on code and carrier observations. Whereas, when only single-frequency data is available, one either can only obtain carrier filtered code observations which are affected by the opposite effect of ionosphere on code and carrier or must use a dynamic model for ionospheric delays to overcome the opposite effect. Since carrier filtered code observations are always correlated in time no matter single or dual frequency data is available, strictly speaking, the correlation should be taken into account when the filtered observations are used. But in practice it is difficult to explicitly show the stochastic model of the filtered observations and therefore they are usually ignored.

### 3.3 Algorithm based on code observations and sequential differences of carrier observations

This algorithm, described in [Loomis 1986], [Loomis et al. 1989], uses code observations and sequential differences of carrier observations as measurements and uses a dynamic model for ionospheric delays. The original algorithm, which is discussed below, is based on single-frequency data. However, it can also be applied to dual frequency observations.

As shown in the previous section, the delta range  $\lambda_1 \Delta \phi_k$  can be formed from two carrier

observations at times  $t_{k-1}$  and  $t_k$ , which is given below again

$$\lambda_1 \Delta \Phi_k = \Delta \rho_k + c(\Delta dt_k - \Delta dt_k^0) + \Delta \nabla_k^{eph} - \Delta I_k + \Delta \nabla_k^{tro} + \Delta \eta_k \quad (3.42)$$

With (3.3) (the definition of DC) it follows that

$$\lambda_1 \Delta \Phi_k - \Delta \rho_k + c \cdot \Delta dt_k^0 = \Delta \nabla_k - 2 \Delta I_k + \Delta \eta_k \quad (3.43)$$

Applying a constant-acceleration dynamic model for the DC (i.e.  $\nabla_k$ ) as in Section 3.1 and assuming that the expectation of the rate of change of ionospheric delays is constant with spectral density  $q_{\nabla}$ , [Loomis 1986] and [Loomis et al. 1989] arrive at the following dynamic model

$$\underbrace{\begin{bmatrix} \nabla_k \\ \dot{\nabla}_k \\ \ddot{\nabla}_k \\ \dot{I}_k \end{bmatrix}}_{x_k} = \underbrace{\begin{bmatrix} 1 & \Delta t_k & \frac{1}{2} \Delta t_k^2 & 0 \\ & 1 & \Delta t_k & 0 \\ & & 1 & 0 \\ & & & 1 \end{bmatrix}}_{\Phi_{k,k-1}} \underbrace{\begin{bmatrix} \nabla_{k-1} \\ \dot{\nabla}_{k-1} \\ \ddot{\nabla}_{k-1} \\ \dot{I}_{k-1} \end{bmatrix}}_{x_{k-1}} + \underbrace{\begin{bmatrix} d_{\nabla_k} \\ d_{\dot{\nabla}_k} \\ d_{\ddot{\nabla}_k} \\ d_{\dot{I}_k} \end{bmatrix}}_{d_k} \quad (3.44)$$

with

$$Q_{d_k} = \begin{bmatrix} \frac{q_{\nabla}}{20} \Delta t_k^5 & & & SYM. \\ \frac{q_{\nabla}}{8} \Delta t_k^4 & \frac{q_{\nabla}}{3} \Delta t_k^3 & & \\ \frac{q_{\nabla}}{6} \Delta t_k^3 & \frac{q_{\nabla}}{2} \Delta t_k^2 & q_{\nabla} \Delta t_k & \\ 0 & 0 & 0 & q_I \Delta t_k \end{bmatrix} \quad (3.45)$$

and the measurement model

$$\underbrace{\begin{bmatrix} P_k - \rho_k - c \cdot dt_k^0 \\ \lambda_1 \Delta \Phi_k - \Delta \rho_k + c \cdot dt_k^0 \end{bmatrix}}_{y_k} = \underbrace{\begin{bmatrix} 1 & 0 & 0 & 0 \\ 0 & \Delta t_k & 0 & -2 \Delta t_k \end{bmatrix}}_{A_k} x_k + e_k \quad (3.46)$$

with

$$Q_y = \begin{bmatrix} (1 \text{ to } 2)^2 & 0 \\ 0 & 10^{-2} \end{bmatrix} m^2 \quad (3.47)$$

From a practical point of view, this is a good algorithm to generate DCs when only single frequency data is available, because the corrections are not affected by the opposite effect of ionosphere on code and carrier observations. There are, however, some remarks which have to be made.

First of all, from the assumptions that DCs have a constant acceleration and that the ionospheric delays have a constant velocity, it follows that

$$\begin{aligned} \Delta \nabla_k &= \nabla_k - \nabla_{k-1} \\ &= (\nabla_{k-1} + \dot{\nabla}_{k-1} \Delta t_k + \frac{1}{2} \ddot{\nabla}_{k-1} \Delta t_k^2 + d_{\nabla_k}) - \nabla_{k-1} \\ &= \dot{\nabla}_{k-1} \Delta t_k + \frac{1}{2} \ddot{\nabla}_{k-1} \Delta t_k^2 + d_{\nabla_k} \\ &= (\dot{\nabla}_k - \ddot{\nabla}_{k-1} \Delta t_k - d_{\nabla_k}) \Delta t_k + \frac{1}{2} \ddot{\nabla}_{k-1} \Delta t_k^2 + d_{\nabla_k} \\ &= \dot{\nabla}_k \Delta t_k - \frac{1}{2} (\ddot{\nabla}_k - d_{\nabla_k}) \Delta t_k^2 - d_{\nabla_k} \Delta t_k + d_{\nabla_k} \\ &= \dot{\nabla}_k \Delta t_k - \frac{1}{2} \ddot{\nabla}_k \Delta t_k^2 + d_{\nabla_k} - d_{\nabla_k} \Delta t_k + \frac{1}{2} d_{\nabla_k} \Delta t_k^2 \\ &= \dot{\nabla}_k \Delta t_k - \frac{1}{2} \ddot{\nabla}_k \Delta t_k^2 + \begin{bmatrix} 1 & -\Delta t_k & \frac{1}{2} \Delta t_k^2 & 0 \end{bmatrix} d_k \end{aligned} \quad (3.48)$$

and

$$\begin{aligned} \Delta I_k &= I_k - I_{k-1} \\ &= \dot{I}_{k-1} \Delta t_k + d_{I_k} \\ &= \dot{I}_k \Delta t_k - d_{I_k} \Delta t_k + d_{I_k} \end{aligned} \quad (3.49)$$

Therefore, after inserting (3.48) and (3.49) into (3.43) and combining the result with (3.4) the measurement model (3.46) should be

$$y_k = \underbrace{\begin{bmatrix} 1 & 0 & 0 & 0 \\ 0 & \Delta t_k & -\frac{1}{2} \Delta t_k^2 & -2 \Delta t_k \end{bmatrix}}_{A_k} x_k + \underbrace{\begin{bmatrix} e_k \\ \Delta \eta_k \end{bmatrix} + \begin{bmatrix} [0 & 0 & 0 & 0] & 0 \\ [1 & -\Delta t_k & \frac{1}{2} \Delta t_k^2 & 2 \Delta t_k] & -2 \end{bmatrix}}_{e_k} \begin{bmatrix} d_k \\ d_{I_k} \end{bmatrix} \quad (3.50)$$

which shows the observation noise  $e_k$  is correlated with the dynamic noise  $d_k$ . Therefore,

strictly speaking the standard algorithm of the Kalman filter cannot be used in this algorithm.

Secondly, since DCs are functions of ionospheric delays, the covariance matrix (3.45) of system dynamic noises should be

$$Q_{d_k} = \begin{bmatrix} \frac{q_{\bar{v}}}{20} \Delta t_k^5 & & & & \text{SYM.} \\ \frac{q_{\bar{v}}}{8} \Delta t_k^4 & \frac{q_{\bar{v}}}{3} \Delta t_k^3 & & & \\ \frac{q_{\bar{v}}}{6} \Delta t_k^3 & \frac{q_{\bar{v}}}{2} \Delta t_k^2 & q_{\bar{v}} \Delta t_k & & \\ \frac{q_{\bar{f}}}{2} \Delta t_k^2 & q_{\bar{f}} \Delta t_k & 0 & q_{\bar{f}} \Delta t_k & \\ & & & & \end{bmatrix} \quad (3.51)$$

Thirdly, although this algorithm can generate DCs which are not affected by the opposite effect of ionosphere on code and carrier observations even in the single frequency case, the correlations between delta ranges in time are still ignored. It was reported in [Roberts and Cross 1993] that ignoring the correlations will result in too optimistic precision for state estimates.



## Chapter 4

# Algorithm for generating carrier adjusted differential corrections and implementation of quality control

This chapter consists of three sections. First, it derives a new algorithm for generating DCs, which are referred to as carrier adjusted DCs, analogously to [Teunissen 1991]. Next, it shows how to integrate this algorithm with the recursive quality control procedure discussed in Chapter 2. Finally, it analyses the effect of input a priori parameters of the algorithm on the estimated precision and reliability.

### 4.1 Dynamic model and measurement model

For the algorithm which is derived in this section, we introduce a bias term in each of the L1 and L2 code observation equations presented in Chapter 3 as follows

$$P_k = \rho_k + c(dT_k - dt_k) + \nabla_k^{eph} + I_k + \nabla_k^{tro} + b_k + \epsilon_k \quad (4.1)$$

$$\tilde{P}_k = \rho_k + c(dT_k - dt_k) + \nabla_k^{eph} + r \cdot I_k + \nabla_k^{tro} + \tilde{b}_k + \tilde{\epsilon}_k \quad (4.2)$$

where

$b_k$ : L1 code observation bias (m)

$\tilde{P}_k$ : L2 code observation (m)

$\tilde{b}_k$ : L2 code observation bias (m)

$\tilde{\epsilon}_k$ : L2 code observation noise (m)

As will be shown in Section 7.2, the L1 and L2 code biases  $b_k$  and  $\tilde{b}_k$  may be significantly present in L1 and L2 code observations, respectively, and they may behave differently for different receivers and different observation environments. Without introducing  $b_k$  and  $\tilde{b}_k$  in L1 and L2 code observation equations, code observation noises may be biased and their time series may appear to have linear and/or periodic behaviour. Whereas after introducing a code-bias parameter in a code observation equation, code observation noises become unbiased random noises. The L1 and L2 code biases  $b_k$  and  $\tilde{b}_k$  consist of all systematic errors in a code observation, which could have resulted from, for example, multipath and instrumental delays.

With the improvement of GPS receivers and antenna designs, this bias may become less and less significant in the future. Note that when the code bias  $b_k$  is present in an L1 code observation, the DC computed by the algorithm based on code observations (see Section 3.1) is actually not what one expects, instead it is a DC biased by  $b_k$ , i.e.,  $\nabla_k + b_k$ . In that algorithm (as well as other existing algorithms), the code bias is implicitly assumed to be zero. The biased DC includes the effect of the code bias  $b_k$ , which is varying with time, and its corresponding rate of change and acceleration are affected by the dynamic behaviour of the code biases. Incidentally, a quantity similar to code biases  $b_k$  and  $\tilde{b}_k$  is defined as inter-frequency bias in [Chao et al. 1995a] and [Chao et al. 1995b].

The L1 and L2 carrier observation equations, which were already discussed in Chapter 3, are

$$\lambda_1 \phi_k = \rho_k + c(dt_k - dt_k) + \nabla_k^{eph} - I_k + \nabla_k^{tro} - \lambda_1 N + \eta_k \quad (4.3)$$

$$\lambda_2 \tilde{\phi}_k = \rho_k + c(dt_k - dt_k) + \nabla_k^{eph} - r \cdot I_k + \nabla_k^{tro} - \lambda_2 \tilde{N} + \tilde{\eta}_k \quad (4.4)$$

Let us denote the combination of receiver-clock bias, correction to the approximate value of satellite-clock bias, effect of ephemeris error and tropospheric delay by  $S_k$ , i.e.

$$S_k = c(dt_k - \delta t_k) + \nabla_k^{eph} + \nabla_k^{tro} \quad (4.5)$$

According to the definition of the DC (see (3.3)), the DC can then be expressed as

$$\nabla_k = S_k + I_k \quad (4.6)$$

Combining (4.1) to (4.4) with (4.5) gives the following system of code and carrier observation equations

$$\begin{bmatrix} P_k - \rho_k + c \cdot dt_k^0 \\ \lambda_1 \phi_k - \rho_k + c \cdot dt_k^0 \\ \lambda_2 \tilde{\phi}_k - \rho_k + c \cdot dt_k^0 \\ \tilde{P}_k - \rho_k + c \cdot dt_k^0 \end{bmatrix} = \begin{bmatrix} 1 & 1 & 0 & 0 & 1 & 0 \\ 1 & -1 & -1 & 0 & 0 & 0 \\ 1 & -r & 0 & -1 & 0 & 0 \\ 1 & r & 0 & 0 & 0 & 1 \end{bmatrix} \begin{bmatrix} S_k \\ I_k \\ \lambda_1 N \\ \lambda_2 \tilde{N} \\ b_k \\ \tilde{b}_k \end{bmatrix} + \begin{bmatrix} e_k \\ \eta_k \\ \tilde{\eta}_k \\ \tilde{e}_k \end{bmatrix} \quad (4.7)$$

The ambiguities  $N$  and  $\tilde{N}$  are constant in time, provided that no cycle slips occur in L1 and L2 carrier observations, respectively. All other parameters generally change with time and have to be solved every epoch. Equation (4.7) cannot be used directly because the number of unknowns is larger than that of observations, regardless of the number of epochs for which data is available. It is, however, possible to estimate the variations of  $b_k$  and  $\tilde{b}_k$  with respect to  $b_0$  and  $\tilde{b}_0$ , respectively. This can be achieved by the following parameter transformation which results in



$$\begin{bmatrix} S_k + \frac{r}{r-1} b_0 - \frac{1}{r-1} \tilde{b}_0 \\ I_k - \frac{1}{r-1} b_0 + \frac{1}{r-1} \tilde{b}_0 \\ \lambda_1 N + \frac{r+1}{r-1} b_0 - \frac{2}{r-1} \tilde{b}_0 \\ \lambda_2 \tilde{N} + \frac{2r}{r-1} b_0 - \frac{r+1}{r-1} \tilde{b}_0 \\ b_k - b_0 \\ \tilde{b}_k - \tilde{b}_0 \end{bmatrix} = \begin{bmatrix} 1 & & & & & \\ & 1 & & & & \\ & & 1 & & & \\ & & & 1 & & \\ & & & & 1 & \\ & & & & & 1 \end{bmatrix} \begin{bmatrix} \frac{r}{r-1} & -\frac{1}{r-1} \\ -\frac{1}{r-1} & \frac{1}{r-1} \\ \frac{r+1}{r-1} & -\frac{2}{r-1} \\ \frac{2r}{r-1} & -\frac{r+1}{r-1} \\ -1 & 0 \\ 0 & -1 \end{bmatrix} \begin{bmatrix} S_k \\ I_k \\ \lambda_1 \tilde{N} \\ b_k \\ \tilde{b}_k \\ b_0 \\ \tilde{b}_0 \end{bmatrix} \quad (4.8)$$

$$\begin{bmatrix} P_k - \rho_k + c dt_k^0 \\ \lambda_1 \Phi_k - \rho_k + c dt_k^0 \\ \lambda_2 \tilde{\Phi}_k - \rho_k + c dt_k^0 \\ \tilde{P}_k - \rho_k + c dt_k^0 \end{bmatrix} = \begin{bmatrix} 1 & 1 & 0 & 0 & 1 & 0 \\ 1 & -1 & -1 & 0 & 0 & 0 \\ 1 & -r & 0 & -1 & 0 & 0 \\ 1 & r & 0 & 0 & 0 & 1 \end{bmatrix} \begin{bmatrix} S_k + \frac{r}{r-1} b_0 - \frac{1}{r-1} \tilde{b}_0 \\ I_k - \frac{1}{r-1} b_0 + \frac{1}{r-1} \tilde{b}_0 \\ \lambda_1 N + \frac{r+1}{r-1} b_0 - \frac{2}{r-1} \tilde{b}_0 \\ \lambda_2 \tilde{N} + \frac{2r}{r-1} b_0 - \frac{r+1}{r-1} \tilde{b}_0 \\ b_k - b_0 \\ \tilde{b}_k - \tilde{b}_0 \end{bmatrix} + \begin{bmatrix} e_k \\ \eta_k \\ \tilde{\eta}_k \\ \tilde{e}_k \end{bmatrix} \quad (4.9)$$

This system can be solved for every epoch. For epoch  $k=0$ , the first four parameters are computed, and for the remaining epochs parameters 1, 2, 5 and 6 are solved, while parameters 3 and 4 are constant.

In order to improve the precision of the estimates of the parameters and also to produce the rate of change of DCs along with the DCs themselves, we introduce dynamic models for  $S_k$ ,  $I_k$ ,  $b_k$  and  $\tilde{b}_k$ . It will be shown in Section 5.2 that the third-order time derivative of  $S_k$  and the second-order time derivative of  $I_k$ , denoted by  $\ddot{S}_k$  and  $\ddot{I}_k$ , respectively, can be modelled as zero-mean white noise processes with constant spectral densities  $q_S$  ( $m^2/s^5$ ) and  $q_I$  ( $m^2/s^3$ ). The second-order time derivatives of  $b_k$  and  $\tilde{b}_k$ , denoted by  $\ddot{b}_k$  and  $\ddot{\tilde{b}}_k$ , can be modelled as zero-mean white noise processes with the same constant spectral density  $q_b$  ( $m^2/s^3$ ). Therefore, it follows from (4.9) that the estimable state vector related to epoch  $k$  ( $k>0$ ) reads

$$\begin{bmatrix} S_k + \frac{r}{r-1}b_0 - \frac{1}{r-1}\tilde{b}_0 & \dot{S}_k & \ddot{S}_k & I_k - \frac{1}{r-1}b_0 + \frac{1}{r-1}\tilde{b}_0 & \dot{I}_k \\ \lambda_1 N + \frac{r+1}{r-1}b_0 - \frac{2}{r-1}\tilde{b}_0 & \lambda_2 \tilde{N} + \frac{2r}{r-1}b_0 - \frac{r+1}{r-1}\tilde{b}_0 & b_k - b_0 & \dot{b}_k & \ddot{b}_k - \ddot{b}_0 & \dot{\tilde{b}}_k \end{bmatrix}^* \quad (4.10)$$

The corresponding original non-estimable state vector is

$$\begin{bmatrix} S_k & \dot{S}_k & \ddot{S}_k & I_k & \dot{I}_k & \lambda_1 N & \lambda_2 \tilde{N} & b_k & \dot{b}_k & \ddot{b}_k & b_0 & \tilde{b}_0 \end{bmatrix}^* \quad (4.11)$$

Our goal is to compute DCs. Additionally, it is preferred to build up a model that links the L2 code bias  $\tilde{b}_k$  only with the L2 code observable so that the model can easily be adapted to situations when the L2 code observable is missing or L2 and/or L1 carrier is missing. For these purposes, a transformation has to be applied to (4.10) or (4.11). For reasons of convenience, we transform (4.11) as follows

$$\begin{bmatrix} \nabla_k + b_0 \\ \dot{\nabla}_k \\ \ddot{S}_k \\ I_k + \frac{\lambda_1 N + b_0}{2} \\ \dot{I}_k \\ I_k + \frac{\lambda_2 \tilde{N} + b_0}{r+1} \\ I_k - \frac{b_0 - \tilde{b}_0}{r-1} \\ b_k - b_0 \\ \dot{b}_k \\ \ddot{b}_k - \ddot{b}_0 \\ \dot{\tilde{b}}_k \end{bmatrix} = \underbrace{\begin{bmatrix} 1 & 0 & 0 & 1 & 0 & 0 & 0 & 0 & 0 & 0 & 1 & 0 \\ 0 & 1 & 0 & 0 & 1 & 0 & 0 & 0 & 0 & 0 & 0 & 0 \\ 0 & 0 & 1 & 0 & 0 & 0 & 0 & 0 & 0 & 0 & 0 & 0 \\ 0 & 0 & 0 & 1 & 0 & \frac{1}{2} & 0 & 0 & 0 & 0 & \frac{1}{2} & 0 \\ 0 & 0 & 0 & 0 & 1 & 0 & 0 & 0 & 0 & 0 & 0 & 0 \\ 0 & 0 & 0 & 1 & 0 & 0 & \frac{1}{r+1} & 0 & 0 & 0 & \frac{1}{r+1} & 0 \\ 0 & 0 & 0 & 1 & 0 & 0 & 0 & 0 & 0 & 0 & \frac{-1}{r-1} & \frac{1}{r-1} \\ 0 & 0 & 0 & 0 & 0 & 0 & 0 & 1 & 0 & 0 & -1 & 0 \\ 0 & 0 & 0 & 0 & 0 & 0 & 0 & 0 & 1 & 0 & 0 & 0 \\ 0 & 0 & 0 & 0 & 0 & 0 & 0 & 0 & 0 & 1 & 0 & -1 \\ 0 & 0 & 0 & 0 & 0 & 0 & 0 & 0 & 0 & 0 & 1 & 0 \end{bmatrix}}_T \begin{bmatrix} S_k \\ \dot{S}_k \\ \ddot{S}_k \\ I_k \\ \dot{I}_k \\ \lambda_1 N \\ \lambda_2 \tilde{N} \\ b_k \\ \dot{b}_k \\ \ddot{b}_k \\ b_0 \\ \tilde{b}_0 \end{bmatrix} \quad (4.12)$$

Note that the first transformed state is the sum of the first two parameters of (4.9), i.e.

$\nabla_k + b_0 = S_k + I_k + b_0 = \left( S_k + \frac{r}{r-1}b_0 - \frac{1}{r-1}\tilde{b}_0 \right) + \left( I_k - \frac{1}{r-1}b_0 + \frac{1}{r-1}\tilde{b}_0 \right)$ . The rate of change of  $\nabla_k$  is the sum of the rates of change of  $S_k$  and  $I_k$ , i.e.  $\dot{\nabla}_k = \dot{S}_k + \dot{I}_k$ .

It follows from (4.12) and (4.7) that the measurement model for the Kalman filter we use reads

$$\underbrace{\begin{bmatrix} P_k - \rho_k + c \cdot dt_k^0 \\ \lambda_1 \Phi_k - \rho_k + c \cdot dt_k^0 \\ \lambda_2 \tilde{\Phi}_k - \rho_k + c \cdot dt_k^0 \\ \tilde{P}_k - \rho_k + c \cdot dt_k^0 \end{bmatrix}}_{y_k} = \underbrace{\begin{bmatrix} 1 & 0 & 0 & 0 & 0 & 0 & 0 & 1 & 0 & 0 & 0 \\ 1 & 0 & 0 & -2 & 0 & 0 & 0 & 0 & 0 & 0 & 0 \\ 1 & 0 & 0 & 0 & 0 & -(r+1) & 0 & 0 & 0 & 0 & 0 \\ 1 & 0 & 0 & 0 & 0 & 0 & r-1 & 0 & 0 & 1 & 0 \end{bmatrix}}_{A_k} \underbrace{\begin{bmatrix} \nabla_k + b_0 \\ \dot{\nabla}_k \\ \ddot{S}_k \\ I_k + \frac{\lambda_1 N + b_0}{2} \\ \dot{I}_k \\ I_k + \frac{\lambda_2 \tilde{N} + b_0}{r+1} \\ I_k - \frac{b_0 - \tilde{b}_0}{r-1} \\ b_k - b_0 \\ \dot{b}_k \\ \tilde{b}_k - \tilde{b}_0 \\ \dot{\tilde{b}}_k \end{bmatrix}}_{x_k} + \underbrace{\begin{bmatrix} e_k \\ \eta_k \\ \tilde{\eta}_k \\ \tilde{e}_k \end{bmatrix}}_{e_k} \quad (4.13)$$

with

$$E\{e_k\} = 0 \quad (4.14)$$

$$E\{e_k e_l^*\} = \delta_{kl} Q_y, \quad Q_y = \begin{bmatrix} \sigma_e^2 & & & \\ & \sigma_\eta^2 & & \\ & & \sigma_{\tilde{\eta}}^2 & \\ & & & \sigma_{\tilde{e}}^2 \end{bmatrix} \quad (4.15)$$

For the sake of simplicity, herein the measurement noises are assumed not only to be uncorrelated among observables and epochs but also to have constant standard deviations. It will be shown in Chapter 6, however, that the standard deviation of code observations is a function of satellite elevation.

To derive the dynamic model for  $x_k$ , we need to note that  $N$  and  $\tilde{N}$  are constant like  $b_0$  and  $\tilde{b}_0$ , unless a cycle slip occurs. The second-order time derivative of DCs  $\ddot{\nabla}_k$  is equal to that of the ionosphere-free DCs  $\ddot{S}_k$ , because  $\dot{I}_k$  is a white noise and is included in the dynamic





$$\begin{bmatrix} \nabla_k + b_k \\ \dot{\nabla}_k + \dot{b}_k \\ \ddot{S}_k \\ I_k + \frac{b_k + \lambda_1 N}{2} \\ I_k + \frac{1}{2} \dot{b}_k \end{bmatrix} = \underbrace{\begin{bmatrix} 1 & 0 & 0 & 1 & 0 & 0 & 1 & 0 \\ 0 & 1 & 0 & 0 & 1 & 0 & 0 & 1 \\ 0 & 0 & 1 & 0 & 0 & 0 & 0 & 0 \\ 0 & 0 & 0 & 1 & 0 & \frac{1}{2} & \frac{1}{2} & 0 \\ 0 & 0 & 0 & 0 & 1 & 0 & 0 & \frac{1}{2} \end{bmatrix}}_T \begin{bmatrix} S_k \\ \dot{S}_k \\ \ddot{S}_k \\ I_k \\ \dot{I}_k \\ \lambda_1 N \\ b_k \\ \dot{b}_k \end{bmatrix} \quad (4.12')$$

$$\underbrace{\begin{bmatrix} P_k - \rho_k + c dt_k^0 \\ \lambda_1 \Phi_k - \rho_k + c dt_k^0 \end{bmatrix}}_{y_k} = \underbrace{\begin{bmatrix} 1 & 0 & 0 & 0 & 0 \\ 1 & 0 & 0 & -2 & 0 \end{bmatrix}}_{A_k} \underbrace{\begin{bmatrix} \nabla_k + b_k \\ \dot{\nabla}_k + \dot{b}_k \\ \ddot{S}_k \\ I_k + \frac{b_k + \lambda_1 N}{2} \\ I_k + \frac{1}{2} \dot{b}_k \end{bmatrix}}_{x_k} + \underbrace{\begin{bmatrix} e_k \\ \eta_k \end{bmatrix}}_{e_k} \quad (4.13')$$

$$E\{e_k e_l^*\} = \delta_{kl} Q_y, \quad Q_y = \begin{bmatrix} \sigma_e^2 \\ \sigma_\eta^2 \end{bmatrix} \quad (4.15')$$

$$\mathbf{x}_k = \underbrace{\begin{bmatrix} 1 & \Delta t_k & \frac{1}{2}\Delta t_k^2 & 0 & 0 \\ 0 & 1 & \Delta t_k & 0 & 0 \\ 0 & 0 & 1 & 0 & 0 \\ 0 & 0 & 0 & 1 & \Delta t_k \\ 0 & 0 & 0 & 0 & 1 \end{bmatrix}}_{\Phi_{k,k-1}} \mathbf{x}_{k-1} + T \int_{t_{k-1}}^{t_k} \underbrace{\begin{bmatrix} \frac{1}{2}(t_k-t)^2 \ddot{S}(t) \\ (t_k-t)\ddot{S}(t) \\ \ddot{S}(t) \\ (t_k-t)\ddot{I}(t) \\ \ddot{I}(t) \\ 0 \\ (t_k-t)\ddot{b}_k \\ \ddot{b}_k \end{bmatrix}}_{\mathbf{d}_k} dt \quad (4.16')$$

$$E\{d_k d_l^*\} = \delta_{kl} Q_{d_k}, \quad Q_{d_k} = T \begin{bmatrix} q_s Q_{11} & & & \\ & q_f Q_{22} & & \\ & & 0 & \\ & & & q_b Q_{22} \end{bmatrix} T^* \quad (4.18')$$

The explicit form of  $Q_{d_k}$  in (4.18') can be found in [Jin 1995a].

Note that the three ionospheric-delay related states  $I_k + \frac{\lambda_1 N + b_0}{2}$ ,  $I_k + \frac{\lambda_2 \tilde{N} + b_0}{r+1}$  and  $I_k - \frac{b_0 - \tilde{b}_0}{r-1}$  in the state vector  $\mathbf{x}_k$  can be used to analyse the variation of ionospheric delays. Often dual-frequency GPS code observations are used to estimate the first-order ionospheric delay. Strictly speaking, it should only be done in the case that L1 and L2 code biases are absent or the same or negligible. In general, by using dual frequency GPS code observations, one can only estimate the first-order ionospheric delay contaminated by code biases  $b_k$  and  $\tilde{b}_k$  (or  $b_0$  and  $\tilde{b}_0$ ), like the state  $I_k - \frac{b_0 - \tilde{b}_0}{r-1}$ .

The time-varying states  $S_k$ ,  $I_k$ ,  $b_k$  and  $\tilde{b}_k$  are affected by different factors. The ionosphere-free DC  $S_k$  is related with receiver and satellite clock biases (including SA clock errors), ephemeris errors (including SA orbit errors) and tropospheric delays. The ionospheric delay  $I_k$  is related with the condition of the ionosphere. The code biases  $b_k$  and  $\tilde{b}_k$  are related with receivers, antennas and the observation environment.

There are some essential differences in the generation of carrier adjusted DCs and of their rates of changes between using dual frequency data and using single frequency data. In the

former case, the carrier adjusted DCs at all epochs are biased by a constant which is the initial value of L1 code bias (see (4.13)); their rates of changes are not biased. In the latter case, the DCs and their rates are biased by L1 code biases and the rates of the changes of the biases at the same epochs (see (4.13')), respectively. Thus, the quality of the rates of carrier adjusted DCs based on dual frequency data is much better than that based on single frequency data. It should be noted that when code biases become negligible, this algorithm can still be used after simply removing the columns and rows related to code biases and their rates of changes. Both carrier adjusted DCs and their rates of change are then no longer biased.

Apart from the above properties, there are some differences between the algorithm presented here and other published ones. First of all, this new algorithm directly uses code and carrier observations in the measurement model of a Kalman filter, so that the measurements are not correlated in time if code and carrier observations can be assumed to have no time correlations. This makes it possible to use a simple stochastic observation model and to use the standard algorithm of the Kalman filter. Secondly, the algorithm accounts for biases like multipath errors and instrumental delays in code observations. It explicitly shows how code biases affect carrier adjusted DCs when dual or single frequency data are used. Thirdly, in addition to generating carrier adjusted DCs, it can also be used to analyse the significance of code biases and to produce information related to the ionosphere (e.g. the variation of ionospheric delays and their rates of change). Finally, all state estimates including carrier adjusted DC are not affected by the opposite influence of ionospheric delay on code and carrier observations.

Note that when code biases are present, one can only obtain DCs biased by  $b_0$  or  $b_k$ . Since the bias  $b_0$  or  $b_k$  will not be the same for reference and mobil stations, it cannot be cancelled when DCs are applied by a mobil user. It will be shown in Section 5.3 that code biases are usually different from satellite to satellite, they will, therefore, result in a bias in the estimate of user's position when DCs are used at the user site. This is one of the prices we pay for the use of DCs.

## 4.2 Implementation of quality control

In Section 2.2, we reviewed how to perform model testing so that the assumptions underlying the models (or say, the null hypothesis  $H_0$ ) can be validated and optimal estimated states can be obtained. This section discusses the implementation of the model testing theory for generation of carrier adjusted DCs.

Suppose in the detection step the null hypothesis  $H_0$  of (2.12) is rejected by the LOM test (2.20). What we need to do is to identify the model error. The identification step is based on the so-called conventional alternative hypothesis or data snooping [Baarda 1968] in combination with the local slippage test statistic (2.22). The model error which is tested is

$$\nabla_i = c_i \nabla \quad (4.20)$$

with



$$c_i = [0 \dots 0 \underset{\substack{\uparrow \\ \text{element } i}}{1} 0 \dots 0]^* \quad (4.21)$$

In other words, the residuals are tested one by one so that all outliers in the observations can be identified. Note that state slippages in dynamic processes are not accounted for here.

For  $m_k$  predicted residuals, we have  $m_k$  independent local slippage test statistics (2.22). The alternative hypothesis for which  $|t^j|$  is at a maximum is then considered as the one that contains the most likely model error. Determine  $j$  such that

$$j = \{ i \mid |t^i| = \max\{|t^1|, \dots, |t^{m_k}|\} \} \quad (4.22)$$

In the case that

$$|t^j| \geq N_{\frac{\alpha}{2}}(0, 1) \quad (4.23)$$

one may accept the alternative hypothesis  $H_a$  of (2.23) at confidence level of  $1-\alpha$  and consider predicted residual  $j$  in  $v_k$  to be the most likely predicted residual containing the detected model error. Since other residuals may also contain unspecified model errors, remove predicted residual  $j$  and corresponding covariances from  $v_k$  and  $Q_{v_k}$ , respectively, and repeat the same procedure as above until (4.23) is not fulfilled for any of the remaining predicted residuals any more.

After identification of the most likely alternative hypotheses, the recursive filter needs to be adapted. In Section 2.2, a general adaptation procedure has been described. But for the particular filter we are considering here, the adaptation can be simplified. Consider the general case that L1 and L2 code and carrier observables are available, i.e.  $m_k=4$ . It will be shown later that the adaptation procedure can be applied to any case, as long as L1 code observable is available.

Depending on accepted alternative hypotheses  $j$  from (2.23), the adaptation can be carried out for different cases as follows.

- $j=1$  or  $j=4$  This is most likely corresponding to the situation that the L1 and/or L2 code measurement contains an outlier. In this case one can simply eliminate predicted residual  $j$  from the residual vector  $v_k$  and then continue the measurement update by using the other residuals.
- $j=2$  or  $j=3$  This case happens most likely due to the occurrence of a cycle slip or an outlier in the L1 and/or L2 carrier measurement. When a cycle slip occurs in a carrier measurement, a new ambiguity is introduced. As can be seen from the measurement model, the L1-carrier

and L2-carrier related states are  $I_k + \frac{\lambda_1 N + b_0}{2}$  and  $I_k + \frac{\lambda_2 \tilde{N} + b_0}{r-1}$ , which contain their own ambiguities respectively. In this case the L1-carrier or L2-carrier related state should be reinitialized (see [Jin 1995a]) and the filter can continue the measurement update by using the other unbiased predicted residuals. It can be expected that if the unspecified model error is an outlier instead of a cycle slip, this adaptation will be repeated in the following epoch.

•  $j=1, j=2, j=3$ , and  $j=4$  Since all predicted residuals are considered to have an unspecified model error in this case, it is probably caused by a slip in the state of the DC  $\nabla_k$  (e.g., a jump in the receiver clock bias). In this case, the states  $\nabla_k + b_0$ ,  $I_k + \frac{\lambda_1 N + b_0}{2}$ ,  $I_k + \frac{\lambda_2 \tilde{N} + b_0}{r-1}$ ,  $b_k - b_0$  and  $\tilde{b}_k - b_0$  should be reinitialized.

We have discussed how to adapt the recursive filter in such three cases that an unspecified model error occurs in the code measurement, in the carrier measurement, and in all measurements. Apparently if unspecified model errors occur in some of code and carrier measurements, the adaptation of the recursive filter can still be done in the same way. In short, if an unspecified model error is identified in a code predicted residual, then exclude the residual in the measurement update; if an unspecified model error is identified in a carrier predicted residual, then initialize its carrier ambiguity related state; but if an unspecified model error is identified in all measurements, then reinitialize all states related to the measurements.

### 4.3 Effect of input parameters on estimated precision and reliability

For all algorithms used to generate DCs, it is essential that outliers, cycle slips and other model errors can be detected in time. Because of this reason, the algorithm for carrier adjusted DCs uses the DIA quality control procedure. This section investigates the influence of the input parameters of the algorithm on the DC and DC-rate precision and on the internal and external reliability of code and carrier observations. Through these investigations, we also show the usual sizes of the precision and the reliability.

As can be seen from Chapter 2 and the previous two sections, the estimated precision (i.e. covariance matrix) of DCs and DC rates (i.e. rate of change of DCs) is function of

- processing epoch  $k$
- observation interval  $\Delta t_k$
- spectral densities  $q_f$ ,  $q_s$  and  $q_b$
- variances of observables  $Q_y$
- number and types of observables

The MDB and BNR related with the local slippage test statistic  $t'$  are functions of the above parameters plus

- significance level  $\alpha_0$
- power of the test  $\gamma_0$

Following the suggestions of [LGR 1982], we choose  $\alpha_0$  and  $\gamma_0$  to be 0.001 and 0.8, respectively. To show how sensitive the precision of DC and DC-rate, MDB and BNR are to the above parameters and how they vary when these parameters vary in realistic ranges, the following analysis is based on the case of three observables (i.e. L1 code and L1 as well as L2 carrier). As will be shown at the end of this section, using four observables (i.e. L1 and L2 code and carrier) cannot much improve the precision and the reliability based on three observables.

Figures 4.1 and 4.2 illustrate the behaviour of the MDB of the L1 carrier and L1 code observables as a function of processing epoch. As can be seen from Figure 4.1, during the first few epochs after filter initialization the L1 carrier MDB decreases very quickly with increasing processing epoch. Then it becomes quite stable. The basic behaviour of the L1 code MDB shown in Figure 4.2 is quite similar to that of the L1 carrier MDB, except that the L1 code MDB needs more time than the L1 carrier MDB to reach a steady state. It has been found that the effects of the processing epoch  $k$  on the L2 carrier MDB and on the DC-rate standard deviation are very similar to that on the L1 carrier MDB. The effect on the DC standard deviation is similar to that on the L1 code MDB and the behaviour of the BNR is similar to the corresponding MDB. Therefore, it can be concluded that the DC and DC-rate precision, MDBs and BNRs become quite stable after few epochs of processing since filter initialization. This is an important property because the precision and the reliability can be approximately regarded as constants, after the first few epochs of processing since filter initialization.

Tables 4.1 to 4.6 show the variations of DC and DC-rate standard deviations, MDB and  $\text{BNR}^{1/2}$  by choosing only one parameter as a variable, while keeping the other parameters fixed. The BNRs are computed from the three DC related states, i.e. DC itself, DC rate and DC acceleration (i.e., the second-order time derivative of DCs), and this can be realized by

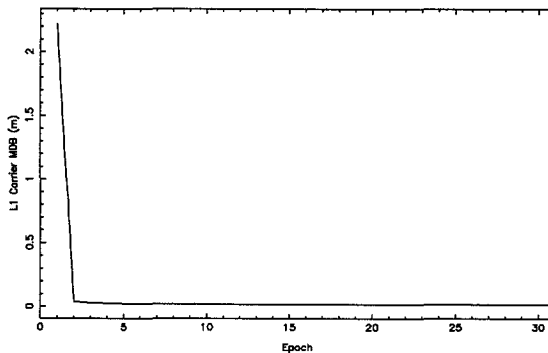


**Figure 4.1:** L1 carrier MDB over processing epoch with sampling interval of 1 second.



observation. In fact, we can even see from the L1 code extremely small  $\text{BNR}^{1/2}$  that L1 code observations hardly play a role in the measurement update of DC related states. One final remark should be given for the difference between the L1 and L2 carrier reliability. In all the cases concerned in the table, the L1 and L2 carrier MDBs are always the same but the L1 carrier  $\text{BNR}^{1/2}$  is always larger than the L2 carrier MDB. Therefore, the contributions of L1 and L2 carrier observations to the measurement update of the DC related states are not the same and the former is larger than the latter. The reason for this is that the L1 and L2 carrier observation equations have different coefficients in the measurement update model.

Table 4.2 shows the effect of the spectral density of dynamic noises of ionospheric delays on the precision, MDBs and BNRs. As can be seen from this table, the effect is quite similar to that of ionosphere-free DCs. When the spectral density increases from  $10^{-9}$  to  $10^{-7} \text{ m}^2/\text{s}^3$ , the DC precision is very stable, and the DC-rate standard deviation, L1 code MDB and  $\text{BNR}^{1/2}$ , and L1 and L2 carrier MDBs increase very slowly. The variation of the spectral density has opposite impacts on L1 and L2 carrier BNRs. By increasing the spectral density, the L1 carrier  $\text{BNR}^{1/2}$  increases whereas the L2 carrier  $\text{BNR}^{1/2}$  decreases.

Table 4.3 shows the effect of the spectral density of dynamic noises of code biases on the DC as well as DC-rate precision, MDBs and BNRs. This spectral density has visible effect only on the DC precision and the L1 code MDB as well, and it has very small effect on the L1 code BNR and no visible effect on the MDBs and BNRs of L1 and L2 carriers. When it increases from  $10^{-4}$  to  $10^{-2} \text{ m}^2/\text{s}^3$ , the standard deviation of DCs varies from about 0.3 to 0.5 m and the L1 code MDB from about 6.6 to 7.4 m. Since the precision of carrier observations is much better than that of code observations, the DC-rate estimate is almost fully determined by carrier measurements. Therefore, code observations can hardly play any role in the DC-rate estimation and the spectral density of code-bias noises has little effect on the precision of DC-rate estimates.

Table 4.4 displays the influence of the standard deviation of L1 carrier observations on the DC and DC-rate precision, MDBs and BNRs. By varying the standard deviation, the DC precision and L1 code MDB are very stable and the L1 code BNR has only a small change. The influence of the standard deviation on the DC-rate precision and carrier MDBs as well as BNRs is obvious. When the standard deviation is increasing, the L1 and L2 carrier MDBs and the L2 carrier BNR are increasing but the L1 carrier BNR is decreasing. The impact of the L2 carrier standard deviation on the DC and DC-rate precision, MDBs and BNRs is very similar to that of the L1 carrier standard deviation. The difference in the impact between code and carrier precision is that the code precision has only visible impact on the DC precision and the code MDB and BNR, whereas the carrier precision has only impact on the DC-rate precision and the carrier MDB and BNR. Note that when the standard deviation is chosen as 0.004 m, the L1 carrier  $\text{BNR}^{1/2}$  is smaller than the L2 carrier  $\text{BNR}^{1/2}$  and they are 2.457 and 3.098, respectively. This is because the standard deviation of L2 carrier observations is chosen as 0.003 m, which is smaller than that of L1 carrier observations.

$q_s (\frac{m^2}{s^5})$	$\sigma_{\nabla}$ (m)	$\sigma_{\dot{\nabla}}$ (m/s)	L1 Code		L1 Carrier		L2 Carrier	
			MDB (m)	BNR <sup>1/2</sup>	MDB (m)	BNR <sup>1/2</sup>	MDB (m)	BNR <sup>1/2</sup>
10 <sup>-6</sup>	0.429	0.002	6.868	0.006	0.017	2.963	0.017	1.932
10 <sup>-5</sup>	0.429	0.003	6.868	0.006	0.018	3.102	0.018	2.342
10 <sup>-4</sup>	0.429	0.006	6.868	0.005	0.019	2.886	0.019	2.366
10 <sup>-3</sup>	0.429	0.010	6.868	0.004	0.019	2.192	0.019	1.867
10 <sup>-2</sup>	0.429	0.026	6.868	0.002	0.019	1.075	0.019	0.926
10 <sup>-1</sup>	0.429	0.078	6.868	0.001	0.019	0.370	0.019	0.320

with:  $Q_y^{1/2} = \text{diag}(1.5, 0.003, 0.003)$  m;  $q_f = 10^{-8} \text{ m}^2/\text{s}^3$ ;  $q_b = 10^{-3} \text{ m}^2/\text{s}^3$ ;  $\Delta t_k = 1$  s and 400 epochs of processing after the filter initialization.

**Table 4.1:** The variations of DC and DC-rate standard deviations, MDB and BNR<sup>1/2</sup> with the spectral density of dynamic noises of ionosphere-free DCs.

$q_f (\frac{m^2}{s^3})$	$\sigma_{\nabla}$ (m)	$\sigma_{\dot{\nabla}}$ (m/s)	L1 Code		L1 Carrier		L2 Carrier	
			MDB (m)	BNR <sup>1/2</sup>	MDB (m)	BNR <sup>1/2</sup>	MDB (m)	BNR <sup>1/2</sup>
10 <sup>-9</sup>	0.429	0.003	6.868	0.004	0.017	2.870	0.017	2.614
10 <sup>-8</sup>	0.429	0.003	6.868	0.006	0.018	3.102	0.018	2.342
10 <sup>-7</sup>	0.429	0.004	6.869	0.010	0.019	3.420	0.019	1.576

with:  $Q_y^{1/2} = \text{diag}(1.5, 0.003, 0.003)$  m;  $q_s = 10^{-5} \text{ m}^2/\text{s}^5$ ;  $q_b = 10^{-3} \text{ m}^2/\text{s}^3$ ;  $\Delta t_k = 1$  s and 400 epochs of processing after the filter initialization.

**Table 4.2:** The variations of DC and DC-rate standard deviations, MDB and BNR<sup>1/2</sup> with the spectral density of dynamic noises of ionospheric delays.

$q_b (\frac{m^2}{s^3})$	$\sigma_{\nabla}$ (m)	$\sigma_{\dot{\nabla}}$ (m/s)	L1 Code		L1 Carrier		L2 Carrier	
			MDB (m)	BNR <sup>1/2</sup>	MDB (m)	BNR <sup>1/2</sup>	MDB (m)	BNR <sup>1/2</sup>
10 <sup>-4</sup>	0.337	0.003	6.567	0.007	0.018	3.102	0.018	2.342
10 <sup>-3</sup>	0.429	0.003	6.868	0.006	0.018	3.102	0.018	2.342
10 <sup>-2</sup>	0.531	0.003	7.440	0.005	0.018	3.102	0.018	2.342

with:  $Q_y^{1/2} = \text{diag}(1.5, 0.003, 0.003)$  m;  $q_f = 10^{-8} \text{ m}^2/\text{s}^3$ ;  $q_s = 10^{-5} \text{ m}^2/\text{s}^5$ ;  $\Delta t_k = 1$  s and 400 epochs of processing after the filter initialization.

**Table 4.3:** The variations of DC and DC-rate standard deviations, MDB and BNR<sup>1/2</sup> with the spectral density of dynamic noises of code biases.

$\sigma_{\eta}$ (m)	$\sigma_{\nabla}$ (m)	$\sigma_{\dot{\nabla}}$ (m/s)	L1 Code		L1 Carrier		L2 Carrier	
			MDB (m)	BNR <sup>1/2</sup>	MDB (m)	BNR <sup>1/2</sup>	MDB (m)	BNR <sup>1/2</sup>
0.004	0.429	0.004	6.868	0.006	0.022	2.457	0.020	3.098
0.003	0.429	0.003	6.868	0.006	0.018	3.102	0.018	2.342
0.002	0.429	0.003	6.868	0.005	0.015	4.253	0.016	1.440
0.001	0.429	0.002	6.868	0.003	0.012	6.816	0.014	0.392

with:  $\mathbf{Q}_y^{1/2} = \text{diag}(1.5, \dots, 0.003)$  m;  $\mathbf{q}_f = 10^{-8} \text{ m}^2/\text{s}^3$ ;  $\mathbf{q}_s = 10^{-5} \text{ m}^2/\text{s}^5$ ;  $\mathbf{q}_b = 10^{-3} \text{ m}^2/\text{s}^3$ ;  $\Delta t_k = 1$  s and 400 epochs of processing after the filter initialization.

**Table 4.4:** The variations of DC and DC-rate standard deviations, MDB and BNR<sup>1/2</sup> with the standard deviation of L1 carrier observable.

$\Delta t_k$ (s)	$\sigma_{\nabla}$ (m)	$\sigma_{\dot{\nabla}}$ (m/s)	L1 Code		L1 Carrier		L2 Carrier	
			MDB (m)	BNR <sup>1/2</sup>	MDB (m)	BNR <sup>1/2</sup>	MDB (m)	BNR <sup>1/2</sup>
1	0.429	0.003	6.868	0.006	0.018	3.102	0.018	2.342
2	0.521	0.004	7.367	0.006	0.020	2.989	0.020	1.869
3	0.576	0.005	7.833	0.005	0.021	2.382	0.021	1.137

with:  $\mathbf{Q}_y^{1/2} = \text{diag}(1.5, 0.003, 0.003)$  m;  $\mathbf{q}_f = 10^{-8} \text{ m}^2/\text{s}^3$ ;  $\mathbf{q}_s = 10^{-5} \text{ m}^2/\text{s}^5$ ;  $\mathbf{q}_b = 10^{-3} \text{ m}^2/\text{s}^3$  and 400 epochs of processing after the filter initialization.

**Table 4.5:** The variations of DC and DC-rate standard deviations, MDB and BNR<sup>1/2</sup> with the sampling interval.

Number of observables	$\sigma_{\nabla}$ (m)	$\sigma_{\dot{\nabla}}$ (m/s)	L1 Code		L1 Carrier		L2 Carrier		L2 Code	
			MDB (m)	BNR <sup>1/2</sup>	MDB (m)	BNR <sup>1/2</sup>	MDB (m)	BNR <sup>1/2</sup>	MDB (m)	BNR <sup>1/2</sup>
1	0.747	0.140	7.147	2.375						
2	0.646	0.096	6.868	1.973	0.034	3.237				
3	0.429	0.003	6.868	0.006	0.018	3.102	0.018	2.342		
4	0.413	0.003	6.868	0.006	0.018	3.102	0.018	2.342	6.868	0.006

with:  $\mathbf{Q}_y^{1/2} = \text{diag}(1.5, 0.003, 0.003, 1.5)$  m;  $\mathbf{q}_f = 10^{-8} \text{ m}^2/\text{s}^3$ ;  $\mathbf{q}_s = 10^{-5} \text{ m}^2/\text{s}^5$ ;  $\mathbf{q}_b = 10^{-3} \text{ m}^2/\text{s}^3$ ;  $\Delta t_k = 1$  s and 400 epochs of processing after the filter initialization.

**Table 4.6:** The variations of DC and DC-rate standard deviations, MDB and BNR<sup>1/2</sup> with the number of observables.

The sampling interval of the observations has a quite significant effect on the precision, MDBs and BNRs considered here. As can be seen from Table 4.5, with increasing sampling interval, both DC and DC-rate standard deviations and all MDBs are increasing. The BNRs are slightly decreasing, but this is because it is a ratio.

The variations of standard deviations of DCs and DC-rates, MDBs and BNRs with the number of observables can be found in Table 4.6. Obviously, the greater the number of observables available, the better the precision, the MDBs and BNRs, except that using L2 code observations along with L1 code and L1 as well as L2 carrier observations has only a small contribution to the DC precision. The improvement of the DC and DC-rate precision is significant by using carrier observations along with L1 code observations. In addition, using L2 carrier observations along with L1 code and carrier observations can make important contributions to the DC and DC-rate precision, L1 code BNR and L1 carrier MDB as well. Note that when the number of observables increases from two to three, the L1 code BNR<sup>1/2</sup> decreases sharply from 1.973 to 0.006 but the corresponding MDB remains the same. From this we can conclude that the biases caused by the L1 code MDB in DC related states with three observables available are much smaller than those with two observables available. In other words, when the types of observables are L1 code and carrier, L1 code observations can still play certain roles in the measurement update of DC related states. But when L2 carrier observable is used as well, L1 code observations can hardly make any contributions to the measurement update. In this case, the only role played by L1 code observations in the DC estimation is the determination of the initial DC state.

Based on the above analysis, some properties of the DC and DC-rate precision and the reliability of code and carrier observations can be concluded. First, in addition to the sampling interval and the number of observables, the DC precision and L1 code MDB are mainly determined by the L1 code precision and the spectral density of dynamic noises of code biases, whereas the DC-rate precision and carrier MDBs are mainly determined by the L1 and L2 carrier precision and the spectral densities of dynamic noises of ionospheric delays and ionosphere-free DCs. Second, using L2 code along with L1 code and L1 as well as L2 carrier observations does not improve the DC-rate precision and the MDBs and BNR<sup>1/2</sup>s of the other three types of observations. Third, the DC and DC-rate precision and the MDBs and BNR<sup>1/2</sup>s of code and carrier observations are quite insensitive to the choices of the spectral densities  $q_f$ ,  $q_s$  and  $q_b$ , when they are varying within a realistic range. Therefore, their approximations are good enough for generation of DCs, since the state estimates are not sensitive to their choices either ([Brown and Hwang 1992], [Roberts and Cross 1993]). Fourth, in most cases the L1 code BNR<sup>1/2</sup> is very small, therefore the impact of an undetected model error with size of MDB in code observations is negligible. Fifth, the main role played by L1 code observations in the estimation of DC-related states is in the determination of the initial DC and they can hardly make contributions in the measurement update of DC-related states, especially when three or more observables are available. Sixth, carrier observations dominate the measurement update of DC-related states. When L1 and L2 observations have the same precision, the contribution of L1 carrier observations to the measurement update is larger than that of L2 carrier observations.



## Chapter 5

# Some numerical results and discussion

The previous chapter derived the algorithm for carrier adjusted DCs and showed how this algorithm can be integrated with the DIA quality control procedure. By using the algorithm and real data, this chapter investigates the modelling of dynamic behaviours of SA clock errors and ionospheric delays, the dynamic behaviour of code biases, the performance of the real time model testing, and the accuracy of DC prediction.

### 5.1 Description of data sets

This section gives details of the data that has been used in this and next chapters and of the choices of the a priori parameters for processing the data.

#### 5.1.1 TurboRogue SNR-8000 data

This data consists of two files and each of them contains three hours of observations collected by a TurboRogue SNR-8000 receiver on 29 June 1993 at a known station in Kootwijk of The Netherlands. Four types of observations in the data were used: P-code and carrier on L1 and L2. The sampling interval of the data was one second and an external rubidium clock with a day stability of  $5 \cdot 10^{-12}$  (Allan variance [Fruehauf 1991]) was used during the data collection. Based on the processing results of the data, it was concluded that SA was present in most Block II satellites during the data collection.

In the processing of the data, the a priori standard deviations of code and carrier observations were chosen to be 0.3 and 0.003 m, and the spectral densities of dynamic noises of ionosphere-free DCs, ionospheric delays and code biases were chosen to be  $10^{-5} \text{ m}^2/\text{s}^5$ ,  $10^{-8} \text{ m}^2/\text{s}^3$  and  $10^{-3} \text{ m}^2/\text{s}^3$ , respectively.

#### 5.1.2 Trimble 4000 SSE data

Soon after GPS was officially declared to be at the phase of initial operational capability, a campaign with four Trimble 4000 SSE receivers was conducted. At this time AS was not active. The campaign consisted of five sessions of one hour. The first four sessions took place on 11 December 1993, while the last session was on 12 December 1993. Four receivers simultaneously occupied the known stations YP01, YP05, YP07 and YP08 which are located along a runway at a former air force base near Delft, except for the third

session, when the receiver at YP05 was removed to DE18 (a station in Delft). The distances between YP01, YP05, YP07 and YP08 are from 100 to 700 metres and DE18 is six kilometres apart from them. At YP01 a kinematic L1/L2 antenna was used in the collection of the data, whereas at the other stations geodetic L1/L2 antennas were used. The main difference between these two types of antennas is that there is a ground plane in a geodetic L1/L2 antenna so as to reduce multipath effects on the observations. The sampling interval of the data was one second and the types of observables used were P-code and carrier on L1 and L2.

The a priori parameters were chosen to be the same as those for the TurboRogue SNR-8000 data, except that the spectral density of the dynamic noises of ionosphere-free DCs was replaced by  $0.1 \text{ m}^2/\text{s}^5$ , since no stable clock was available.

### **5.1.3 Trimble 4000 SSE data under AS conditions**

This Trimble 4000 SSE data was simultaneously collected on 5 May 1994 (when AS was turned on) at stations YP01, DE18 and YP08. The observations at YP01 and DE18 consisted of six one-hour sessions, and those at YP08 of three one-hour sessions. The sampling interval of the data was one second. Since under AS conditions P1 and P2 codes are encrypted, the types of observations available in the data are C1 (i.e. C/A) code, L1 and L2 carriers, and C2 (the combination of C1 and the difference between the two encrypted P1 and P2 codes denoted by Y1 and Y2, i.e.  $C2=C1+(Y2-Y1)$ ).

## **5.2 Validation of dynamic models**

In the previous chapter, we assumed that the third-order time derivatives of ionosphere-free DCs and the second-order time derivatives of ionospheric delays are random noises. In other words, we use a quadratic function to model the dynamic behaviour of ionosphere-free DCs and a linear function to model that of ionospheric delays. Since ionosphere-free DCs are functions of many factors such as receiver and satellite clock biases, tropospheric delays and since ionospheric delays are functions of satellite elevation and observation time, etc., it is necessary to study how well the dynamic behaviour of ionosphere-free DCs and that of ionospheric delays can be modelled by such quadratic and linear functions.

Of all terms contained in a DC, satellite clock biases under SA condition (i.e. SA clock errors) and receiver clock biases are the least stable. Since the receiver clock bias at a reference station has the same effect on all DCs related to different satellites, it affects only the estimate of the receiver clock bias at a DGPS user station when the corrections are applied. It has no impact on estimates of user positions. Therefore, whether or not the dynamic behaviour of receiver clock biases in DCs can well be modelled is not important for DGPS positioning applications. This means that the least stable terms that we need to account for in the modelling of ionosphere-free DCs are SA clock errors.

As we know, the carrier predicted residuals consist of carrier observation noises and prediction errors of ionosphere-free DCs and ionospheric delays. Therefore, the difference between the accuracy of carrier predicted residuals and that of carrier observations reflects the accuracy of the modelling of DCs and ionospheric delays. The accuracy of carrier observations is usually in the order of a few millimetres. The accuracy of the residuals can be estimated by their RMS error, i.e.  $\left(\frac{1}{m}\sum_{i=1}^m w_i^2\right)^{\frac{1}{2}}$ , where  $w_i$ ,  $i=1,\dots,m$ , are the residuals.

Table 5.1 presents RMS errors of nine groups of carrier predicted residuals. Each group is related to a particular satellite. The data was collected by a TurboRogue SNR-8000 receiver and its details were already given in Section 5.1.1. It was confirmed that the mean of each group of the residuals was zero. Figure 5.1 gives a histogram of the residuals related to satellite 29. As can be seen from Table 5.1, all RMS errors range from 0.001 to 0.003 metres, which means that the accuracy of carrier predicted residuals is consistent with the accuracy of carrier observations. In other words, this shows that the prediction errors of ionosphere-free DCs and ionospheric delays are at most of the order of a few millimetres. In addition, it can be seen from Figure 5.1 that the predicted residuals are quite well normally distributed. This shows that the prediction errors consist of random noises. Since in the data collection a good external clock was used, the dynamic behaviour of DCs was dominated by SA clock errors rather than receiver clock biases. Therefore, the dynamic behaviours of SA clock errors and ionospheric delays can indeed well be modelled by quadratic and linear functions, respectively.

Satellite number	Number of residuals	RMS (m)
15	1024	0.002
7	3576	0.003
25	3259	0.003
14	8165	0.003
13	8280	0.001
29	10470	0.003
24	7634	0.002
19	5640	0.002
16	2240	0.002

**Table 5.1:** RMS errors of carrier predicted residuals.

### 5.3 Dynamic behaviour of code biases

As indicated in the previous chapter, one property of carrier adjusted DCs is that code biases can be accounted for in the generation of DCs. This section gives some examples of the properties of code biases based on data collected by Trimble 4000 SSE and TurboRogue SNR-8000 receivers. In addition, two plots of code predicted residuals without and with the impact of code biases are also presented.

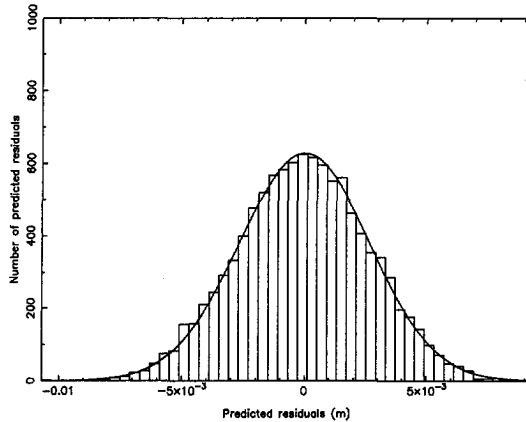


**Figure 5.1:** A histogram of carrier predicted residuals.

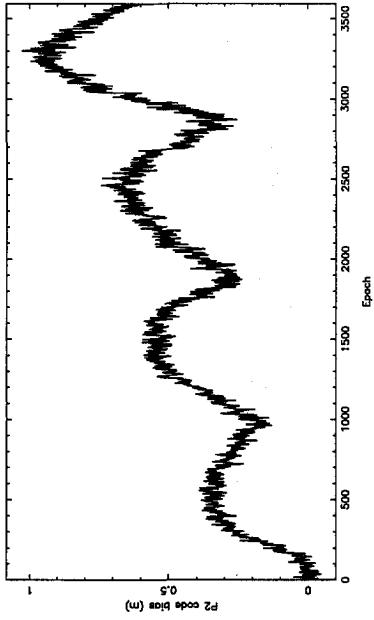
Figures 5.2 to 5.5 show P1 and P2 code biases found in a Trimble 4000 SSE data set. The data was collected on 12 December 1993 at the known station YP05; more details about the data were given in Section 5.1.2. Figures 5.2 and 5.3 plot the dynamic behaviour of P2 and P1 code biases for one satellite at the same period. It can be easily seen from Figure 5.2 that the P2 code biases show a periodic behaviour plus a trend and that the size finally reaches about one metre within one hour. The behaviour of the P1 code biases shown in Figure 5.3 is quite different from that of the P2 code biases. For example, the periodic behaviour in the P1 code biases is less obvious than in the P2 code biases and the size in the former, which is about 0.7 meters within one hour, is smaller than that in the latter. But the trends of the P1 and P2 code biases are quite similar.

Figure 5.4 illustrates the behaviour of the P2 code biases in observations from satellite 19. Its main property is the comparatively high frequency in the code biases. Figure 5.5 graphs the P1 code biases in satellite 21 observations, where the trend is rather insignificant.

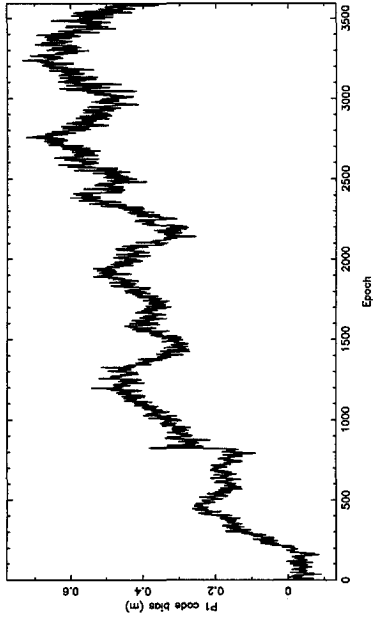
Figure 5.6 shows the C1 code biases found in a Trimble 4000 SSE data set. The data was collected on 5 May 1994 at the known station YP01 and their details can be found in Section 5.1.3. As graphed in the figure, the behaviour of the C1 code biases is dominated by a trend, the maximum size of which reaches about 1.5 metres. After the filter starts, the code bias linearly increases until epoch 3200, then it decreases again.

Figure 5.7 shows the P2 code biases found in a TurboRogue SNR-8000 data set, details of which were given in Section 5.1.1. As can be seen from the figure, there is hardly any trend in the P2 code biases although periodic variations are apparent.

On the basis of the same data and the same a priori parameters as Figure 5.6, Figures 5.8 and 5.9 illustrate the C1 code predicted residuals without and with the impact of code



**Figure 5.2:** P2 code biases in satellite 3 observations collected by a Trimble 4000 SSE receiver.



**Figure 5.3:** P1 code biases in satellite 3 observations collected by a Trimble 4000 SSE receiver.

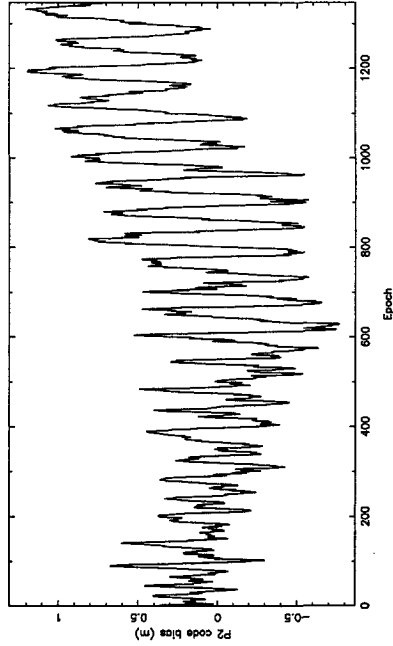


**Figure 5.4:** P2 code biases in satellite 19 observations collected by a Trimble 4000 SSE receiver.

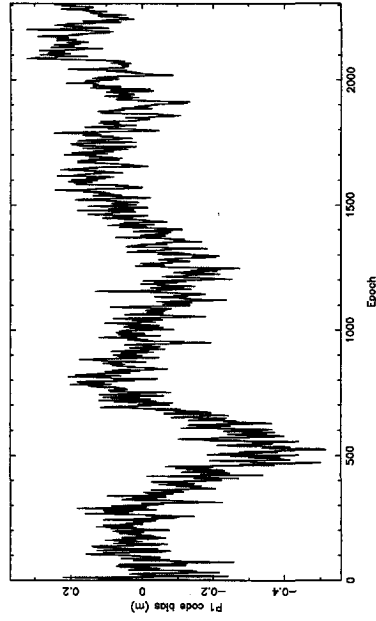


**Figure 5.5:** P1 code biases in satellite 21 observations collected by a Trimble 4000 SSE receiver.

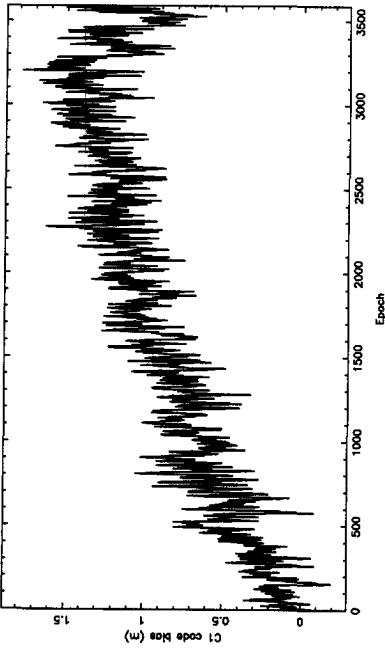


Figure 5.6: C1 code biases for a Trimble 4000 SSE data set.

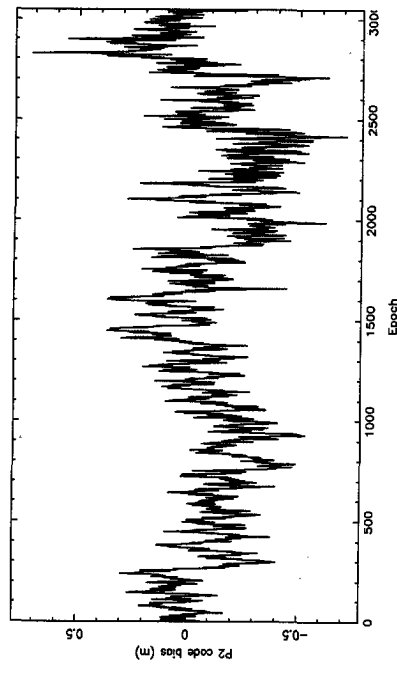


Figure 5.7: P2 code biases for a TurboRogue SNR-8000 data set.

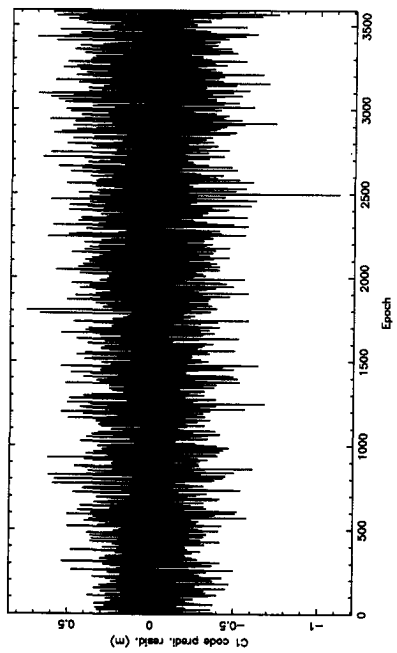


Figure 5.8: C1 code predicted residuals without the impact of code biases.

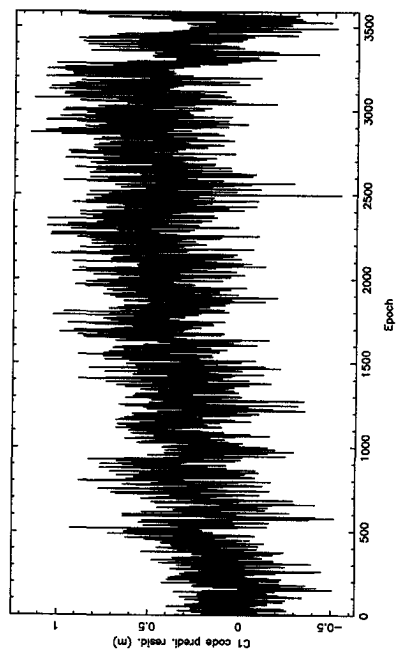


Figure 5.9: C1 code predicted residuals with the impact of code biases.

biases, respectively. The only difference in processing the data between these two figures is that Figure 5.8 is based on a filter in which code biases were taken into account, whereas Figure 5.9 is based on a filter where code biases were ignored. Obviously, the predicted residuals shown in Figure 5.8 seem quite normal, which were confirmed by their zero mean. This means that the measurement and dynamic models of the filter are correct. However, the residuals shown in Figure 5.9 are clearly biased by a trend, which is actually the trend appearing in Figure 5.6. Therefore, when code bias are significantly present in code observations, it is necessary to introduce a code-bias parameter in the filter so that the effect of the bias on code predicted residuals and consequently on the estimated states can be avoided or reduced. The code bias parameter can be modelled by a dynamic model with constant velocity.

A few remarks should be made. First of all, the code biases shown in Figures 5.2 to 5.7 are actually the variation of the code biases with respect to the code bias at the initial epochs. They are not the absolute biases in the code observation at the corresponding epochs. Second, the periodic behaviour of code biases are likely caused by multipath effects. Since multipath errors may have different frequencies, the periods of code biases may not be the same for different satellites observed at the same time. Third, the size and behaviour of code biases on L1 and L2 frequencies may not be the same for the same satellite. Fourth, when code biases are significantly present, introducing code-bias parameters with a constant-velocity dynamic model can efficiently reduce the effect of code biases on code predicted residuals and in turn on estimated states.

#### 5.4 Performance of real time model testing

In Section 4.2, we discussed how to carry out real time model testing along with the generation of carrier adjusted DCs. This section uses a small TurboRogue SNR-8000 data set to show some examples of the testing performance.

The data set used in this section was collected at the same location as the two data sets described in Section 5.1.1, but one day later. The data collection lasted only seven minutes. At the beginning of the collection there were five satellites (i.e., satellites 15, 14, 1, 7, and 31) in view and two minutes later one more satellite (i.e. satellite 29) became visible. Since it will be shown in the next chapter that there is an apparent relationship between satellite elevation and the precision of code observations, Table 5.2 gives the information on the elevations of the satellites.

Table 5.3 shows the sensitivity of the mean of the normalized LOM test statistic to the standard deviations of code and carrier observations and to the spectral densities of dynamic noises of ionospheric delays, ionosphere-free DCs and code biases. Note that the five statistical parameters  $\sigma_{code}$ ,  $\sigma_{carrier}$ ,  $q_f$ ,  $q_g$ , and  $q_b$  are chosen to be 0.3 m, 0.003 m,  $10^{-8} \text{ m}^2/\text{s}^3$ ,  $10^{-5} \text{ m}^2/\text{s}^5$  and  $10^{-3} \text{ m}^2/\text{s}^3$ , respectively, when they are not treated as variables in the analysis. In the choices of the code standard deviation, we accounted for the results of the relationship between satellite elevation and the precision of code observations to be shown in Section 6.3. In other words, choosing the code standard deviations to be 0.07,

Satellite number	Elevation (deg)
15	76.0 - 72.7
14	52.3 - 55.4
1	30.4 - 28.5
7	26.7 - 29.0
31	17.9 - 14.8
29	14.2 - 17.3

**Table 5.2:** The Varying ranges of satellite elevations.

0.15 and 0.30 m is because satellites 15, 1 and 31 are at elevations of about 70°, 30°, and 15°, respectively. Therefore these three standard deviations can be considered as realistic choices for the three satellites. Here the difference in the standard deviation between P1 and P2 code observables is ignored. As can be seen from the table, the mean of the LOM test statistic is quite sensitive to the choices of the standard deviations of both code and carrier observations. By increasing one of the standard deviations, all of the means decrease with no exception. For example, when the code standard deviation increases from 0.07 to 0.15 and 0.30 m, the mean of the LOM test statistics of satellite 15 decreases from 0.21 to 0.06 and 0.02, respectively. When the carrier standard deviation increases from 0.001 to 0.002 and 0.003 m, the mean decrease from 0.07 to 0.03 and 0.02. From a theoretical point of view, if all statistical parameters are correctly chosen and the specified dynamic and measurement models are valid, the mean should be close to its expectation value of one. But as can be seen from the results in Table 5.3, the means are always a bit too small, when the code standard deviation is correctly chosen. For instance, when the code standard deviations of satellites 15, 1 and 31 are chosen to be 0.07, 0.15 and 0.30 m, respectively, their corresponding means are 0.21, 0.60 and 0.66, i.e., all of them are less than one. It is not clear yet what are the reasons to cause the mean of the LOM test statistic to be too small. Some possible reasons might be that the real code and carrier observation noises are not normally distributed; there are correlations between observables; code and carrier observations are correlated in time; or others.

Different from the standard deviations of code and carrier observations, the spectral densities of dynamic noises of ionospheric delays, ionosphere-free DCs, and code biases have no or very small impact on the mean of the LOM test statistic when they vary in certain ranges. Therefore, how to choose the spectral densities is not really a problem for performing real time model testing along with generation of carrier adjusted DCs.

Cycle slips are probably the most likely model errors to appear in carrier observations. In order to see if such errors can be indeed successfully detected and identified in the model testing procedure in practice, five testing experiments were conducted by using the same data as used in Table 5.3 with different size and combinations of simulated errors in L1 and L2 carrier observations. Table 5.4 shows the information on the simulated error(s) and the LOM testing result of each experiment as well as a LOM testing result without any



		Satellite number					
		15	14	1	7	31	29
$\sigma_{code}$ (m)	0.07	0.21	0.31	1.40	1.19	4.77	4.43
	0.15	0.06	0.10	0.60	0.30	1.41	1.08
	0.30	0.02	0.05	0.42	0.10	0.66	0.30
$\sigma_{carrier}$ (m)	0.001	0.07	0.17	1.24	0.17	1.63	0.41
	0.002	0.03	0.07	0.65	0.11	0.94	0.32
	0.003	0.02	0.05	0.42	0.10	0.66	0.30
$q_f$ ( $\frac{m^2}{s^3}$ )	$10^{-8}$	0.02	0.05	0.42	0.10	0.66	0.30
	$10^{-7}$	0.02	0.05	0.41	0.10	0.66	0.29
	$10^{-6}$	0.02	0.05	0.39	0.09	0.63	0.29
$q_g$ ( $\frac{m^2}{s^5}$ )	$10^{-5}$	0.02	0.05	0.42	0.10	0.66	0.30
	$10^{-4}$	0.02	0.04	0.22	0.09	0.43	0.29
	$10^{-3}$	0.02	0.03	0.12	0.08	0.32	0.28
$q_h$ ( $\frac{m^2}{s^3}$ )	$10^{-3}$	0.02	0.05	0.42	0.10	0.66	0.30
	$10^{-2}$	0.02	0.04	0.41	0.09	0.62	0.26
	$10^{-1}$	0.02	0.04	0.39	0.07	0.57	0.20

**Table 5.3:** Means of normalized LOM test statistics based on different standard deviations and spectral densities.

experiment number	simulated errors (cycles)		$T^k_{LOM}$
	L1	L2	
1	1	0	477.57
2	1	1	298.53
3	1	-1	2211.69
4	77	60	1214956.50
5	-77	60	10016474.62
6	0	0	0.02

Note: with the choices of  $\alpha = 0.001$  and  $\gamma = 0.8$ , the critical value  $F_{0.001}(4, \infty, 0) = 3.38$

**Table 5.4:** Results of LOM testing experiments with or without simulated cycle-slip errors in carrier observations.

simulated errors. Experiment 1 is concerned with a single model error of one cycle slip in the L1 carrier observation, while experiments 2 and 3 are related to two model errors of the same or opposite signs with one in the L1 carrier and the other in the L2 carrier. Since the wave lengths of L1 and L2 carrier are not the same due to the ratio of L1 and L2 frequencies being 77/60, experiments 4 and 5 were designed for testing a special combination of cycle slips in the L1 and L2 so that they could result in model errors with the same size and the same or opposite signs. The last experiment was a test without any simulated errors. As can be seen from Table 5.4, all the simulated cycle-slip model errors were indeed correctly detected, no matter they occurred as single model errors, multi model errors, or some special combinations. Moreover, they were also successfully identified. Therefore, the real time model testing approach discussed in Sections 2.2 and 4.2 can indeed work well with cycle slip model errors.

### 5.5 Accuracy of differential-correction prediction

Some latency is unavoidable when DCs are applied at a mobile station. Therefore, when a mobile user is going to use DCs at time  $t_l$ , they will actually be using predicted DCs which are usually computed from DC and DC-rate estimates at time  $t_k$  ( $t_k < t_l$ ) [Clynch et al. 1992], [van Dierendonck and Enge 1994]. Because of error propagation, the accuracy of predicted DCs will decrease when the latency ( $t_l - t_k$ ) increases. One may wonder, in this case, how the accuracy of predicted DCs varies with the latency and how large the maximum latency can be so as to have predicted DCs with a certain accuracy.

Obviously the accuracy variation of predicted DCs can be explored by using the covariance matrix of DC and DC-rate estimates, provided the actual observation model is identical to the one assumed in generation of DCs. But because many unexpected factors may occur in actual observations, such as, measurement correlations in time and in observables, the theoretical precision of DC and DC-rate estimates may not exactly reflect the actual accuracies of them. In the following, we will, therefore, investigate the accuracy of DC prediction by analyzing RMS errors of DC prediction residuals. The RMS error can be computed as follows.

- Estimate the parameters DC, DC-rate and DC-acceleration for each epoch.
- Choose a latency  $\Delta t$ .
- Compute the predicted DC at time  $t_l$  ( $l=\Delta t+1, \Delta t+2, \dots$ ) by using DC and DC-rate estimates at time  $t_k$  ( $t_k=t_l-\Delta t$ ).
- Compute DC prediction residuals by taking the difference of the predicted and estimated DCs at time  $t_l$ ,  $l=\Delta t+1, \Delta t+2, \dots$
- Compute the RMS of the residuals

By repeating the above steps, except for the first one for a new latency, all RMS errors of DC prediction residuals as functions of latency can be obtained.

Note that the RMS error of DC prediction residuals can only reflect the accuracy of DC prediction rather than the accuracy of predicted DCs, since the latter depends on the

accuracy of DC and DC-rate estimations as well as on the accuracy of DC prediction.

Figure 5.10 illustrates some typical RMS errors of DC prediction residuals, which were based on DC and DC-rate estimates obtained by using the data described in Section 5.1.1. As can be seen from this figure, the RMS errors may vary in two different ways: quadratically and linearly. It was found that this behaviour difference is related to presence or absence of SA clock errors. For satellites with SA clock errors, the RMS errors increase quadratically with increasing latencies; they are about 0.05, 0.2 and 0.5 meters when latencies are 5, 10 and 15 seconds, respectively. On the other hand, for satellites without SA clock errors, the RMS errors increase linearly and grow more slowly. For 15 seconds latency, they are about 0.02 meters.

In most practical cases, DC latencies will be within 15 seconds [Kremer et al. 1990], [Langley 1994] but sometimes, for instance, when transmitted DCs are not received, old DCs with ages of tens of seconds may have to be used [Ashkenazi et al. 1994]. Therefore it would be interesting to know how the accuracy of DC prediction varies when DC latency is up to one minute. Some examples of the accuracy are give in Figure 5.11, from which it can be seen that the RMS error of DC prediction residuals is within 8.3 metres when the latency is one minute.

In order to see how the accuracy of DC prediction will be affected by the use of DC-acceleration estimates as well, we computed the RMS errors based on not only DC and DC-rate estimates but also DC-acceleration estimates. The results are plotted in Figures 5.12 and 5.13. Note that the only difference between Figures 5.10 and 5.11 and Figures 5.12 and 5.13 is that DC-acceleration estimates were used in the latter two figures. By comparing Figures 5.10 and 5.11 with Figures 5.12 and 5.13, it can be seen that for satellites with SA clock errors implemented, the accuracy of DC prediction is clearly improved by using DC-acceleration estimates in DC predictions. For example, for 15 seconds latency, the RMS error drops from about 0.38–0.54 metres to about 0.16–0.21 metres. The larger the latency, the more apparent the improvement. Using DC-acceleration estimates in DC predictions for satellites without SA clock errors, on the contrary, will worsen the accuracy of DC prediction. For example, for a 15-second latency the RMS error of the DC prediction increases from 0.02 metres to 0.09 metres due to the use of DC-acceleration estimates in the DC prediction. But note that the deteriorated accuracies related to satellites without SA clock errors are still better than the improved ones related to satellites with SA clock errors.

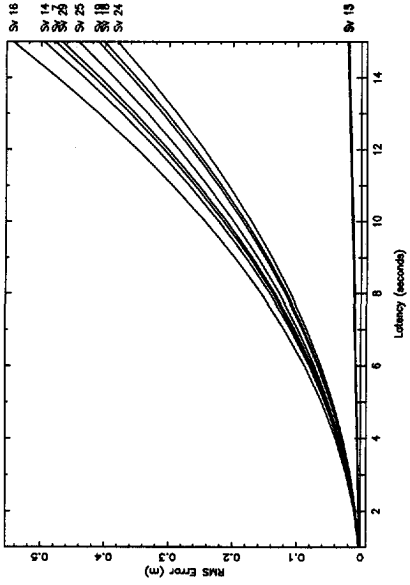


Figure 5.10: RMS errors of DC prediction versus latency between 1 and 15 seconds.

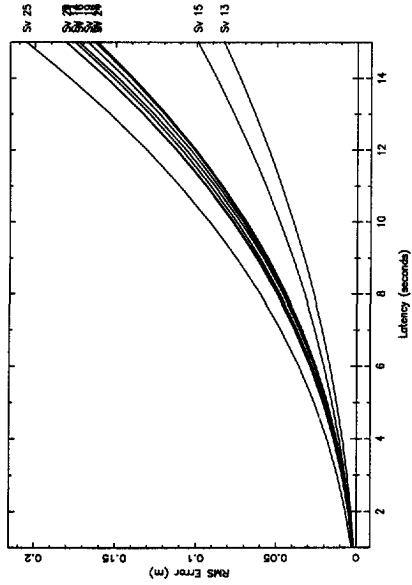


Figure 5.12: RMS errors of DC prediction versus latency between 1 and 15 seconds, where predicted DCs are computed based not only on DC and DC-rate estimates but also on DC-acceleration estimates.

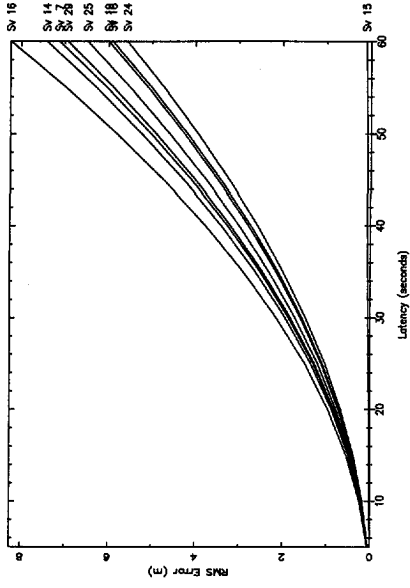


Figure 5.11: RMS errors of DC prediction versus latency between 5 and 60 seconds.

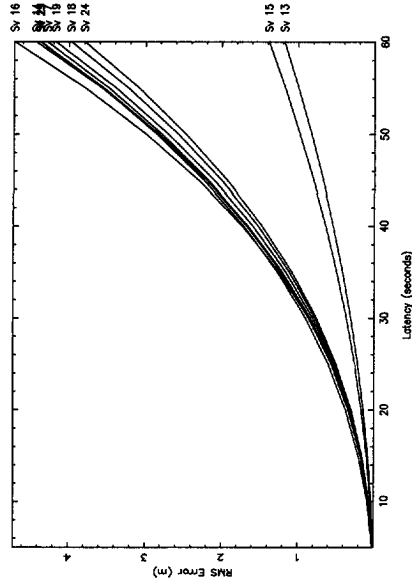


Figure 5.13: RMS errors of DC prediction versus latency between 5 and 60 seconds, where predicted DCs are computed based not only on DC and DC-rate estimates but also on DC-acceleration estimates.

## Chapter 6

# Relationship between satellite elevation and precision of code observations

### 6.1 Introduction

In GPS data reduction, the stochastic model of GPS code observations is usually assumed to be constant, i.e., a fixed value for the standard deviation of code observations is used for an entire satellite pass. It is shown below, however, that this assumption may not be realistic and that the precision of code observations may deteriorate with decreasing satellite elevation. As indicated in [Brown and Hwang 1992], when a priori uncertainty is not correctly given to a certain extent, it may not have much influence on the estimates of unknowns (e.g. states of a Kalman filter) but it can result in incorrect variances of the estimates. Variances of estimates play important roles not only in evaluating the precision of estimates but also in performing quality control of geodetic networks and navigation systems [Teunissen 1984, 1990a]. It is, therefore, important to investigate the stochastic behaviour of GPS code and carrier observations so that correct stochastic models for these observables can be used in GPS data processing.

Note the difference between the accuracy and the precision of an observation. The former is the closeness of an estimate (or measurement) to its true (but unknown) value. It, therefore, depends on both systematic errors and random noises in the observation. Whereas the latter is the closeness of an estimate to its mean estimate and thus it depends on only random noises in it (cf. [Mikhail 1976], [NGS 1986] or [GSD 1993]). Since our goal is to analyse the precision, rather than the accuracy, of code observations, which often contain significant systematic errors (i.e. code biases), successful isolation of code observation noises from the systematic errors is the key to the investigation on the precision of code observations.

This chapter analyses the relationship between satellite elevation and the precision of code observations. This analysis is based on code predicted residuals computed by using the algorithm presented in Chapter 4 and on data collected by TurboRogue SNR-8000, Trimble 4000 SSE and Trimble 4000 SST receivers.

### 6.2 Analytic approach of the precision of code observations

To analyse the precision of code observations, we need to compute code observation noises, which are the random part of code observation errors. Since the algorithm for

carrier adjusted DCs has accounted for all systematic errors in code observations, estimation of the noises become not only possible but also quite easy.

As can be seen from the dynamic and measurement models given in Chapter 4, code predicted residuals consist of code observation noises and prediction errors of DCs and code biases. As already indicated in Section 5.2, the least stable terms in DCs are receiver clock biases and SA clock errors. It was shown in that section that SA clock errors could be modelled and predicted quite well under certain conditions and that the modelling accuracy could be within a few millimetres. Concerning the modelling of receiver clock biases, it is, of course, very much dependent on the quality of receivers. Based on our experiments with data collected by Trimble 4000 SSE receivers (see its details in Section 5.1) and data collected by a Trimble 4000 SST receiver, it was found that the modelling accuracy of receiver clock biases could be within 3 centimetres. Since a code bias is a combination of all systematic errors in a code observation, its dynamic behaviour is easy to model and predict. Therefore, the prediction errors of DCs and code biases are negligible compared with code observation noises and code predicted residuals reflect appropriately the properties of code observation noises. In order to study the relationship between satellite elevation and the precision of code observations, we assume that the relationship at epoch  $t_k$  can be reflected by the code predicted residuals 5 minutes before and after  $t_k$ . We choose, therefore, every 10 minutes of code predicted residuals as one group and for each group the RMS error of the residuals is computed along with the elevation at the centre of the 10 minute period. Since the code predicted residuals are dominated by code observation noises, the RMS errors of code predicted residuals are equivalent to those of code observation noises, i.e. the precision of code observations.

### 6.3 Numerical results and discussion

Figure 6.1 shows the RMS errors of P1 and P2 code predicted residuals based on the data described in Section 5.1.1. Note that it has been verified that the choices of the a priori parameters to a certain extent have no visible impact on the values of the RMS errors, the standard deviations were still chosen to be constant for computing the RMS errors here and afterwards. From this figure, the following conclusions can be drawn. First, comparing Figure 6.1 (a) and (b) shows that the precision of P1 is slightly better than that of P2 at low elevation. For example, the average of the RMS errors of P1 at 20° elevation is about 0.19 m, whereas the P2 related one is about 0.22 m. Second, the relationship between satellite elevation and the precision of P code observations is obvious, especially at low elevations. At elevations of about 15°, the mean of the P1 related RMS errors is about 0.24 m, when the elevation increases to 40°, it decreases to about 0.1 m. Once the elevation is above 50°, the RMS error becomes more and more stable. Third, as suggested by [Euler and Goad 1991], the relationship between satellite elevation and the RMS errors can quite well be modelled by an exponential function like

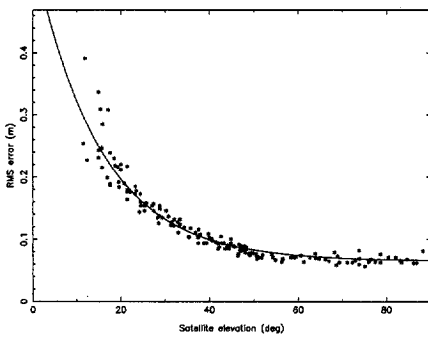
$$y = a_0 + a_1 \cdot \exp\left\{\frac{-x}{x_0}\right\} \tag{6.1}$$

where  $y$  (the RMS error),  $a_0$  and  $a_1$  have units of metres and  $x$  (the elevation) and  $x_0$  are in degrees. Obviously,  $a_0+a_1$  is the RMS error at zero-degree elevation,  $a_0$  approximately the RMS error at 90° elevation (if  $x_0 < 90^\circ$ ) and  $-a_1/x_0$  the rate of change of the RMS errors with respect to elevation at zero degrees. The following coefficients were found for the TurboRogue SNR-8000 data

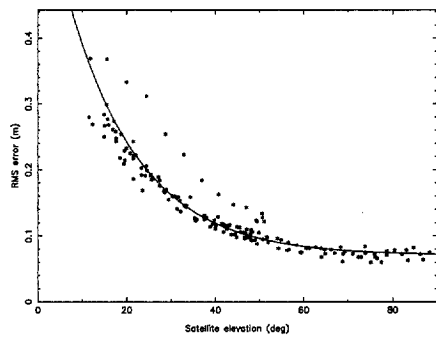
	$a_0$ (m)	$a_1$ (m)	$x_0$ (deg)
P1	0.065	0.5	15
P2	0.07	0.6	16

Figures 6.2 to 6.5 present the RMS errors related to the Trimble 4000 SSE receivers at four stations. As can be seen from the figures, the precision of the P1 and P2 code observations is almost the same at all stations and it decreases quickly at low elevations. The relationship between satellite elevation and the P-code precision of Trimble 4000 SSE can also be modelled by an exponential function with the following coefficients

	$a_0$ (m)	$a_1$ (m)	$x_0$ (deg)
P1	0.05 - 0.08	0.7 - 1.0	6 - 9
P2	0.06 - 0.09	0.7 - 1.0	6 - 7

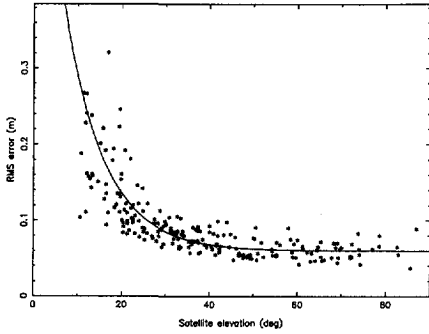


(a): P1

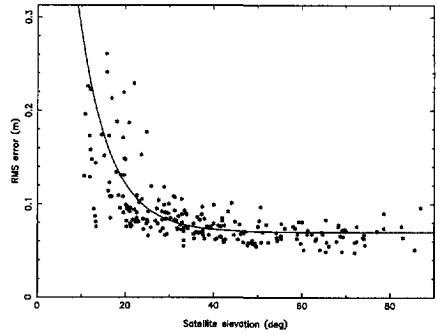


(b): P2

**Figure 6.1:** RMS errors of TurboRogue SNR-8000 code predicted residuals; the solid curves are  $y=0.065+0.5 \cdot \exp\{-x/15\}$  in (a) and  $y=0.07+0.6 \cdot \exp\{-x/16\}$  in (b).

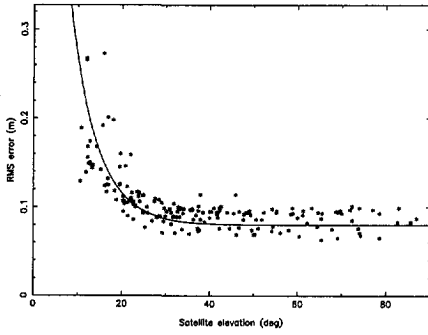


(a): P1

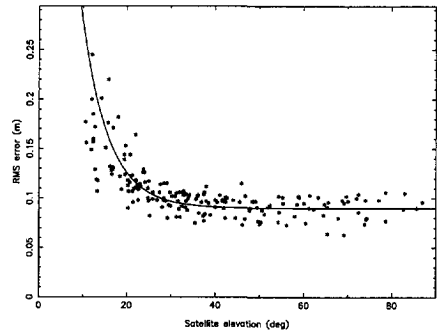


(b): P2

**Figure 6.2:** RMS errors of Trimble 4000 SSE code predicted residuals at station YP01; the solid curves are  $y=0.06+0.7 \exp\{-x/9\}$  in (a) and  $y=0.07+0.9 \exp\{-x/7\}$  in (b).

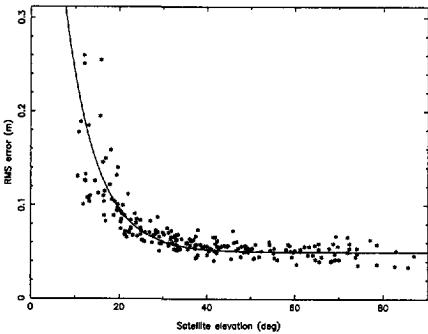


(a): P1

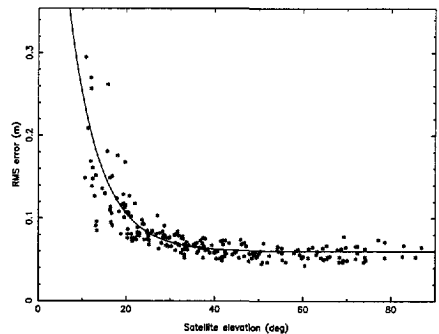


(b): P2

**Figure 6.3:** RMS errors of Trimble 4000 SSE code predicted residuals at station YP05; the solid curves are  $y=0.08+1.0 \exp\{-x/6\}$  in (a) and  $y=0.09+1.0 \exp\{-x/6\}$  in (b).



(a): P1



(a): P2

**Figure 6.4:** RMS errors of Trimble 4000 SSE code predicted residuals at station YP07; the solid curves are  $y=0.05+0.8 \exp\{-x/7\}$  in (a) and  $y=0.06+0.8 \exp\{-x/7\}$  in (b).



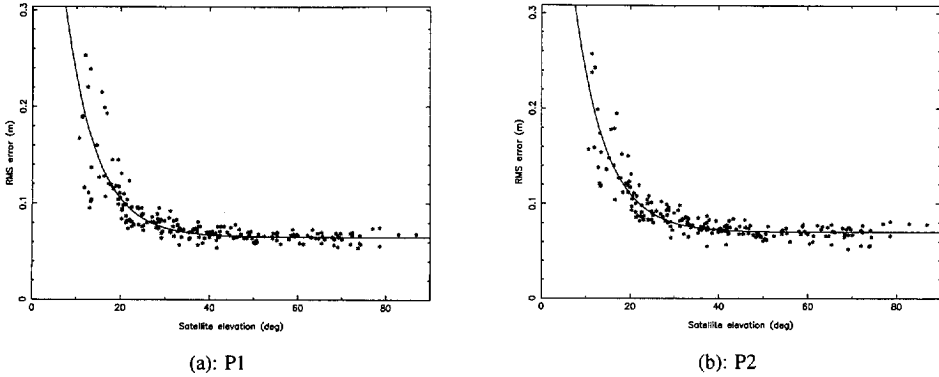
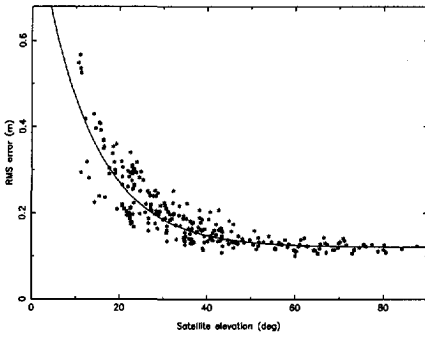


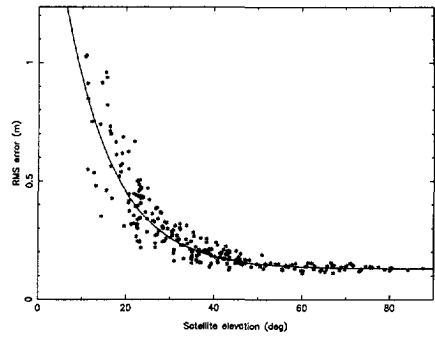
**Figure 6.5:** RMS errors of Trimble 4000 SSE code predicted residuals at station YP08; the solid curves are  $y=0.065+0.7 \cdot \exp\{-x/7\}$  in (a) and  $y=0.07+0.7 \cdot \exp\{-x/7\}$  in (b).

There are some differences in the RMS errors between the TurboRogue SNR-8000 and the Trimble 4000 SSE data. First, the P-code precision of the latter is generally better than that of the former, particularly below  $40^\circ$  elevation. For example, around  $30^\circ$  elevation, the P-code RMS errors of the TurboRogue SNR-8000 are more than 0.12 m, whereas those of the Trimble 4000 SSE are in general less than 0.10 m. Note that this difference is not caused by the different choices of the spectral density of dynamic noises of ionosphere-free DCs in the processing of the two types of data. It has been verified that the behaviour of the RMS errors of the TurboRogue data remains the same when the data is processed with the same input parameters as those chosen for the Trimble 4000 SSE data. Second, the relationship between satellite elevation and P-code precision for the Trimble 4000 SSE appears mainly in a smaller elevation range than that for the TurboRogue SNR-8000.

To investigate the relationship between satellite elevation and the precision of code observations under AS conditions, Figures 6.6 to 6.8 show the RMS errors of Trimble 4000 SSE C1 and C2 code predicted residuals. Similar to the precision of P-code observations, the precision of C1 and C2 code observations improves when satellite elevation increases up to about  $50^\circ$ . As expected, at low elevations, the precision of the C2 code observations is obviously poorer than that of the C1 code observations. With increasing elevation, the differences in the precision become smaller and smaller. In other words, the precision difference between C1 and C2 code observations appears mainly at low elevations, and the higher the elevation, the closer the precision. Again, the relationships between satellite elevation and the RMS errors of the C1 and C2 code predicted residuals can quite well be modelled by the exponential function (6.1); the coefficients  $a_0$ ,  $a_1$  and  $x_0$  read

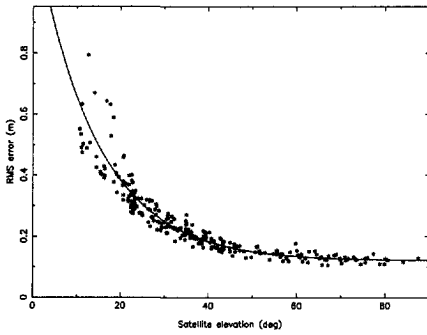


(a): C1

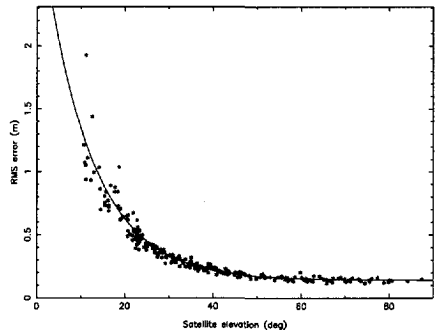


(b): C2

**Figure 6.6:** RMS errors of the Trimble 4000 SSE code predicted residuals at station YP01; the solid curves are  $y=0.12+0.8 \cdot \exp\{-x/12\}$  in (a) and  $y=0.13+2.0 \cdot \exp\{-x/11\}$  in (b).

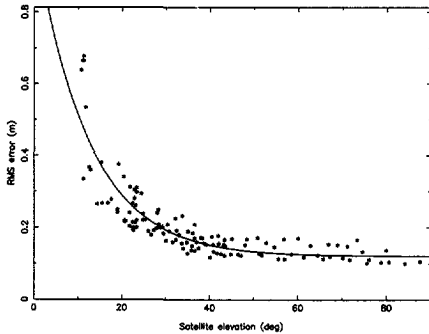


(a): C1

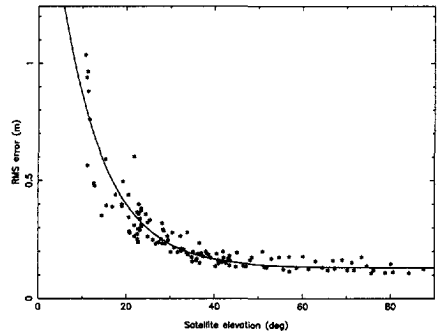


(b): C2

**Figure 6.7:** RMS errors of the Trimble 4000 SSE code predicted residuals at station DE18; the solid curves are  $y=0.12+1.1 \cdot \exp\{-x/14\}$  in (a) and  $y=0.14+3.0 \cdot \exp\{-x/11\}$  in (b).



(a): C1



(b): C2

**Figure 6.8:** RMS errors of the Trimble 4000 SSE code predicted residuals at station YP08; the solid curves are  $y=0.12+0.9 \cdot \exp\{-x/12\}$  in (a) and  $y=0.13+2.0 \cdot \exp\{-x/10\}$  in (b).

	$a_0$ (m)	$a_1$ (m)	$x_0$ (deg)
C1	0.12	0.8 - 1.1	12 - 14
C2	0.13 - 0.14	2.0 - 3.0	10 - 11

Figure 6.9 shows the RMS errors of one hour of Trimble 4000 SST C/A code predicted residuals. The data was collected on 3 October 1991 at the station DE18 and the sampling interval was one second. The observables used were C/A code and L1 as well as squared L2 carrier. As can be seen from the figure, the relationship between satellite elevation and the C/A-code precision is quite obvious below 40° elevation. When satellite elevation increases from 15° to 25° and then to 40°, the mean of the RMS errors decreases from about 2.6 to 1.8 and then to 1.4 metres. This relationship can quite well be modelled by the exponential function  $y=1.0+3.0 \exp\{-x/25\}$ . Above 40° elevation, the relationship becomes less significant.

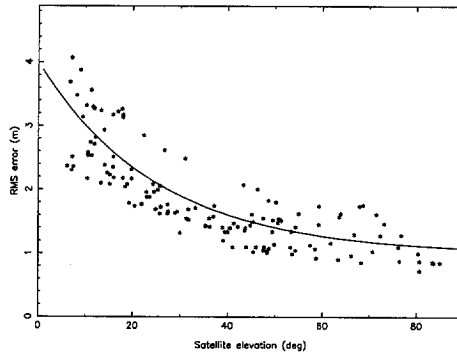


**Figure 6.9:** RMS errors of the Trimble 4000 SST C/A code predicted residuals; the solid curve is  $y=1.0+3.0 \exp\{-x/25\}$ .

It should be indicated that the analytic approach used here is different from approaches based on simply a linear combination of code and carrier observations. For instance, [Euler and Goad 1991] reported a similar analysis based on the RMS errors, within 2° elevation intervals, of the differences between code range changes and carrier range changes. Therefore, code bias errors and the opposite influence of the ionosphere on code and carrier observations were not taken into account there and they were included in the RMS errors. For the same type of Trimble 4000 SST receivers, the RMS errors shown in the above reference are about 1.3 (at high elevation) to 2.2 (at low elevation) times those found here. In addition, as indicated in the same reference, the decrease of code observation precision at low elevations is probably due to a higher likelihood of encountering multipath and lower signal-to-noise ratios at these elevations.



## Chapter 7

# Algorithm for carrier adjusted DGPS positioning and numerical results

### 7.1 Introduction

The performance of DGPS positioning is a function of three elements: i) generation of DCs at a known DGPS reference station, ii) transmission of the corrections from the reference station to mobile stations, and iii) computation of the mobile position. In Chapter 4, we discussed how to generate DCs. This chapter focuses on how to compute unknown mobile positions. As we know, when only code observations are available, the positioning algorithm is quite simple, particularly in the case of single-epoch positioning. But when both code and carrier observations are available, it is still of interest to investigate how to integrate these two types of observables. By using the carrier filtered code observations, one can usually reduce the effect of code observation noises on estimates of the parameters of interest, such as position, velocity and time. But it was shown in Chapter 3 that the stochastic model of carrier filtered code observations is hard to specify correctly, which consequently makes it difficult to obtain the correct precision of the estimates. As is well known, data processing has two tasks: i) to estimate the unknown parameters; ii) to estimate the quality of the parameter estimates. Since precision estimates are used to describe how precise the parameter estimates are, without them the parameter estimates can be useless in some cases. In addition, the precision estimate is also important for quality control of a navigation system [Teunissen 1990a]. Therefore, correct precision estimates are as important as optimal parameter estimates. Furthermore, some methods leads to biased carrier filtered code observations due to the opposite influence of ionosphere on code and carrier observations. The size of the bias may sometimes exceed the code observation noise [Loomis et al. 1989].

This chapter first derives in Section 7.2 an alternative DGPS positioning algorithm based on L1 code and carrier observations, which is referred to as algorithm for carrier adjusted DGPS positioning, analogously to [Teunissen 1991]. Next, we show in Section 7.3 the effect of the number of observables used at reference and mobile stations on the positioning accuracy and investigate the differences in positioning results between using elevation-dependent and constant standard deviations for code observations. Finally, Section 7.4 will give some concluding remarks.

### 7.2 Carrier adjusted DGPS positioning models

### 7.2.1 Positioning models

When we derived the models for generating carrier adjusted DCs in Chapter 4, we introduced code-bias parameters in L1 and L2 code observation equations to account for systematic errors. But now we have to eliminate the parameters, since in the computation of mobile positions it is no longer possible to separate systematic errors from white noises in code observations.

Let us write the L1 code and carrier observation equations given in Chapter 3 again as follows

$$P^i(t_k) = \rho^i(t_k) + c(dT(t_k) - dt^i(t_k)) + \nabla^{eph^i}(t_k) + I^i(t_k) + \nabla^{tro^i}(t_k) + e^i(t_k) \quad (7.1)$$

$$\lambda_1 \Phi^i(t_k) = \rho^i(t_k) + c(dT(t_k) - dt^i(t_k)) + \nabla^{eph^i}(t_k) - I^i(t_k) + \nabla^{tro^i}(t_k) - \lambda_1 N^i + \eta^i(t_k) \quad (7.2)$$

where

*i*: satellite number, when used as a superscript

By using the broadcast navigation data, the approximate value for  $dt^i(t_k)$ , denoted by  $dt^{i^0}(t_k)$ , can be computed. Analogously to what we did in the derivation of the models for generating carrier adjusted DCs, define

$$\left. \begin{aligned} \delta t^i(t_k) &= dt^i(t_k) - dt^{i^0}(t_k) \\ \nabla_m^i(t_k) &= c(dT(t_k) - \delta t^i(t_k)) + \nabla^{eph^i}(t_k) + I^i(t_k) + \nabla^{tro^i}(t_k) \end{aligned} \right\} \quad (7.3)$$

Then it follows from (7.1), (7.2) and (7.3) that

$$\left. \begin{aligned} P^i(t_k) - c dt^{i^0}(t_k) &= \rho^i(t_k) + \nabla_m^i(t_k) + e^i(t_k) \\ \lambda_1 \Phi^i(t_k) - c dt^{i^0}(t_k) &= \rho^i(t_k) + \nabla_m^i(t_k) - 2I^i(t_k) - \lambda_1 N^i + \eta^i(t_k) \end{aligned} \right\} \quad (7.4)$$

The DC and its rate of change, as generated at a reference station and transmitted to a user, read as

$$\left. \begin{aligned} \hat{V}_r^i(t) &= \nabla_r^i(t) + \mu_1^i(t) \\ \frac{d\hat{V}_r^i(t)}{dt} &= \frac{d\nabla_r^i(t)}{dt} + \mu_2^i(t) \end{aligned} \right\} \quad (7.5)$$

with

$$\left. \begin{aligned} E\left\{ \begin{bmatrix} \mu_1^i(t) \\ \mu_2^i(t) \end{bmatrix} \right\} &= \mathbf{0} \\ E\left\{ \begin{bmatrix} \mu_1^i(t) \\ \mu_2^i(t) \end{bmatrix} \begin{bmatrix} \mu_1^i(t) \\ \mu_2^i(t) \end{bmatrix}^* \right\} &= \begin{bmatrix} \sigma_{\mu_1^i}^2(t) & SYM. \\ \sigma_{\mu_2^i \mu_1^i}(t) & \sigma_{\mu_2^i}^2(t) \end{bmatrix} \end{aligned} \right\} \quad (7.6)$$

Usually only the rate of change of DCs is used to account for the unavoidable latency when the corrections are applied at a mobile station [RTCM SC-104 1994]. For reasons of simplicity, let us assume that the second-order time derivative of the DC  $\nabla_r^i(t)$  is a zero-mean white noise with spectral density  $q_{\nabla}$  ( $m^2/s^3$ ). Then we arrive at

$$\begin{aligned} \hat{\nabla}_r^i(t_k) &= \hat{\nabla}_r^i(t_{DC}) + \frac{d\hat{\nabla}_r^i(t_{DC})}{dt}(t_k - t_{DC}) \\ &= \nabla_r^i(t_{DC}) + \mu_1^i(t_{DC}) + \left( \frac{d\nabla_r^i(t_{DC})}{dt} + \mu_2^i(t_{DC}) \right) (t_k - t_{DC}) \\ &= \nabla_r^i(t_{DC}) + \frac{d\nabla_r^i(t_{DC})}{dt}(t_k - t_{DC}) + \mu_1^i(t_{DC}) + \mu_2^i(t_{DC})(t_k - t_{DC}) \\ &= \nabla_r^i(t_k) - w^i(t_k) + \mu_1^i(t_{DC}) + \mu_2^i(t_{DC})(t_k - t_{DC}) \end{aligned} \quad (7.7)$$

with

$$w^i(t_k) = \int_{t_{DC}}^{t_k} \frac{d^2 \nabla_r^i(\tau)}{dt^2} (t_k - \tau) d\tau \sim N\left(0, \frac{q_{\nabla}}{3} (t_k - t_{DC})^3\right) \quad (7.8)$$

$$\begin{aligned} \sigma_{\nabla_r^i}^2(t_k) &= \sigma_w^2(t_k) + \sigma_{\mu_1^i}^2(t_{DC}) + (t_k - t_{DC})^2 \sigma_{\mu_2^i}^2(t_{DC}) + (t_k - t_{DC}) \sigma_{\mu_2^i \mu_1^i}(t_{DC}) \\ &= \frac{q_{\nabla}}{3} (t_k - t_{DC})^3 + \sigma_{\mu_1^i}^2(t_{DC}) + (t_k - t_{DC})^2 \sigma_{\mu_2^i}^2(t_{DC}) + (t_k - t_{DC}) \sigma_{\mu_2^i \mu_1^i}(t_{DC}) \end{aligned} \quad (7.9)$$

In Appendix B, it is shown that the dynamic noise  $w^i(t_k)$  is not correlated with the errors  $\mu_1^i(t_{DC})$  and  $\mu_2^i(t_{DC})$  of the DC estimates.

If we assume that the mobile station is located close to the reference station where the DCs are generated, it follows that





determination of  $c \delta T(t_k)$  and the position parameters contained in  $\rho^i(t_k)$ , when four or more satellites are tracked. To overcome the dependency between the columns related to the last two parameters, which makes it impossible to estimate  $I^i(t_k)$  and  $\lambda_1 N^i$  individually, let us define

$$\bar{I}^i(t_k) = I^i(t_k) + \frac{1}{2} \lambda_1 N^i \quad (7.15)$$

Then (7.14) becomes

$$\begin{bmatrix} P^i(t_k) - c dt^{i^0}(t_k) - \hat{V}_r^i(t_k) \\ \lambda_1 \Phi^i(t_k) - c dt^{i^0}(t_k) - \hat{V}_r^i(t_k) \end{bmatrix} = \begin{bmatrix} 1 & 1 \\ 1 & 1 & -2 \end{bmatrix} \begin{bmatrix} \rho^i(t_k) \\ c \delta T(t_k) \\ \bar{I}^i(t_k) \end{bmatrix} + \begin{bmatrix} e^i(t_k) - \mu^i(t_k) \\ \eta^i(t_k) - \mu^i(t_k) \end{bmatrix} \quad (7.16)$$

In order to estimate the mobile position, linearize the satellite-receiver range  $\rho^i$  as follows

$$\rho^i(t_k) = \rho^{i^0}(t_k) + \sum_{j=1}^3 \frac{\partial \rho^{i^0}(t_k)}{\partial x_j} \Delta x_j(t_k) \quad (7.17)$$

where

$\rho^{i^0}$ : approximate value of  $\rho^i$  computed from the ephemeris data and the approximate position of the mobile station

$\Delta x_j = x_j - x_j^0$

$x_j$ : coordinate of the mobile station in cartesian or geocentric coordinate system ( $j=1,2,3$ )

$x_j^0$ : approximate value of  $x_j$

Inserting (7.17) into (7.16) yields

$$y^i(t_k) = \begin{bmatrix} \frac{\partial \rho^{i^0}(t_k)}{\partial x_1} & \frac{\partial \rho^{i^0}(t_k)}{\partial x_2} & \frac{\partial \rho^{i^0}(t_k)}{\partial x_3} & 1 & 0 \\ \frac{\partial \rho^{i^0}(t_k)}{\partial x_1} & \frac{\partial \rho^{i^0}(t_k)}{\partial x_2} & \frac{\partial \rho^{i^0}(t_k)}{\partial x_3} & 1 & -2 \end{bmatrix} \begin{bmatrix} \Delta x_1(t_k) \\ \Delta x_2(t_k) \\ \Delta x_3(t_k) \\ c \delta T(t_k) \\ \bar{I}^i(t_k) \end{bmatrix} + \begin{bmatrix} e^i(t_k) - \mu^i(t_k) \\ \eta^i(t_k) - \mu^i(t_k) \end{bmatrix} \quad (7.18)$$

where

$$y^i(t_k) = \begin{bmatrix} P^i(t_k) - c dt^{i^0}(t_k) - \hat{V}_r^i(t_k) - \rho^{i^0}(t_k) \\ \lambda_1 \Phi^i(t_k) - c dt^{i^0}(t_k) - \hat{V}_r^i(t_k) - \rho^{i^0}(t_k) \end{bmatrix} \quad (7.19)$$

In most situations, the dynamic behaviour of mobile positions or receiver clock biases is





$$\underbrace{\begin{bmatrix} y^1(t_k) \\ \vdots \\ y^m(t_k) \end{bmatrix}}_{y_k} = \underbrace{\begin{bmatrix} A^1(t_k) & \left| \begin{bmatrix} 0 & 0 \\ -2 & 0 \end{bmatrix} \\ \vdots & \ddots \\ A^m(t_k) & \left| \begin{bmatrix} 0 & 0 \\ -2 & 0 \end{bmatrix} \end{bmatrix}}_{A_k} \underbrace{\begin{bmatrix} \Delta x_1(t_k) \\ \Delta \dot{x}_1(t_k) \\ \Delta x_2(t_k) \\ \Delta \dot{x}_2(t_k) \\ \Delta x_3(t_k) \\ \Delta \dot{x}_3(t_k) \\ c \cdot \delta T(t_k) \\ c \cdot \delta \dot{T}(t_k) \\ \hline \bar{I}^1(t_k) \\ \dot{I}^1(t_k) \\ \vdots \\ \bar{I}^m(t_k) \\ \dot{I}^m(t_k) \end{bmatrix}}_{x_k} + \underbrace{\begin{bmatrix} e^1(t_k) \\ \vdots \\ e^m(t_k) \end{bmatrix}}_{e_k} \quad (7.26)$$

with

$$E\{e_k\} = 0 \quad (7.27)$$

$$E\{e_k e_l^*\} = \delta_{kl} \begin{bmatrix} \left[ \begin{array}{cc} \sigma_e^2 + \sigma_{\hat{v}_r^1}^2(t_k) & SYM. \\ \sigma_{\hat{v}_r^1}^2(t_k) & \sigma_\eta^2 + \sigma_{\hat{v}_r^1}^2(t_k) \end{array} \right] & \dots \\ \dots & \left[ \begin{array}{cc} \sigma_e^2 + \sigma_{\hat{v}_r^m}^2(t_k) & SYM. \\ \sigma_{\hat{v}_r^m}^2(t_k) & \sigma_\eta^2 + \sigma_{\hat{v}_r^m}^2(t_k) \end{array} \right] \end{bmatrix} \quad (7.28)$$

and the full dynamic model reads

$$x_k = \underbrace{\begin{bmatrix} F_k & & & & & \\ & F_k & & & & \\ & & F_k & & & \\ & & & F_k & & \\ & & & & F_k & \\ & & & & & \ddots \\ & & & & & & F_k \end{bmatrix}}_{\Phi_{k,k-1}} x_{k-1} + \underbrace{\begin{bmatrix} \tilde{d}(t_k) \\ \bar{d}(t_k) \\ d^1(t_k) \\ \vdots \\ d^m(t_k) \end{bmatrix}}_{d_k} \quad (7.29)$$

with

$$E\{d_k\} = 0 \quad (7.30)$$

$$E\{d_k d_l^*\} = \delta_{kl} \begin{bmatrix} S_k & & & & & \\ q_x & S_k & & & & \\ & & S_k & & & \\ & & & S_k & & \\ & & & & q_c S_k & \\ & & & & & q_f S_k \\ & & & & & & \ddots \\ & & & & & & & q_f S_k \end{bmatrix} \quad (7.31)$$

For the sake of simplicity, herein the measurement noises are assumed not only to be uncorrelated among observables and epochs but also to have a constant standard deviation. It was shown in Chapter 6, however, that the standard deviation for code observations should better be modelled as a function of satellite elevations.

On the basis of the above dynamic and measurement models, solutions of the state vector can be recursively obtained by using the standard Kalman filter algorithm. The initial values of the filter state vector and their covariance matrix can be determined by solving the first two epochs simultaneously by least squares.

**7.2.2 Discussion**

In the previous sub-section, we derived the carrier adjusted DGPS positioning models based

on the assumptions that L1 code and carrier observations are available and that the dynamic behaviours of both receiver clock biases and mobile positions can be modelled. Although in many cases the assumption on the dynamic behaviours may not be realistic, it may not be a problem in practice. As we know, the spectral density is a measure of the uncertainty of dynamic noises. A large spectral density represents great dynamic noises, i.e., a rather random dynamic behaviour. Whereas a small spectral density represents less dynamic noises, i.e., a quite smooth dynamic behaviour. Therefore, when the dynamic behaviour of mobile positions or receiver clock biases cannot be well modelled, it can be in practice approximately treated as a random process with a very large spectral density. Whereas, when mobile positions are static, their dynamic behaviour can be considered as a random process with a spectral density of zero [Axelrad and Brown 1996]. It can be proved that for a random process with an infinite variance of dynamic noises, its solutions by using a Kalman filter are equivalent to the least-square simultaneous solutions, when there are enough observations at a single epoch. Therefore, the previously derived positioning models can be applied when the dynamic behaviours of receiver clock biases and mobile positions can or cannot well be modelled. In the former case, the models can sufficiently use the dynamic information in the estimation of mobile positions so as to provide recursive solutions of mobile positions. In the latter case, the models can provide single-epoch solutions.

In the derivation of the positioning models, we assumed that the second-order time derivatives of both mobile positions and receiver clock biases are zero-mean white noises. In fact, the assumption can also be others like, for example, the first-order time derivatives of mobile positions and the third-order time derivatives of receiver clock biases are zero-mean white noises. Naturally, in this case the measurement and dynamic models need to be adapted appropriately.

It is probably the most usual situation that DGPS mobile stations are equipped with single frequency receivers. But it is possible that dual frequency data is available at a mobile station. It is shown in Appendix C that in this case the positioning models can be easily adapted.

Since the positioning models directly use code and carrier observations as inputs, the stochastic observation model has a simple structure and can be easily specified. In addition, as long as four or more satellites are tracked, the positioning models always (except for the initial two epochs) have redundancy, even though no dynamic models are introduced for mobile positions and receiver clock biases. Let us look at such a situation that only four satellites are tracked and no dynamic models are introduced for the position and clock bias states. The states to be estimated are the three position components  $\Delta x_j(t_k)$ ,  $j=1, \dots, 3$ , the clock bias  $c \delta T(t_k)$ , the four pairs of satellite related parameters  $\bar{I}^i(t_k)$  (combination of L1 carrier ambiguity and ionospheric delay) and  $\dot{I}^i(t_k)$  (rate of change of ionospheric delays),  $i=1, \dots, 4$ . Therefore, the total number of states is 12. The measurements that are available in this case consist of two types: the four pairs of L1 code and carrier observations  $P^i(t_k)$  and  $\phi^i(t_k)$ ,  $i=1, \dots, 4$ ; and the four pairs of predicted observations  $\bar{I}^i(t_k|t_{k-1})$  and  $\dot{I}^i(t_k|t_{k-1})$ ,  $i=1, \dots, 4$ . Therefore, the total number of measurements is 16. Thus the redundancy is 4. Note that the predicted observations result from the modelling of the dynamic behaviour of ionospheric delays and the constant property of the carrier ambiguity. Concerning the modelling of ionospheric delays, it was shown in Chapter 5 that the modelling accuracy could be within

a few millimetres. As can be easily seen, the redundancy is actually identical to the number of tracked satellites multiplied by the number of carrier observables, no matter dynamic models are introduced for mobile positions and receiver clock biases or not.

Another important property of the carrier adjusted positioning models is that they are easy to integrate with the DIA quality control procedure as shown in Sections 2.2 and 4.2 so that the quality of position estimates can be assured with a certain probability. Since the positioning models always have redundancy unless the position parameters are not estimable, the quality control procedure can even be performed when only four satellites are tracked. With respect to the performance of quality control at DGPS mobile stations, more investigations need to be conducted in the future.

Note that the approach used in the previous derivation to solve the problem that the ionospheric delay  $I^i(t_k)$  and the L1 carrier ambiguity  $\lambda_1 N^i$  are not individually estimable is to combine them into a new state (see (7.15)). In fact the problem can also be solved by estimating the change of  $I^i(t_k)$  with respect to  $I^i(t_0)$  and a combination of  $\lambda_1 N^i$  and  $I^i(t_0)$ . From a theoretical point of view, the latter should be used since the solutions based on the former are only sub-optimal [Hwang and Brown 1990]. But the former has the advantage that it reduces the order of the filter (one state per satellite) and consequently saves computational time and memory. Since most DGPS users may need real-time solutions by the use of only personal computers, the compromise on the optimality was assumed necessary in the derivation of the positioning models.

### 7.3 DGPS positioning experiments

#### 7.3.1 Data description and choices of a priori parameters

The GPS data used in this chapter was collected at two known stations: DE18 in Delft and KO25 in Kootwijk, The Netherlands, on 7 June 1995. At the DE18 station a Trimble 4000 SSE receiver was used, whereas at the KO25 station a TurboRogue SNR-8000 receiver was used. The data collection lasted one hour from 8:00 to 9:00 UTC and the sampling interval was one second. During the data collection, the cut-off angle was  $10^\circ$  at the two stations and there were seven to eight satellites in view. Figure 7.1 pictures the information on the number of visible satellites and DOP values versus time. It was found that during the data collection, both AS and SA were active. Since under AS condition P1 and P2 codes are encrypted, the types of observables available in the RINEX data were C1 (i.e. C/A) code, L1 and L2 carriers, and C2 code. The distance between the two stations is about 100 kilometres.

The DE18 station was chosen as a reference station and the KO25 station as a mobile station. The Trimble 4000 SSE data collected at the reference station was processed by using the algorithm for carrier adjusted DCs. The TurboRogue SNR-8000 data collected at the mobile station was processed by using the algorithm derived in the previous section. In order to see the positioning accuracy in the worst case that a DGPS user is in random dynamic conditions, we computed the single-epoch positioning accuracy by assuming that the dynamic behaviours

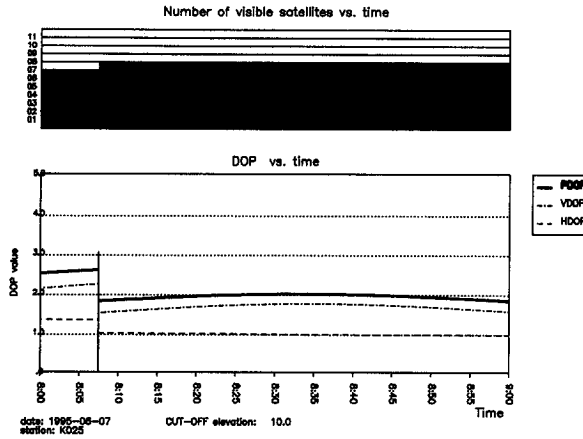


**Figure 7.1:** Number of visible satellites and PDOP, VDOP and HDOP values at the KO25 station.

of both mobile positions and receiver clock biases could not be modelled. The latency between computing the DCs and applying them was chosen to be five seconds. In addition, to investigate the importance of choosing an elevation-dependent standard deviation for code observations, the processing was carried out twice with the two sets of a priori parameters given in Table 7.1.

Set 1		Set 2	
Reference	Mobile	Reference	Mobile
$\sigma_e = 0.12 + 1.3 e^{-El/18}$ m	$\sigma_e = 0.3 + 1.0 e^{-El/14}$ m	$\sigma_e = 0.3$ m	$\sigma_e = 0.5$ m
$\sigma_\eta = 0.003$ m	$\sigma_\eta = 0.003$ m	$\sigma_\eta = 0.003$ m	$\sigma_\eta = 0.003$ m
$\sigma_{\bar{\eta}} = 0.003$ m	$\sigma_{\bar{\eta}} = 0.003$ m	$\sigma_{\bar{\eta}} = 0.003$ m	$\sigma_{\bar{\eta}} = 0.003$ m
$\sigma_{\bar{e}} = 0.15 + 1.3 e^{-El/18}$ m	$\sigma_{\bar{e}} = 0.5 + 1.0 e^{-El/14}$ m	$\sigma_{\bar{e}} = 0.5$ m	$\sigma_{\bar{e}} = 0.8$ m
$q_{\bar{f}} = 10^{-8}$ m <sup>2</sup> /s <sup>3</sup>	$q_{\bar{f}} = 10^{-8}$ m <sup>2</sup> /s <sup>3</sup>	$q_{\bar{f}} = 10^{-8}$ m <sup>2</sup> /s <sup>3</sup>	$q_{\bar{f}} = 10^{-8}$ m <sup>2</sup> /s <sup>3</sup>
$q_{\bar{s}} = 10^{-2}$ m <sup>2</sup> /s <sup>5</sup>	$q_{\bar{c}} = 10^4$ m <sup>2</sup> /s	$q_{\bar{s}} = 10^{-2}$ m <sup>2</sup> /s <sup>5</sup>	$q_{\bar{c}} = 10^4$ m <sup>2</sup> /s
$q_{\bar{b}} = 10^{-3}$ m <sup>2</sup> /s <sup>3</sup>	$q_{\bar{x}} = 10^4$ m <sup>2</sup> /s	$q_{\bar{b}} = 10^{-3}$ m <sup>2</sup> /s <sup>3</sup>	$q_{\bar{x}} = 10^4$ m <sup>2</sup> /s

*El*: satellite elevation

**Table 7.1:** Two sets of a priori parameters used in DGPS positioning experiments.

Note that the only difference between these two sets of a priori parameters is that at both reference and mobile stations, set 1 accounts for the information of satellite elevation in the standard deviation of code observations, whereas set 2 does not. In addition, it is worth mentioning that [Ashkenazi et al. 1994] reported the similar work to account for the satellite



elevation information in DGPS positioning, but no details can be found in the reference.

### 7.3.2 Numerical results and discussion

Based on different types of observables used at the reference and mobile stations, Table 7.2 shows the RMS errors of DGPS positioning experiments in north, east, and height components by using set 1 of a priori parameters. As an example, Figures 7.2 to 7.4 show the typical behaviour of the positioning errors in north, east and height components based on three observables (i.e. L1 code and L1 as well as L2 carrier) at the reference station and only one observable (i.e. L1 code) at the mobile station.

As can be seen from Table 7.2, the improvement of the positioning accuracy by using carrier observations along with L1 code observations is evident. For example, when three observables were used at the reference station, the RMS error in the position component was 0.912 metres in the case of only one observable used at the mobile station, and it decreased to 0.738 metres

			Number of observables used at reference station			
			1	2	3	4
Number of observables used at mobile station	1	north	0.833 m	0.588 m	0.441 m	0.443 m
		east	0.489 m	0.329 m	0.259 m	0.258 m
		height	1.279 m	0.900 m	0.755 m	0.753 m
		position	1.603 m	1.124 m	0.912 m	0.911 m
	2	north	0.778 m	0.506 m	0.335 m	0.337 m
		east	0.454 m	0.262 m	0.180 m	0.179 m
		height	1.207 m	0.793 m	0.632 m	0.629 m
		position	1.506 m	0.976 m	0.738 m	0.736 m
	3	north	0.754 m	0.481 m	0.237 m	0.238 m
		east	0.438 m	0.228 m	0.107 m	0.106 m
		height	1.153 m	0.687 m	0.425 m	0.422 m
		position	1.446 m	0.869 m	0.498 m	0.496 m
	4	north	0.754 m	0.481 m	0.237 m	0.238 m
		east	0.438 m	0.228 m	0.107 m	0.106 m
		height	1.153 m	0.687 m	0.425 m	0.422 m
		position	1.446 m	0.869 m	0.498 m	0.496 m

**Table 7.2:** RMS errors of DGPS positioning experiments with an elevation-dependent standard deviation for code observations.

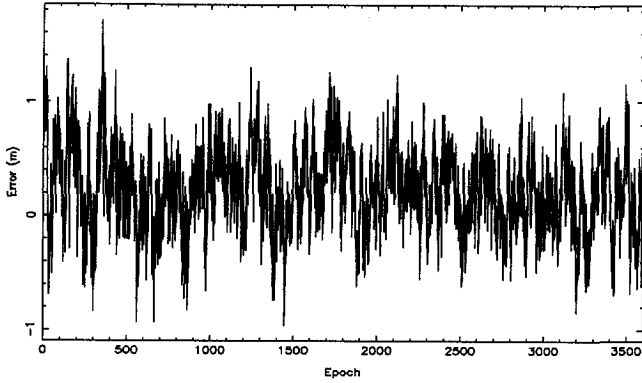


**Figure 7.2:** DGPS positioning errors in the north component.

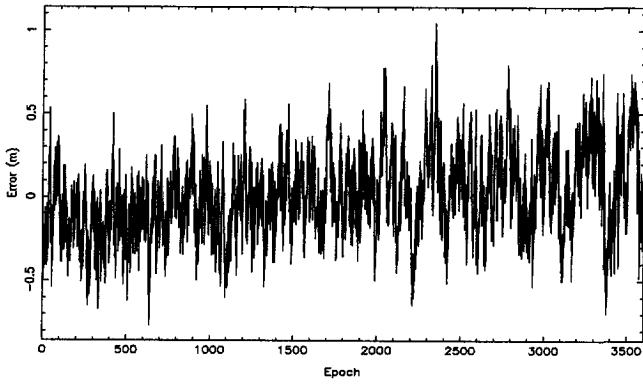


**Figure 7.3:** DGPS positioning errors in the east component.

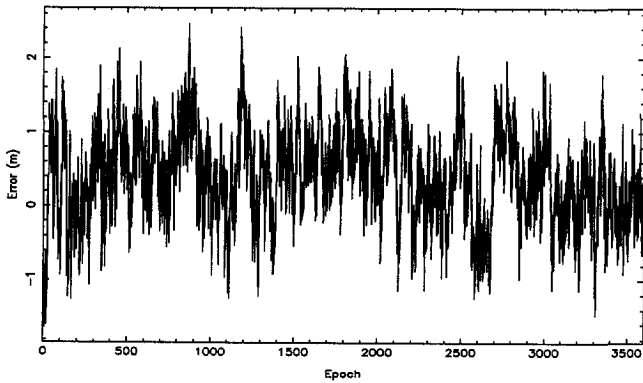


**Figure 7.4:** DGPS positioning errors in the height component.

in the case of two observables (i.e. L1 code and carrier) used at the mobile station. Moreover, the use of carrier observations is more important at the reference station than at the mobile station. For instance, the RMS error in the position component was 1.506 metres when one observable was used at the reference station and two observables at the mobile station, whereas it was improved to 1.124 metres when two observables were used at the reference station and one observable at the mobile station. The reason for these phenomena is that when only L1 code observations were used at the reference station, code noises had great influences on the estimates of both DCs and correction rates. When such noisy estimates were applied at the mobile station, the noises were propagated to the corrected code and carrier observations. This then made the positioning errors include noises in code observations collected at reference and mobile stations. Whereas when carrier observations were used at the reference station, carrier observations played much greater roles than code observations in the generation of DCs, since the former are much more precise than the latter. In this case, the estimates of DCs and particular correction rates were much less noisy. When these estimates were applied at the mobile station, the corrected observations were actually not affected by code noises from the reference station. This then made the positioning errors be less or much less than those in the previous case. In short, in the case of carrier observations used at the mobile station, the positioning errors mainly resulted from code noises at both reference and mobile stations. Whereas, in the case of carrier observations used at the reference station, the positioning errors mainly resulted from code noises at only the mobile station. Therefore, using carrier observations is more important in the generation of DCs than in the estimation of mobile positions.

Additionally, we can also see from Table 7.2 that the RMS error related to four observables (i.e. L1 and L2 code and carrier) used at the mobile or reference station is either identical or very close to its corresponding one related to three observables used at the same station. This means that the use of L2 code observations along with L1 code and L1 as well as L2 carrier observations at the reference or mobile station cannot make real contributions to the positioning accuracy. As we know, when very precise L1 and L2 carrier observations are used, the estimated parameters (e.g. DC or mobile position) obtain much greater contributions from the carrier observations than from code observations. Therefore, when L1 and L2 carrier observations have already been used along with L1 code observations, adding L2 code observations at the reference or mobile station cannot really improve the positioning accuracy.

Furthermore, Table 7.2 shows that the use of different types of receivers at reference and mobile stations may not be a problem in DGPS positioning applications, since the positioning accuracies in all cases concerned were better than two metres, which were based on the use of a Trimble 4000 SSE receiver at the reference station and the use of a TurboRogue SNR-8000 receiver at the mobile station.

Table 7.3 gives the RMS errors of DGPS positioning experiments by using set 2 of a priori parameters. After comparisons of this table with Table 7.2, it can be seen that when single-frequency data (i.e. L1 code alone or along with carrier) was used at the reference or mobile station, choosing an elevation-dependent standard deviation for code observations can clearly improve the positioning accuracy, particularly in the height component. Table 7.4 shows the difference between the RMS errors in the position component by using sets 1 and 2 of a

			Number of observables used at reference station			
			1	2	3	4
Number of observables used at mobile station	1	north	0.931 m	0.611 m	0.445 m	0.446 m
		east	0.574 m	0.358 m	0.271 m	0.271 m
		height	1.536 m	1.038 m	0.836 m	0.835 m
		position	1.886 m	1.257 m	0.985 m	0.985 m
	2	north	0.880 m	0.520 m	0.332 m	0.333 m
		east	0.537 m	0.284 m	0.168 m	0.168 m
		height	1.465 m	0.910 m	0.695 m	0.692 m
		position	1.791 m	1.077 m	0.788 m	0.786 m
	3	north	0.853 m	0.490 m	0.220 m	0.220 m
		east	0.515 m	0.239 m	0.081 m	0.081 m
		height	1.391 m	0.773 m	0.429 m	0.427 m
		position	1.711 m	0.946 m	0.489 m	0.487 m
	4	north	0.853 m	0.490 m	0.220 m	0.220 m
		east	0.515 m	0.237 m	0.081 m	0.081 m
		height	1.391 m	0.773 m	0.428 m	0.427 m
		position	1.711 m	0.945 m	0.488 m	0.487 m

**Table 7.3:** RMS errors of DGPS positioning experiments with a constant standard deviation for code observations.

		# of observables used at reference station			
		1	2	3	4
# of obser. used at mobile station	1	0.283 m	0.133 m	0.073 m	0.074 m
	2	0.285 m	0.101 m	0.050 m	0.050 m
	3	0.265 m	0.077 m	-0.009 m	-0.009 m
	4	0.265 m	0.076 m	-0.009 m	-0.009 m

**Table 7.4:** Improvement of DGPS positioning accuracy by choosing an elevation-dependent standard deviation for code observations.

priori parameters. As can be seen from this table, when only one observable was used at the reference station, it was particularly important to choose an elevation-dependent standard deviation for code observations, no matter how many number of observables were used at the mobile station. When using more and more types of carrier observables at the reference station, the improvement of the accuracy by choosing an elevation-dependent standard deviation for code observations became smaller and smaller. When the types of observables used at both reference and mobile stations included L1 and L2 carriers, choosing an elevation-dependent standard deviation for code observations could not improve the positioning accuracy any more. Again, this is because code observations could not play an important role in the estimation of the position parameters and therefore precisely choosing the standard deviation for code observations became less important.

Note that the improvement of the positioning accuracy by choosing an elevation-dependent standard deviation for code observations may vary with many factors, for example, the number of satellites at low elevations, the quality of the receivers, the observation environment, and the number of carrier observables in uses. In our DGPS positioning experiments the greatest improvement we found was about three decimeters. In some cases it may be greater.

By using three observables at the reference station and only one observable at the mobile station, Figures 7.5 and 7.6 illustrate the DGPS positioning precision obtained from the covariance matrix in north, east and height components. Figure 7.5 was based on set 1 of a priori parameters, whereas Figure 7.6 was based on set 2 of a priori parameters. The sudden jump of the precision at about epoch 500 was because of a rising satellite, whereas those after epoch 2500 were because the tracking of a satellite at low elevation stopped and then started again at the reference station. In other words, the sudden changes of the precision after epoch 2500 resulted from the quality of DCs instead of some reasons related to the mobile station.

By comparing Figures 7.5 and 7.6 as well as the RMS errors given in Tables 7.2 and 7.3, a number of properties of the precision can be stated. First of all, when a satellite rises, the change of the precision based on an elevation-dependent standard deviation for code observations is less than that based on a constant standard deviation for code observations. For example, the changes of the precision at about epoch 500 due to a rising satellite were about 7, 3 and 18 centimetres in north, east and height components respectively, when set 1 of a priori parameters were used, whereas they increased to 14, 11 and 40 centimetres, when set 2 of a priori parameters were used. The reason of this phenomenon is that a rising or setting satellite is always at very low elevation and it can, therefore, only make less or much less contributions to the precision than other satellites, when an elevation-dependent standard deviation for code observations is used. Whereas when a constant standard deviation for code observations is used, a rising or setting satellite can make the same contributions to the precision as other satellites. Thus, choosing an elevation-dependent standard deviation for code observations can make the precision more insensitive to the sudden change of constellation geometry caused by rising and setting satellites.

Secondly, the precision based on an elevation-dependent standard deviation for code observations, particularly in the height component, is clearly better than that based on a

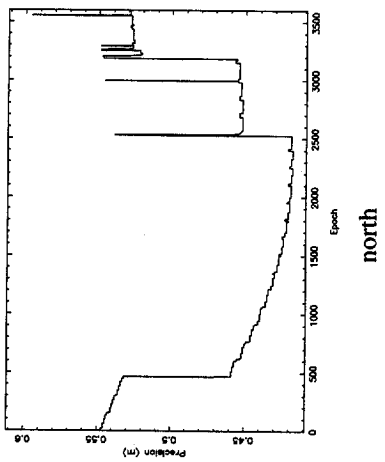


**Figure 7.5:** DGPS positioning precision in north, east and height components with an elevation-dependent standard deviation for code observations.

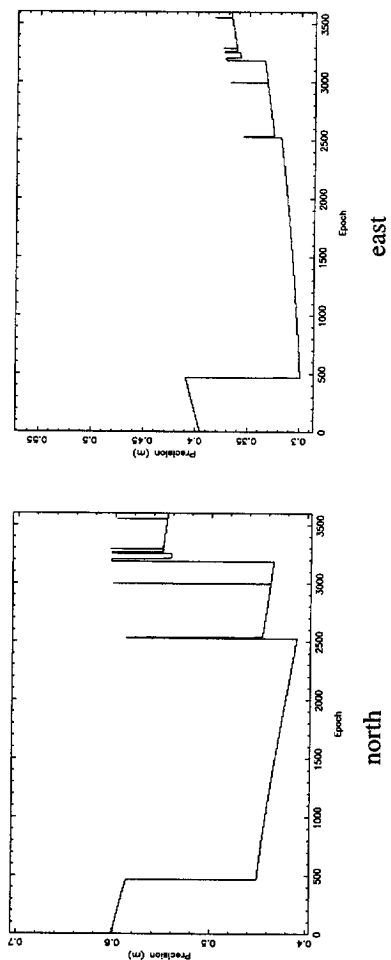


**Figure 7.6:** DGPS positioning precision in north, east and height components with a constant standard deviation for code observations.

constant standard deviation for code observations. Let us take the precision at the middle epoch of the whole observation period (i.e. epoch 1800) as an example. In Figure 7.5, the precision in north, east and height components are 0.42, 0.29 and 0.77 metres respectively. While in Figure 7.6, they are 0.43, 0.31 and 0.94 meters respectively. Obviously, the difference in the height component is greater than those in the horizontal components. This is consistent with the conclusions obtained in the previous analysis of the RMS errors in Tables 7.2 and 7.3.

Thirdly, the precision based on an elevation-dependent or constant standard deviation for code observations is in general quite consistent with the RMS errors (i.e. the accuracy), but the consistency in the former case is still better than that in the latter case. Strictly speaking, it is hard to compare the RMS error in Table 7.2 or 7.3 with the precision in Figure 7.5 or 7.6, because the RMS error is a measure of the positioning accuracy concerned with the whole observation period, whereas the precision describes the accuracy at a particular epoch. It may be, however, acceptable to choose the precision at the middle epoch as the average precision over the whole observation period, so that we can compare the RMS error with the precision. Based on sets 1 and 2 of a priori parameters, Table 7.5 shows the RMS errors, the precision at epoch 1800 and their differences in such a typical positioning case that three observables were used at the reference station and only one observable was used at the mobile station. As can be seen from the table, when set 1 of a priori parameters was used, the difference between the RMS error and the precision in each of the north, east and height components was really small. Whereas when set 2 of a priori parameters was used, the difference in the height component increased. This means that when an elevation-dependent standard deviation for code observations was used, the precision more precisely reflected the accuracy than when a constant standard deviation for code observations was used.

Set	Component	RMS error (m)	Precision (m)	Difference (m)
1	North	0.44	0.42	0.02
	East	0.26	0.29	-0.03
	Height	0.76	0.77	-0.01
2	North	0.45	0.43	0.02
	East	0.27	0.31	-0.04
	Height	0.84	0.94	-0.10

**Table 7.5:** Difference between the RMS error and the precision in the use of an elevation-dependent or a constant standard deviation for code observations.

## 7.4 Concluding remarks

We have developed the algorithm for carrier adjusted DGPS positioning. This algorithm can be applied by a DGPS user when code as well as carrier observations are available. Since the algorithm directly uses code and carrier observations in the measurement model of a Kalman

filter, the stochastic model of observations has a simple structure and can be easily specified. The algorithm always has, except for the initialization of the filter, redundancy as long as four or more satellites are tracked. Therefore, it can integrate well with the DIA quality control procedure so as to guarantee the quality of position estimates with a certain probability. The algorithm can take into account the dynamic behaviour of mobile positions and that of receiver clock biases. When the dynamic behaviour of mobile positions can be modelled, the algorithm can provide recursive solutions for the positions. When the behaviour cannot be modelled, it can provide instantaneous solutions.

By using the algorithm and real GPS data collected at a 100-km baseline, some DGPS positioning experiments have been conducted. In general, using carrier observations along with code observations at the reference or mobile station can indeed improve the DGPS positioning accuracy. But using carrier observations is more important at the reference station than at the mobile station. The greater the number of carrier observables used in generating DCs, the more significant the improvement of the positioning accuracy. Note that this does not mean the greater the number of observables, the better the accuracy, because adding L2 code observations to L1 code and L1 as well as L2 carrier observations at the reference or mobile station will not actually improve the positioning accuracy.

It is important to account for the satellite elevation in choosing the standard deviation of code observations, particularly when code observations make important contributions in the estimation of unknown parameters. It has been shown that choosing an elevation-dependent standard deviation for code observations can improve the DGPS positioning accuracy. The improvement is related to the number of carrier observables used at reference and mobile stations. When only code observations were available at the reference station, the improvement was the most significant. When L1 code and L1 as well as L2 carrier observations were available in both reference and mobile stations, choosing an elevation-dependent standard deviation for code observations is less important.

For a 100-km baseline with a PDOP value of about 2, half-metre single epoch positioning accuracy was achieved, when L1 code and L1 as well as L2 carrier observations were used at both reference and mobile stations. When the observations used at the mobile station were replaced by L1 code and carrier, the positioning accuracy was better than 7.5 decimeters.



## Chapter 8

# Reduction of GPS observation biases by using a local DGPS network

### 8.1 Introduction

In the previous chapters, we mainly investigated how to design a local DGPS positioning system from the points of generating DCs at a DGPS reference station and computing mobile positions at user sites. The operation of local DGPS positioning systems is based on the basic premise that the primary error sources of the system are spatially correlated. By the use of such a system, one needs only one reference station, but the user distance to the station is usually limited to be within a few hundred kilometres, if metre-level positioning accuracy is required [NATO 1991a]. With increasing distances, the positioning accuracy will deteriorate, because the effect of ephemeris errors and atmospheric (ionospheric and tropospheric) delays at a user site cannot be sufficiently reduced by using the DCs computed at the reference station.

Investigations have shown that using a network of DGPS reference stations is an economic and efficient way to overcome the spatial decorrelation of DCs. From the standpoint of algorithms, there are two basic types of networks [Loomis et al. 1991]. The simpler type is the local (or say, common view) network (see, e.g., [Tang et al. 1989] and [Mueller 1994a]); and the more complex type is the wide area network (see, e.g., [Brown 1989], [Kee et al. 1991] and [Ashkenazi et al. 1993]). The algorithms used in these two types of networks are sometimes referred to as measurement domain algorithms and state-space domain algorithms, respectively [Mueller 1994b]. In addition to the difference in algorithms, these two types of networks are also different in many other aspects such as the size of the network, the communication link, and the type of corrections [Loomis et al. 1991]. Both local and wide-area DGPS networks have advantages and disadvantages.

Many field tests and analyses of the positioning accuracy by using DGPS or a DGPS network have been conducted under various conditions (see, e.g. [McNally et al. 1991], [Clynych et al. 1992], [de Cevins and Ponsot 1995], [Lachapelle et al. 1995]). But most of them have a common property that the analyses were conducted in state (for example, position parameters  $x$ ,  $y$ , and  $z$ ) domain. One advantage of the analyses is that they can directly address the issue with which we are most concerned, i.e., positioning accuracy. But the result of the analyses is highly depended on a certain satellite constellation and consequently the conclusions of the analyses are generally only applicable for a particular constellation. In addition, since the analyses are based on positioning errors, which are functions of a combination of all error sources, it is usually hard to show the main error source of the positioning errors in certain

situations.

This chapter focuses on the subject of local DGPS networks. We will first in Section 8.2 discuss the computation of DC vectors. Next, we will individually analyse how well the effect of ephemeris errors, ionospheric delays, and tropospheric delays at a user station can be reduced by using the correction vector. Finally, we will quantitatively give some concluding remarks.

## 8.2 Computation of differential correction vectors

Assume that at  $n_r$  reference stations  $n^s$  satellites have been simultaneously observed and the DC  $\nabla_j^i$  ( $i=1, \dots, n^s$ ;  $j=1, \dots, n_r$ ) and its rate of change as well as its acceleration (i.e., the second-order time derivative of DCs) have been computed at each of these reference stations. By means of a communication link, all the DCs are transmitted to a master station, which can be one of the  $n_r$  reference stations, for instance, station 1. Since a DC is related to its position, it can be expressed as

$$\nabla_j^i = \nabla_1^i + \frac{\partial \nabla_1^i}{\partial x} (x_j - x_1) + \frac{\partial \nabla_1^i}{\partial y} (y_j - y_1) + \frac{\partial \nabla_1^i}{\partial z} (z_j - z_1) + \dots \quad (8.1)$$

where  $x$ ,  $y$  and  $z$  are coordinates in the WGS 84 system or in a local coordinate system. Assume that the area occupied by the  $n_r$  reference stations is so large that the first-order derivatives of a DC with respect to  $x$ ,  $y$ , and  $z$  should be accounted for but the second as well as higher order derivatives of a DC with respect to  $x$ ,  $y$ , and  $z$  are negligible, for a certain positioning accuracy. Let us define

$$a^i = \frac{\partial \nabla_1^i}{\partial x}, \quad b^i = \frac{\partial \nabla_1^i}{\partial y}, \quad c^i = \frac{\partial \nabla_1^i}{\partial z} \quad (8.2)$$

It follows from (8.1) that for a DGPS network with four reference stations, we have

$$\begin{bmatrix} \nabla_2^i - \nabla_1^i \\ \nabla_3^i - \nabla_1^i \\ \nabla_4^i - \nabla_1^i \end{bmatrix} = \begin{bmatrix} \Delta x_2 & \Delta y_2 & \Delta z_2 \\ \Delta x_3 & \Delta y_3 & \Delta z_3 \\ \Delta x_4 & \Delta y_4 & \Delta z_4 \end{bmatrix} \begin{bmatrix} a^i \\ b^i \\ c^i \end{bmatrix} \quad (8.3)$$

or

$$\begin{bmatrix} a^i \\ b^i \\ c^i \end{bmatrix} = \begin{bmatrix} \Delta x_2 & \Delta y_2 & \Delta z_2 \\ \Delta x_3 & \Delta y_3 & \Delta z_3 \\ \Delta x_4 & \Delta y_4 & \Delta z_4 \end{bmatrix}^{-1} \begin{bmatrix} \nabla_2^i - \nabla_1^i \\ \nabla_3^i - \nabla_1^i \\ \nabla_4^i - \nabla_1^i \end{bmatrix} \quad (8.4)$$

where  $\Delta x_j = x_j - x_1$ ,  $\Delta y_j = y_j - y_1$  and  $\Delta z_j = z_j - z_1$ .

An appropriate DC vector concerning satellite  $i$  reads

$$\left( \nabla_1^i \quad \dot{\nabla}_1^i \quad a^i \quad b^i \quad c^i \right)^* \quad (8.5)$$

Some remarks should be made. First,  $a^i$ ,  $b^i$  and  $c^i$  are the gradients of a DC with respect to  $x$ ,  $y$ , and  $z$ , respectively, and they are coefficients of a hyper (3 dimensional) plane which is fitted to DCs in the area. Second, the difference in DCs between reference stations  $j$  and 1 for a particular satellite does not include the satellite clock bias. It is, therefore, only a function of the differences of ephemeris errors, tropospheric delays, ionospheric delays, and receiver clock biases between these two stations, so are  $a^i$ ,  $b^i$  and  $c^i$ . Third, the difference of receiver clock biases included in  $(\nabla_j^i - \nabla_1^i)$  has the same effect on  $a^i$ ,  $b^i$  and  $c^i$ ,  $i=1, \dots, n^i$ , for all satellites, thus it will only result in a bias in the estimate of the receiver clock bias of a user, after they have been applied at the user site. It will not affect the estimate of user positions. Fourth, since ephemeris errors and atmospheric (including tropospheric and ionospheric) delays are generally very stable for a period of a few seconds, which is the usual interval used to generate DCs, and since any prediction errors of receiver clock biases in DCs have no effect on the estimate of user position, the rates of changes of the coefficients  $a^i$ ,  $b^i$  and  $c^i$  are not necessarily computed and transmitted along with them. Fifth, the number of reference stations can be less than four and it depends on the number of the gradients which need to be taken into account at the considered area. For example, when the area is so small that the effect of ephemeris errors, tropospheric delays, and ionospheric delays can be regarded as quantities independent of user locations, one reference station is sufficient. When the area is a quite long and narrow zone, one may only need to consider a one-dimensional effect on the DC. Therefore the number of reference stations can be two. For a rather large but flat area, one may need three reference stations so that the variation of DCs in north and east components can be accounted for. Sixth, the above DGPS network design is based on the essential assumption that the second and higher order derivatives of a DC with respect to  $x$ ,  $y$ , and  $z$  are negligible, thus the area covered by the reference stations should not be too large. Finally, it can be shown that the above algorithm for DC vectors is equivalent to the algorithm given in [Loomis et al. 1991].

Apparently, within a certain area and a certain required positioning accuracy, one can always assume that DCs vary linearly with positions. But one may immediately wonder for how large area how well the effect of ephemeris errors and atmospheric delays can be reduced by using the DC vector and how much improvement one can expect by using multiple reference stations instead of only one reference station.

### 8.3 Reduction of effect of ephemeris errors in a local DGPS network

Consider the situation (see Figure 8.1) that a satellite  $S$  at location  $S_{true}$  is believed to be at location  $S_{assumed}$  and a user station is apart from a reference station at distance  $\delta$ . Beser and Parkinson (1982) derived the following upper bound for the correction error introduced by using, at the user station, the DC calculated at the reference station

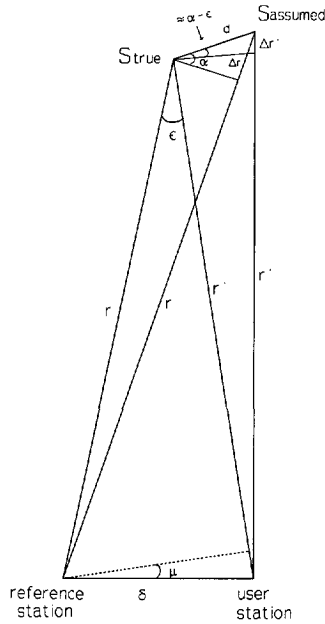


**Figure 8.1:** The effect of satellite orbit error on reference and user stations, after [Beser and Parkinson 1982].

$$|e| \leq \frac{d\delta}{r} \cos\alpha \tag{8.6}$$

with

$$e = \Delta r - \Delta r' \tag{8.7}$$

or

$$|e| \leq \frac{d}{r} \delta \tag{8.8}$$

for  $\alpha=0$ , i.e., the ephemeris error  $d$  is an along or cross track offset.

In the following, we give a similar upper bound for the correction error in the case of a DGPS network. We assume that in the DGPS network area, the effect of height differences on DCs is negligible and that only those, due to horizontal differences in east and/or north component, denoted by  $x$  and  $y$  respectively, have to be accounted for. Therefore, we only

need three reference stations to determine the coefficients  $a^i$  and  $b^i$  for a linear function fitted to DCs in this area.

It follows from

$$\begin{bmatrix} a \\ b \end{bmatrix} = \begin{bmatrix} \Delta x_2 & \Delta y_2 \\ \Delta x_3 & \Delta y_3 \end{bmatrix}^{-1} \begin{bmatrix} \nabla_2 - \nabla_1 \\ \nabla_3 - \nabla_1 \end{bmatrix} \quad (8.9)$$

that the DC applied by a user located at  $(x_j, y_j)$  reads

$$\begin{aligned} \hat{\nabla}_j &= \nabla_1 + [\Delta x_j \ \Delta y_j] \begin{bmatrix} a \\ b \end{bmatrix} \\ &= \nabla_1 + [\Delta x_j \ \Delta y_j] \begin{bmatrix} \Delta x_2 & \Delta y_2 \\ \Delta x_3 & \Delta y_3 \end{bmatrix}^{-1} \begin{bmatrix} \nabla_2 - \nabla_1 \\ \nabla_3 - \nabla_1 \end{bmatrix} \end{aligned} \quad (8.10)$$

Note that the superscript  $i$  standing for the satellite is omitted here and below.

Obviously, its error reads

$$\hat{\nabla}_j - \nabla_j = -(\nabla_j - \nabla_1) + [\Delta x_j \ \Delta y_j] \begin{bmatrix} \Delta x_2 & \Delta y_2 \\ \Delta x_3 & \Delta y_3 \end{bmatrix}^{-1} \begin{bmatrix} \nabla_2 - \nabla_1 \\ \nabla_3 - \nabla_1 \end{bmatrix} \quad (8.11)$$

The DC error  $\hat{\nabla}_j - \nabla_j$  results from four sources: the error of estimated effect of ephemeris errors, that of estimated ionospheric delays, that of estimated tropospheric delays, and a combination of receiver clock biases at all reference stations and the user station. Again since the last error source in  $\hat{\nabla}_j - \nabla_j$  has no effect on the estimates of user positions, we are only concerned with the error sizes of the remaining three sources. Note that the second term on the right-hand side of (8.11) is the contribution of reference stations 2 and 3 and it plays the role to compensate the spatial decorrelation of DCs. In the case of local DGPS positioning, only one reference station is used and therefore there is only the first term on the right-hand side of (8.11).

To see the error size of the estimated effect of ephemeris errors at a user station by using a DC vector, replacing DC  $\nabla_j$  in the above equation by ranging error  $\Delta r_j$  gives

$$\Delta \hat{r}_j - \Delta r_j = -(\Delta r_j - \Delta r_1) + [\Delta x_j \ \Delta y_j] \begin{bmatrix} \Delta x_2 & \Delta y_2 \\ \Delta x_3 & \Delta y_3 \end{bmatrix}^{-1} \begin{bmatrix} \Delta r_2 - \Delta r_1 \\ \Delta r_3 - \Delta r_1 \end{bmatrix} \quad (8.12)$$

As is shown in [Jin and de Jong 1996b]

$$\Delta r_j - \Delta r_1 \approx \frac{d \cos \alpha_1}{r_1} \delta_{1,j} \cos \mu_{1,j} \tag{8.13}$$

where  $\delta_{1,j}$  is the distance between reference station 1 and user station  $j$  and  $\mu_{1,j}$  the angle between the line from reference station 1 to user station  $j$  and the line which is orthogonal to the line from user station  $j$  to the satellite. Thus, we arrive at

$$\Delta \hat{r}_j - \Delta r_j \approx \frac{d \cos \alpha_1}{r_1} \left\{ -\delta_{1,j} \cos \mu_{1,j} + [\Delta x_j \ \Delta y_j] \begin{bmatrix} \Delta x_2 & \Delta y_2 \\ \Delta x_3 & \Delta y_3 \end{bmatrix}^{-1} \begin{bmatrix} \delta_{1,2} \cos \mu_{1,2} \\ \delta_{1,3} \cos \mu_{1,3} \end{bmatrix} \right\} \tag{8.14}$$

As is shown in Appendix D.1,  $\mu_{1,j}$  can be expressed as a function of satellite elevation and the horizontal angle of the line from station  $j$  to the satellite with respect to the line from station 1 to station  $j$ . Appendix D.2 proves that when the satellite elevation is zero, the error  $\Delta \hat{r}_j - \Delta r_j$  is zero. For reasons of simplicity, we analyse the error size in the case of 90° satellite elevation. Since in this case  $\cos \mu \approx 1$ , (8.14) becomes

$$\Delta \hat{r}_j - \Delta r_j \approx \frac{d \cos \alpha_1}{r_1} \left\{ -\delta_{1,j} + [\Delta x_j \ \Delta y_j] \begin{bmatrix} \Delta x_2 & \Delta y_2 \\ \Delta x_3 & \Delta y_3 \end{bmatrix}^{-1} \begin{bmatrix} \delta_{1,2} \\ \delta_{1,3} \end{bmatrix} \right\} \tag{8.15}$$

or

$$|\Delta \hat{r}_j - \Delta r_j| \leq \frac{d}{r_1} \left| -\delta_{1,j} + [\Delta x_j \ \Delta y_j] \begin{bmatrix} \Delta x_2 & \Delta y_2 \\ \Delta x_3 & \Delta y_3 \end{bmatrix}^{-1} \begin{bmatrix} \delta_{1,2} \\ \delta_{1,3} \end{bmatrix} \right| \tag{8.16}$$

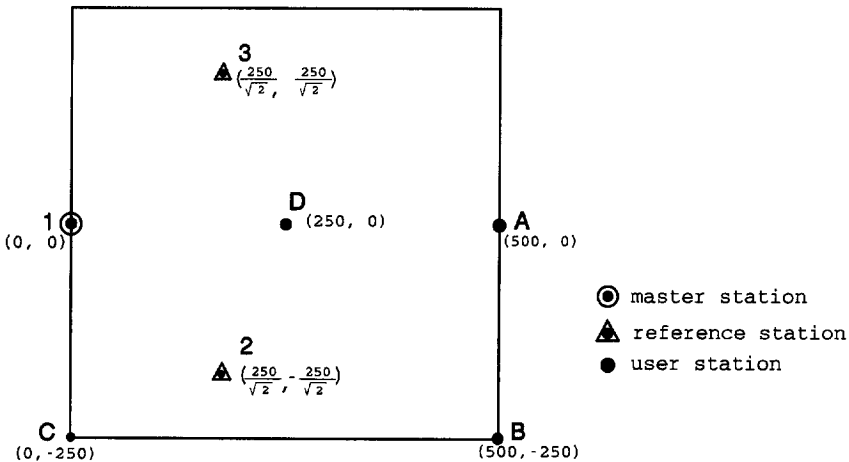


Figure 8.2: A simulated 500x500 km<sup>2</sup> DGPS network with three reference stations.

Let us simulate a  $500 \times 500 \text{ km}^2$  DGPS network with three reference stations as shown in Figure 8.2 (note that it may not be the best design). Note that  $r_1$  is approximately  $2 \cdot 10^4$  km and assume that the ephemeris error  $d$  is in the worst direction (along track or cross track). The maximum remaining effect of ephemeris errors at some user stations of the DGPS network are given in Table 8.1.

Station	Remaining error
A	$0.01d$
B	$0.007d$
C	$0.0075d$
D	$0.005d$

**Table 8.1:** Remaining effect of an ephemeris error with size of  $d$  for DGPS network users.

A typical ephemeris error even in SA conditions is usually less than 10 metres [Parkinson and Engle 1996]. Therefore, it can be seen from Table 8.1 that the effects of such an error in the worst direction (along track or cross track) on DGPS network users can be reduced to less than *one decimeter*. To compare the reductions of effects of ephemeris errors by using DGPS network and by using local DGPS, let us assume in the local DGPS positioning case the reference station is located in the ideal position (i.e. the centre) of the simulated  $500 \times 500 \text{ km}^2$  area. Then it is easy to see in this case the maximum remaining effect of ephemeris errors in the area is less than *1.8 decimeters*. As can be seen from this, using DGPS network can improve the reduction of the effect of ephemeris errors by using DGPS but the improvement is rather small.

#### 8.4 Reduction of ionospheric delays in a DGPS network

This section discusses to which extent the ionospheric delay in a DGPS network can be reduced.

It follows from (8.11) that the remaining ionospheric delay for a DGPS-network user after the application of a DC vector reads

$$\hat{I}_j - I_j = -(I_j - I_1) + [\Delta x_j \ \Delta y_j] \begin{bmatrix} \Delta x_2 & \Delta y_2 \\ \Delta x_3 & \Delta y_3 \end{bmatrix}^{-1} \begin{bmatrix} I_2 - I_1 \\ I_3 - I_1 \end{bmatrix} \quad (8.17)$$

Following the approach of [van der Marel 1993], we express the difference in ionospheric delay between two stations as

$$I_j - I_1 = I_{v_1} \left( \frac{1}{\cos z_j} - \frac{1}{\cos z_1} \right) + (I_{v_j} - I_{v_1}) \frac{1}{\cos z_j} \quad (8.18)$$

where  $I_{v_j}$  is the vertical ionospheric delay at station  $j$  and  $z'_j$  the zenith distance at the ionospheric point (see Figure D.2 in Appendix D).

Therefore we arrive at

$$\hat{I}_j - I_j = I_{v_1} \left\{ - \left( \frac{1}{\cos z'_j} - \frac{1}{\cos z'_1} \right) + [\Delta x_j \ \Delta y_j] \begin{bmatrix} \Delta x_2 & \Delta y_2 \\ \Delta x_3 & \Delta y_3 \end{bmatrix}^{-1} \begin{bmatrix} \frac{1}{\cos z'_2} - \frac{1}{\cos z'_1} \\ \frac{1}{\cos z'_3} - \frac{1}{\cos z'_1} \end{bmatrix} \right\} - \frac{I_{v_j} - I_{v_1}}{\cos z'_j} + [\Delta x_j \ \Delta y_j] \begin{bmatrix} \Delta x_2 & \Delta y_2 \\ \Delta x_3 & \Delta y_3 \end{bmatrix}^{-1} \begin{bmatrix} \frac{I_{v_2} - I_{v_1}}{\cos z'_2} \\ \frac{I_{v_3} - I_{v_1}}{\cos z'_3} \end{bmatrix} \quad (8.19)$$

For reasons of simplicity, let us define

$$\text{Part 1} = I_{v_1} \left| - \left( \frac{1}{\cos z'_j} - \frac{1}{\cos z'_1} \right) + [\Delta x_j \ \Delta y_j] \begin{bmatrix} \Delta x_2 & \Delta y_2 \\ \Delta x_3 & \Delta y_3 \end{bmatrix}^{-1} \begin{bmatrix} \frac{1}{\cos z'_2} - \frac{1}{\cos z'_1} \\ \frac{1}{\cos z'_3} - \frac{1}{\cos z'_1} \end{bmatrix} \right| \quad (8.20)$$

$$\text{Part 2} = \left| - \frac{I_{v_j} - I_{v_1}}{\cos z'_j} + (\Delta x_j \ \Delta y_j) \begin{bmatrix} \Delta x_2 & \Delta y_2 \\ \Delta x_3 & \Delta y_3 \end{bmatrix}^{-1} \begin{bmatrix} \frac{I_{v_2} - I_{v_1}}{\cos z'_2} \\ \frac{I_{v_3} - I_{v_1}}{\cos z'_3} \end{bmatrix} \right| \quad (8.21)$$

Note that Part 1 is the homogeneous part of the remaining ionospheric delay, which results from the difference in satellite elevation between the reference stations and between the user and master stations. If a satellite is observed at the same elevation at both the reference stations and the user station, this part of the error will be zero. Part 2 is the inhomogeneous part of the remaining ionospheric delay, which results from the variation of vertical ionospheric delay at different stations. It will be shown later that the size of the inhomogeneous part error is normally much smaller than that of the homogeneous part error.

To facilitate the numerical analysis of the Part 2 error, we express  $I_{v_j} - I_{v_1}$  in (8.21) as [van der Marel 1993]

$$I_{v_j} - I_{v_1} = \frac{dI_{v_1}}{dIp} \Delta Ip_{j,1} \quad (8.22)$$



where  $\frac{dI_{v_1}}{dp}$  is the gradient of the vertical ionospheric delay at station 1 and  $\Delta Ip_{j,1}$  is a function of the distance between stations  $j$  and 1 and of the zenith distance at station 1; its computing formula is given in Appendix D.4. Therefore, (8.22) becomes

$$\text{Part 2} = \frac{dI_{v_1}}{dp} \left[ -\frac{\Delta Ip_{j,1}}{\cos z_j} + [\Delta x_j \ \Delta y_j] \begin{bmatrix} \Delta x_2 & \Delta y_2 \\ \Delta x_3 & \Delta y_3 \end{bmatrix}^{-1} \begin{bmatrix} \frac{\Delta Ip_{2,1}}{\cos z_2} \\ \frac{\Delta Ip_{3,1}}{\cos z_3} \end{bmatrix} \right] \quad (8.23)$$

For the simulated DGPS network as shown in Figure 8.2, the remaining ionospheric delays corrected by a DC vector in the network are analysed and the results are given in Table 8.2.

Station	Part 1	Part 2 (km <sup>-1</sup> )	Direction of Satellite
A	0.018 I <sub>v<sub>1</sub></sub>	10 $\frac{dI_{v_1}}{dp}$	opposite to master station
B	0.037 I <sub>v<sub>1</sub></sub>	37 $\frac{dI_{v_1}}{dp}$	from station 2 to master station
C	0.0001 I <sub>v<sub>1</sub></sub>	4 $\frac{dI_{v_1}}{dp}$	opposite to master station
D	0.002 I <sub>v<sub>1</sub></sub>	$\frac{dI_{v_1}}{dp}$	opposite to master station

**Table 8.2:** Remaining ionospheric delays in a DGPS network, where Part 1 corresponds to the case that satellite zenith distance is 75° and Part 2 corresponds to the case that the satellite zenith distance is 70°.

Note that since a satellite may not be observed at the same zenith distance by two stations if they are not close to each other, a one-degree zenith difference for each 100 kilometre is assumed in the computation of Table 8.2.

With respect to the sizes of the vertical ionospheric delay  $I_{v_1}$  and its gradient  $\frac{dI_{v_1}}{dp}$ , van der Marel and Georgiadou (1994) showed that for the central part of The Netherlands (latitude: 52 °N), the typical vertical ionospheric delay is not more than 4.5 metres and the rate of change of the vertical ionospheric delay is less than 0.3 m/h, which leads to  $\left| \frac{dI_{v_1}}{dp} \right| = \frac{0.3 \text{ m/h}}{2 \cdot \pi \cdot (6356+400) \text{ km}} = 8 \cdot 10^{-5} \text{ m/km}$ . Therefore, even in the case that satellite zenith distance is 75°, the typical Part 1 and Part 2 remaining ionospheric delays in the simulated 500×500 km<sup>2</sup> DGPS network are less than *two decimeters* and *three millimetres*, respectively. It can be shown that if only one reference station is used in the area, the corresponding part 1

remaining delay becomes *one metre*, which is five times as great as that in the DGPS network case.

Some remarks are worth making. First, the Part 1 remaining ionospheric delay increases when the zenith distance increases, whereas the Part 2 remaining ionospheric delay reaches its maximum when the zenith distance is  $70^\circ$  (see Appendix D.5). Therefore, if the cut-off zenith distance is chosen to be  $75^\circ$ , the Part 1 and Part 2 remaining ionospheric delays will not reach their maximums at the same time. Second, based on Table 8.2 and on the typical magnitudes

of  $I_{v_1}$  and  $\frac{dI_{v_1}}{dp}$ , the size of the Part 1 remaining ionospheric delay is much greater than that of the Part 2 remaining ionospheric delay. The latter can, therefore, be ignored in the analysis of the remaining ionospheric delay in DGPS positioning.

## 8.5 Reduction of tropospheric delays in a DGPS network

### 8.5.1 The use of a differential correction vector

From the analysis of the remaining ionospheric delay in a DGPS network, it is easy to see that after the application of a DC vector, the remaining tropospheric delay in a DGPS network reads

$$\hat{\nabla}_j^{tro} - \nabla_j^{tro} = -(\nabla_j^{tro} - \nabla_1^{tro}) + [\Delta x_j \ \Delta y_j] \begin{bmatrix} \Delta x_2 & \Delta y_2 \\ \Delta x_3 & \Delta y_3 \end{bmatrix}^{-1} \begin{bmatrix} \nabla_2^{tro} - \nabla_1^{tro} \\ \nabla_3^{tro} - \nabla_1^{tro} \end{bmatrix} \quad (8.24)$$

According to [Saastamoinen 1973], the tropospheric delay in metres can be modelled by

$$\nabla^{tro} = \frac{0.00227}{\cos z} \left[ p + \left( \frac{1255}{T} + 0.05 \right) e - \tan^2 z \right] \quad (8.25)$$

or

$$\nabla^{tro} = \frac{1}{\cos z} \nabla_v^{tro} - 0.00227 \frac{\tan^2 z}{\cos z} \quad (8.26)$$

with

$$\nabla_v^{tro} = 0.00227 \left[ p + \left( \frac{1255}{T} + 0.05 \right) e \right] \quad (8.27)$$

where

$z$ : zenith distance of the satellite

$p$ : atmospheric pressure (mbar)

- $T$ : temperature (Kelvin)
- $e$ : partial pressure of water vapour (mbar)
- $\nabla_v^{tro}$ : vertical tropospheric delay (m)

Therefore, the difference in tropospheric delays between two stations can be expressed as

$$\nabla_j^{tro} - \nabla_1^{tro} = \nabla_{v_1}^{tro} \left( \frac{1}{\cos z_j} - \frac{1}{\cos z_1} \right) - 0.00227 \left( \frac{\tan^2 z_j}{\cos z_j} - \frac{\tan^2 z_1}{\cos z_1} \right) + \left( \nabla_{v_j}^{tro} - \nabla_{v_1}^{tro} \right) \frac{1}{\cos z_j} \tag{8.28}$$

It will be shown later that the third term on the right-hand side of (8.28) is negligible for GPS positioning applications. Therefore, it follows from (8.24) and (8.28) that

$$\hat{\nabla}_j^{tro} - \nabla_j^{tro} = \nabla_{v_1}^{tro} \left\{ - \left( \frac{1}{\cos z_j} - \frac{1}{\cos z_1} \right) + [\Delta x_j \ \Delta y_j] \begin{bmatrix} \Delta x_2 & \Delta y_2 \\ \Delta x_3 & \Delta y_3 \end{bmatrix}^{-1} \begin{bmatrix} \frac{1}{\cos z_2} - \frac{1}{\cos z_1} \\ \frac{1}{\cos z_3} - \frac{1}{\cos z_1} \end{bmatrix} \right\} - 0.00227 \left\{ - \left( \frac{\tan^2 z_j}{\cos z_j} - \frac{\tan^2 z_1}{\cos z_1} \right) + [\Delta x_j \ \Delta y_j] \begin{bmatrix} \Delta x_2 & \Delta y_2 \\ \Delta x_3 & \Delta y_3 \end{bmatrix}^{-1} \begin{bmatrix} \frac{\tan^2 z_2}{\cos z_2} - \frac{\tan^2 z_1}{\cos z_1} \\ \frac{\tan^2 z_3}{\cos z_3} - \frac{\tan^2 z_1}{\cos z_1} \end{bmatrix} \right\} \tag{8.29}$$

For the simulated DGPS network as shown in Figure 8.2, the remaining tropospheric delays at user locations A, B, C, and D are given in Table 8.3. To assess the size of the remaining errors, we need the size of the vertical tropospheric delay  $\nabla_v^{tro}$ . In practice  $\nabla_v^{tro} \leq 2.6$  m [Mueller and Zerbini 1989]. Therefore, it can be seen from Table 8.3 that the size of the remaining tropospheric delays in the simulated 500x500 km<sup>2</sup> DGPS network is less than 2.5

Station	$\max  \hat{\nabla}_j^{tro} - \nabla_j^{tro} $ (m)	Direction of satellite
A	$0.06 \nabla_{v_1}^{tro} - 0.017$	opposite to master station
B	$0.09 \nabla_{v_1}^{tro} - 0.017$	from station 2 to master station
C	$0.09 \nabla_{v_1}^{tro} - 0.041$	opposite to master station
D	$0.05 \nabla_{v_1}^{tro} - 0.018$	opposite to master station

**Table 8.3:** Remaining tropospheric delays at DGPS network user stations, where the zenith distance at the station is assumed to be 75° and  $\nabla_v^{tro}$  is in metres.

*decimeters*. If only one reference station is used in the area, the corresponding remaining tropospheric delays will increase to **1.8 metres**, which is seven times greater than the one in the DGPS network case.

### 8.5.2 The Use of a tropospheric delay model

As was shown in the previous sub-section, if the tropospheric delay is included in the DC, the sizes of remaining tropospheric delays in GPS observations can be reduced to a few decimeters in a DGPS network. For most users this may be sufficient. But it may be still of interest to investigate if the remaining tropospheric delay can be further reduced.

It follows from (8.27) that

$$\nabla_v^{tro}(p+\Delta p, T+\Delta T, e+\Delta e) = \nabla_v^{tro}(p, T, e) + \frac{d\nabla_v^{tro}}{dp} \Delta p + \frac{d\nabla_v^{tro}}{dT} \Delta T + \frac{d\nabla_v^{tro}}{de} \Delta e \quad (8.30)$$

and

$$\left. \begin{aligned} \frac{d\nabla_v^{tro}}{dp} &= 2.27 \cdot 10^{-3} \quad \frac{\text{m}}{\text{mbar}} \\ \frac{d\nabla_v^{tro}}{dT} &= -2.84885 \frac{e}{T^2} \quad \frac{\text{m}}{\text{K}} \\ \frac{d\nabla_v^{tro}}{de} &= 1.135 \cdot 10^{-4} \quad \frac{\text{m}}{\text{mbar}} \end{aligned} \right\} \quad (8.31)$$

Based on experimental results, Rothacher et al. (1993) suggested to compute meteorological parameters from a standard atmospheric model rather than using observed values. The meteorological parameters can be calculated by using the following formulas:

$$\left. \begin{aligned} p &= p_0 [1 - 2.26 \cdot 10^{-5} (h - h_0)]^{5.225} \quad \text{mbar} \\ T &= T_0 - 6.5 \cdot 10^{-3} (h - h_0) \quad \text{K} \\ e &= \frac{RH_0}{100} \exp\{-6.396 \cdot 10^{-4} (h - h_0) - 37.2465 + 0.213166T - 2.56908 \cdot 10^{-4} T^2\} \quad \text{mbar} \end{aligned} \right\} \quad (8.32)$$

where

- $h$ : station's orthometric height (m)
- $RH$ : relative humidity (%)

and the subscript 0 indicates the related quantity corresponding to the values at sea level.

Assume that in the DGPS network we are considering, the height differences are within 80

meters and  $p_0 = 1013$  mbar,  $T_0 = 291$  K (i.e. 18 °C),  $h_0 = 0$  m,  $RH_0 = 70$  %. Then the differences in atmospheric pressure, temperature, and partial pressure of water vapour between any two stations are not greater than 9.6 mbar, 0.4 K, and 1 mbar, respectively. Therefore, we arrive at

$$\left. \begin{aligned} \left| \frac{d\nabla_v^{tro}}{dp} \Delta p \right| &< 0.022 \text{ m} \\ \left| \frac{d\nabla_v^{tro}}{dT} \Delta T \right| &< 0.0002 \text{ m} \\ \left| \frac{d\nabla_v^{tro}}{de} \Delta e \right| &< 1.2 \cdot 10^{-4} \text{ m} \end{aligned} \right\} \quad (8.33)$$

which shows that for GPS positioning applications, the last three terms on the right-hand side of (8.30) can be ignored, i.e.

$$\nabla_v^{tro}(p+\Delta p, T+\Delta T, e+\Delta e) \approx \nabla_v^{tro}(p, T, e) \quad (8.34)$$

In other words, the difference in the vertical tropospheric delay between stations at less than 80-metre difference in height is not greater than a few centimetres. If the cut-off elevation is chosen to be 15°, then the tropospheric delay at the cut-off elevation is about four times the vertical delay [Saastamoinen 1972]. Therefore, even in this case the difference in the tropospheric delay between two stations is less than nine centimetres, which also shows that the third term on the right-hand side of (8.28) can be ignored. In addition, it follows from (8.33) that of the three atmospheric parameters  $p$ ,  $T$  and  $e$ , the pressure  $p$  plays much bigger roles than the temperature  $T$  and the partial pressure of water vapour  $e$  in the tropospheric delay. The influence of  $T$  or  $e$  is extremely small.

As can be seen from the above analysis, if the Saastamoinen model is used to correct the tropospheric delay in DGPS positioning applications, DGPS users do not need to measure their own atmospheric parameters and they can use the atmospheric parameters measured at a reference station. This approximation will only introduce a bias of centimetre order in the correction of the tropospheric delay. Furthermore, the requirements of measuring the atmospheric parameters at a reference station and transmitting them to mobile users can also be removed by using a set of standard atmospheric parameters such as  $p = 1013$  mbar,  $T = 291$  K and  $e = 12$  mbar, because it was reported in [Brunner and Tregoning 1994] that the use of real atmospheric parameters measured at GPS sites does not lead to more accurate GPS results than the use of standard parameters and a standard model like (8.32).

As a comparison of the above two approaches for the elimination of the tropospheric delay, some characteristics of them are worth mentioning. The use of a DC vector is simple and can be implemented by simply combining the tropospheric delay with the ionospheric delay and the effect of ephemeris errors in DCs. No extra work is needed at all. But its accuracy depends on the location of the user in the network and in the worst cases it may reach a few

decimeters. Instead, the use of a tropospheric delay model can provide an accuracy of better than one decimeter for the correction of the tropospheric delay and the accuracy may be in practice considered to be independent of the user location in the network, although strictly speaking it is a function of the height. A drawback of using a tropospheric delay model is that the elimination of the tropospheric delay is also dependent on the accuracy of the model, which was not accounted for in the above. Fortunately, this may not be a big problem in DGPS positioning applications.

## **8.6 Concluding remarks**

We have individually analysed the reductions of the effect of ephemeris errors, ionospheric delays, and tropospheric delays by using a simulated local DGPS network and local DGPS. Since the analyses were conducted in the measurement domain, they are independent of satellite constellation, so are the results of them.

As shown by the simulated DGPS network of  $500 \times 500 \text{ km}^2$ , when ephemeris errors, vertical ionospheric delays, and vertical tropospheric delays are less than 10, 4.5, and 2.6 metres, respectively, using three reference stations can reduce the effect of ephemeris errors to less than one decimeter, ionospheric delays to less than two decimeters and tropospheric delays to less than 2.5 decimeters. If a tropospheric delay model is used, the tropospheric delays can be further reduced to one decimeter. For the same area and under the same conditions, if only one reference station is used, the remaining effect of ephemeris errors, remaining ionospheric delays, remaining tropospheric delays are less than 0.18, 1, 1.8 metres, respectively.

## Chapter 9

# Taylor expansion of GPS observation equations

### 9.1 Introduction

In order to solve GPS observation equations, one needs to know the transmission time of a GPS signal, which is usually determined by the use of iterations or code observations. Since using iterations is rather time consuming, one should try to avoid this approach, especially in real time GPS applications. It will be shown by a real data set later that a bug of hundreds of kilometres can be included in a code observation. Therefore using a code observation to determine the transmission time may result in biased results.

The main objective of this chapter is to show how to avoid the determination of the transmission time by expanding GPS observations into Taylor series. This chapter consists of six sections. Section 9.2 discusses the derivation of GPS observation equations. In the next section, we discuss some existing approaches used to determine the transmission time of a GPS signal. Section 9.4 will derive the Taylor expansion of GPS observation equations, which is the key part of this chapter. Since solving the Taylor expansion needs to compute partial derivatives of the satellite-receiver distance, Section 9.5 will simplify a formula for the computation. Finally, Section 9.6 will give a summary and some concluding remarks.

Note that the topic of this chapter is somewhat independent from those of the previous chapters. A few notations used in this chapter are not the same as those in the previous chapters for the same quantities. But as will be seen later, this will not cause confusions.

### 9.2 GPS observation equations

The derivation of GPS carrier observation equations can be found in many relevant references (for example, [Remondi 1985], [King et al. 1985] and [Landau 1988]), but they often have one common property that some assumptions are made on the stability of satellite clocks. This section first reviews the derivation of GPS code observation equations and next gives an alternative derivation of carrier observation equations, which does not need any assumptions on the stability of satellite clocks.

#### 9.2.1 GPS code observation equations

The GPS code observable is a measure of the distance between a satellite at the transmission time of a GPS signal and a receiver at the reception time of the signal. The travel time of the signal is determined by comparing (correlating) identical Pseudo Random Noise (PRN) codes generated by the satellite and by the receiver. A code-tracking loop within the receiver is to shift the internal replica of the PRN code in time until maximum correlation occurs. The PRN codes generated at the receiver are derived from the receiver's own clock, and the PRN codes transmitted by the satellite are generated by the satellite clock. In other words, the code observable is the difference between the arrival time (in the receiver time frame) and the transmission time (in the satellite time frame) of a particular signal transmitted by a satellite. Therefore, the unavoidable timing errors in both the satellite clock and the receiver clock will cause the code observable to differ from the true distance between the satellite and the receiver, which will be called satellite-receiver distance herein for simplicity.

Let us define

- $t_R^r$ : reception time of a GPS signal in the receiver time frame
- $t_T^s$ : transmission time of the GPS signal in the satellite time frame
- $t_R$ : GPS time corresponding to the receiver time  $t_R^r$
- $t_T$ : GPS time corresponding to the satellite time  $t_T^s$
- $dt^r$ : receiver clock bias, defined as  $dt^r = t_R^r - t_R$
- $dt^s$ : satellite clock bias, defined as  $dt^s = t_T^s - t_T$

Then the basic code observable reads [Wells et al. 1987]

$$\begin{aligned} t_R^r - t_T^s &= (t_R + dt^r(t_R)) - (t_T + dt^s(t_T)) \\ &= (t_R - t_T) + (dt^r(t_R) - dt^s(t_T)) \end{aligned} \quad (9.1)$$

In this expression, the term  $(t_R - t_T)$  is the travel time (in the GPS time frame) of a signal from a satellite to a receiver. Because of the effect of atmospheric refraction, it is a function of the satellite-receiver distance and the tropospheric and ionospheric refractions. If only the first-order effect of ionospheric delay is taken into account, the travel time  $(t_R - t_T)$  can be written in equation as [Leick 1990]

$$t_R - t_T = \tau(t_R) = \frac{1}{c} \left( \rho(t_R) + \nabla^{i\omega} \rho(t_R) + \frac{40.3}{f^2} TEC(t_R) \right) \quad (9.2)$$

where

- $\tau(t_R)$ : travel time of a GPS code signal received at  $t_R$
- $\rho(t_R)$ : satellite-receiver geometric distance (m), which is not the satellite-receiver distance defined before.
- $TEC(t_R)$ : total electron content, in units of  $10^{16}$  electrons per cubic meter
- $f$ : observable related frequency (Hz)

For reasons of simplicity, the GPS time variable  $t_R$  in the travel time  $\tau(t_R)$  will be omitted



in the following derivation.

Inserting the above equation into (9.1) gives

$$t_R^r - t_T^s = \frac{1}{c} \left( \rho(t_R) + \nabla^{no}(t_R) + \frac{40.3}{f^2} TEC(t_R) \right) + (dt^r(t_R) - dt^s(t_R - \tau)) \quad (9.3)$$

or

$$c(t_R^r - t_T^s) = \rho(t_R) + c \cdot (dt^r(t_R) - dt^s(t_R - \tau)) + \nabla^{no}(t_R) + \frac{40.3}{f^2} TEC(t_R) \quad (9.4)$$

Replacing  $c(t_R^r - t_T^s)$  by the L1 code observation  $P(t_R)$ , and  $f$  by the L1 frequency  $f_1$ , and adding the L1 code observation noise  $\varepsilon(t_R)$  to the right hand side of (9.4) give the L1 code observation equation as

$$P(t_R) = \rho(t_R) + c \cdot (dt^r(t_R) - dt^s(t_R - \tau)) + \nabla^{no}(t_R) + \frac{40.3}{f_1^2} TEC(t_R) + \varepsilon(t_R) \quad (9.5)$$

Analogously, the L2 code observation equation reads

$$\tilde{P}(t_R) = \rho(t_R) + c \cdot (dt^r(t_R) - dt^s(t_R - \tau)) + \nabla^{no}(t_R) + \frac{40.3}{f_2^2} TEC(t_R) + \tilde{\varepsilon}(t_R) \quad (9.6)$$

Since

$$I(t_R) = \frac{40.3}{f_1^2} TEC(t_R) \quad (9.7)$$

and

$$\frac{40.3}{f_2^2} TEC(t_R) = \frac{f_1^2}{f_2^2} \frac{40.3}{f_1^2} TEC(t_R) = \frac{f_1^2}{f_2^2} I(t_R) = r \cdot I(t_R) \quad (9.8)$$

the L1 and L2 code observation equations read, respectively,

$$P(t_R) = \rho(t_R) + c \cdot (dt^r(t_R) - dt^s(t_R - \tau)) + \nabla^{no}(t_R) + I(t_R) + \varepsilon(t_R) \quad (9.9)$$

$$\tilde{P}(t_R) = \rho(t_R) + c \cdot (dt^r(t_R) - dt^s(t_R - \tau)) + \nabla^{no}(t_R) + r \cdot I(t_R) + \tilde{\varepsilon}(t_R) \quad (9.10)$$

## 9.2.2 GPS carrier observation equations

The GPS carrier observable is the difference between the phase generated by a receiver oscillator and that by a satellite oscillator. In equation, the basic form of the carrier observable reads [Remondi 1985]

$$\Phi(t_R^r) = \Phi^r(t_R^r) - \Phi^s(t_T^s) \quad (9.11)$$

where

- $\Phi(t_R^r)$ : carrier phase observable at time  $t_R^r$
- $\Phi^r(t_R^r)$ : carrier phase generated by the receiver oscillator at  $t_R^r$
- $\Phi^s(t_T^s)$ : carrier phase transmitted by the satellite at time  $t_T^s$  and received at  $t_R^r$

In order to let our discussion take place in the GPS time frame, we express  $\Phi^r(t_R^r)$  and  $\Phi^s(t_T^s)$  in this frame by defining

$$\left. \begin{aligned} \Phi^r(t_R^r) &= \phi^r(t_R) \\ \Phi^s(t_T^s) &= \phi^s(t_T) \\ \Phi(t_R^r) &= \phi(t_R) \end{aligned} \right\} \quad (9.12)$$

Note that here  $\phi$  is temporarily not restricted to the L1 carrier observation. Substituting (9.12) into (9.11) yields

$$\phi(t_R) = \phi^r(t_R) - \phi^s(t_T) \quad (9.13)$$

Note that the difference between  $\phi^r(t_R)$  and  $\Phi^r(t_R^r)$  is that the former is evaluated in the GPS time frame, whereas the latter is in the receiver time frame. For one moment,  $t_R$  is generally not equal to  $t_R^r$  due to the receiver clock bias, but  $\phi^r(t_R)$  equals  $\Phi^r(t_R^r)$ . For the pair of  $\phi^s(t_T)$  and  $\Phi^s(t_T^s)$ , this property is also valid.

Since at the first (i.e. initial) epoch there is no knowledge to determine the integer count of the carrier observable, the initial integer-cycle quantity is actually an unknown parameter [Remondi 1984]. In order to acknowledge this initial integer-cycle ambiguity, denoted by  $N(t_0)$ , (9.13) can be updated to

$$\phi(t_R) = \phi^r(t_R) - \phi^s(t_T) + N(t_0) \quad (9.14)$$

It should be pointed out that as long as carrier tracking is maintained, the integer-cycle ambiguity  $N(t_0)$  is a constant. After the first observation is made,  $\phi^r$ ,  $\phi^s$  and  $\phi$  are all continuous quantities, and none of them is restricted to being a fraction of a cycle, and neither are  $\Phi^r$ ,  $\Phi^s$  and  $\Phi$ , of course.

It follows from (9.12) that

$$\phi^r(t_R) = \Phi^r(t_R^r) = \Phi^r(t_0^r) + \int_{t_0^r}^{t_R^r} \frac{d(\Phi^r(t^r))}{dt^r} dt^r \tag{9.15}$$

where

- $t^r$ : time variable in the receiver time frame
- $t_0^r$ : receiver time at the initial epoch, which corresponds to the GPS time  $t_0$

Since the derivative of the phase  $\Phi^r(t^r)$  generated by the receiver oscillator with respect to its own time  $t^r$  is the nominal frequency of the receiver oscillator, denoted by  $f$ , which is a constant, it follows from (9.15) that

$$\begin{aligned} \phi^r(t_R) &= \Phi^r(t_0^r) + \int_{t_0^r}^{t_R^r} f \cdot dt^r \\ &= \Phi^r(t_0^r) + f \cdot (t_R^r - t_0^r) \\ &= \Phi^r(t_0) + f \cdot [t_R + dt^r(t_R) - (t_0 + dt^r(t_0))] \end{aligned} \tag{9.16}$$

Analogous to the derivation of (9.16), it can be shown that the phase  $\phi^s(t_T)$  transmitted by the satellite can be written by

$$\phi^s(t_T) = \Phi^s(t_{T_0}) + f \cdot [t_T + dt^s(t_T) - (t_{T_0} + dt^s(t_{T_0}))] \tag{9.17}$$

where

- $t_{T_0}$ : transmission time (in the GPS time frame) of the carrier signal received at the GPS time  $t_0$

Inserting (9.16) and (9.17) into (9.14) gives

$$\begin{aligned} \phi(t_R) &= \Phi^r(t_0) + f \cdot [t_R + dt^r(t_R) - (t_0 + dt^r(t_0))] - \Phi^s(t_{T_0}) - f \cdot [t_T + dt^s(t_T) - (t_{T_0} + dt^s(t_{T_0}))] + N(t_0) \\ &= f \cdot [(t_R - t_T) + dt^r(t_R) - dt^s(t_T)] - f \cdot (t_0 + dt^r(t_0) - t_{T_0} - dt^s(t_{T_0})) + \Phi^r(t_0) - \Phi^s(t_{T_0}) + N(t_0) \end{aligned} \tag{9.18}$$

Since

$$\left. \begin{aligned} t_R - t_T &= \tau(t_R) \\ t_0 - t_{T_0} &= \tau(t_0) \end{aligned} \right\} \tag{9.19}$$

where

- $\tau(t_R)$ : travel time of a GPS carrier signal received at time  $t_R$

(9.18) becomes

$$\begin{aligned} \phi(t_R) = & f \cdot (\tau(t_R) + dt^r(t_R) - dt^s(t_R - \tau(t_R))) \\ & - f \cdot (\tau(t_0) + dt^r(t_0) - dt^s(t_0 - \tau(t_0))) + \phi^r(t_0) - \phi^s(t_0 - \tau(t_0)) + N(t_0) \end{aligned} \quad (9.20)$$

or

$$\phi(t_R) = f \cdot (\tau(t_R) + dt^r(t_R) - dt^s(t_R - \tau(t_R))) + A(t_0) \quad (9.21)$$

where the initial carrier observable ambiguity  $A(t_0)$  is given by

$$A(t_0) = N(t_0) - f \cdot (\tau(t_0) + dt^r(t_0) - dt^s(t_0 - \tau(t_0))) + \phi^r(t_0) - \phi^s(t_0 - \tau(t_0)) \quad (9.22)$$

As was shown in [Jin 1995b], the ambiguity can also be expressed by

$$A(t_0) = N(t_0) - f \cdot (dt^r(t_0) - dt^s(t_0)) + \phi^r(t_0) - \phi^s(t_0) \quad (9.23)$$

Some remarks are worth making on the ambiguity. First of all, as can be seen from (9.22), the initial carrier observable ambiguity is a function of the following six quantities at different times

- the fractional part of the carrier phase transmitted from the satellite at the initial epoch  $t_0 - \tau(t_0)$ ;
- the satellite clock bias at the epoch  $t_0 - \tau(t_0)$ ;
- the carrier phase generated by the receiver oscillator at the initial epoch  $t_0$ ;
- the receiver clock bias at the initial epoch  $t_0$ ;
- the travel time of the carrier phase signal received at the initial epoch  $t_0$ , which depends on the satellite-receiver geometry and atmospheric effects;
- the initial integer-cycle ambiguity which is an arbitrary integer related to receiver, satellite, and the initial epoch  $t_0$ .

Secondly, it follows from (9.23) that the initial carrier observable ambiguity can also be understood as a linear combination of the following five quantities at the same time  $t_0$  (the initial epoch)

- the fractional part of the carrier phase received from the satellite;
- the initial arbitrary integer-cycle ambiguity;
- the satellite clock bias;
- the carrier phase generated by the receiver oscillator;
- the receiver clock bias.

It should be emphasized here that the initial carrier observable ambiguity has a certain physical meaning which is reflected by expression (9.22). Expression (9.23) only tells us that the *size* of the initial carrier observable ambiguity is equivalent to a combination of five other quantities at the initial epoch  $t_0$ . It becomes evident from (9.22) or (9.23) that the initial

carrier observable ambiguity is a real valued quantity.

Thirdly, the so called carrier observable integer-cycle ambiguity  $N(t_0)$  is an arbitrary integer which is related to the satellite, the receiver, and the initial epoch. But it does not include any information on the satellite-receiver distance.

Now let us return to the derivation of L1 and L2 carrier observation equations. As with code observables, the travel time of the carrier phase signal from a satellite to a receiver is a function of the satellite-receiver distance and the tropospheric and ionospheric refractions. The satellite-receiver distance and the troposphere have the same effect on code and carrier observables, but the ionosphere has an opposite effect on code and carrier observables with the same magnitude (usually called group delay and phase advance, respectively) [Hofmann-Wellenhof et al. 1992]. Based on these properties, it follows from (9.2) that

$$\tau(t_R) = \frac{1}{c} \left( \rho(t_R) + \nabla^{tro}(t_R) - \frac{40.3}{f^2} TEC(t_R) \right) \tag{9.24}$$

Substitution of the above equation into (9.21) yields

$$\phi(t_R) = \frac{f}{c} \left( \rho(t_R) + \nabla^{tro}(t_R) - \frac{40.3}{f^2} TEC(t_R) \right) + f \cdot (dt^r(t_R) - dt^s(t_R - \tau(t_R))) + A(t_0) \tag{9.25}$$

Again let us make use of the symbol  $\phi$  to represent L1 carrier observable and denote the L1 carrier ambiguity by  $A$ . Multiplying both sides of (9.25) by  $\lambda_1$  (note:  $\lambda_1 = c / f_1$ ) and then adding the L1 carrier observation noise to its right-hand side gives the L1 carrier observation equation (in metric units)

$$\lambda_1 \phi(t) = \rho(t) + c \cdot (dt^r(t) - dt^s(t - \tau(t))) + \nabla^{tro}(t) - I(t) + \lambda_1 A(t_0) + \eta(t) \tag{9.26}$$

with

$$A(t_0) = N(t_0) - f_1 \cdot (\tau(t_0) + dt^r(t_0) - dt^s(t_0 - \tau(t_0))) + \phi^r(t_0) - \phi^s(t_0 - \tau(t_0)) \tag{9.27}$$

or

$$A(t_0) = N(t_0) - f_1 \cdot (dt^r(t_0) - dt^s(t_0)) + \phi^r(t_0) - \phi^s(t_0) \tag{9.28}$$

Since the L2 carrier observation equation can be obtained by following the same procedure as for deriving the L1 carrier observation equation, it is directly given below

$$\lambda_2 \check{\phi}(t) = \rho(t) + c \cdot (dt^r(t) - dt^s(t - \tau(t))) + \nabla^{tro}(t) - r \cdot I(t) + \lambda_2 \check{A}(t_0) + \check{\eta}(t) \tag{9.29}$$

with

$$\check{A}(t_0) = \check{N}(t_0) - f_2 \cdot (\tau(t_0) + dt^r(t_0) - dt^s(t_0 - \tau(t_0))) + \check{\phi}^r(t_0) - \check{\phi}^s(t_0 - \tau(t_0)) \tag{9.30}$$

or

$$\tilde{A}(t_0) = \tilde{N}(t_0) - f_2 \cdot (dt^r(t_0) - dt^s(t_0)) + \tilde{\phi}^r(t_0) - \tilde{\phi}^s(t_0) \quad (9.31)$$

where

$\tilde{A}$ : L2 carrier ambiguity (cycles)

$\tilde{N}$ : L2 carrier integer-cycle ambiguity (cycles)

It should be pointed out that strictly speaking, the travel time of a carrier signal is different from that of a code signal and moreover the travel time of an L1 carrier (and code) is different from that of an L2 carrier (and code) due to the different impact of the ionosphere. Therefore the symbol  $\tau$  in (9.26) and (9.29) should be considered as two different quantities, representing the travel times of the L1 and L2 carrier signals, respectively. It will be shown later, however, that it does not make sense to do so here.

### 9.3 Discussion on some existing approaches to compute the travel time of GPS signals

In the previous section, code and carrier observation equations were derived. As can be seen from them, many parameters are included there, for instance, the satellite-receiver distance which is a function of satellite and receiver positions, receiver and satellite clock biases, and some other bias terms like ionospheric and tropospheric delays. For most GPS applications, satellite positions and satellite clock biases, or their approximate values, at the transmission time of a GPS signal are usually computed by means of either broadcast ephemeris or precise ephemeris. In order to determine the transmission time of the signal, one needs to know the signal travel time from the satellite to the receiver.

Several approaches exist for computing the travel time, e.g., using iterations [Remondi 1985] or using code observations [NATO 1991b]. As we know, an iteration algorithm usually needs at least one iteration to reach a solution precise enough and always needs another iteration to check if the iteration procedure may stop. This means that by the use of any iteration algorithm, the same computations are usually carried out at least three times. Therefore, using iterations to determine the travel time of a GPS signal is comparatively time consuming especially when the broadcast ephemeris as such are used. For real time GPS applications, this method should be avoided if possible.

Generally speaking, using a code observation to determine the travel time is very simple and thus very efficient, because the code observable is actually a direct measure of the travel time of a signal from the satellite to the receiver. But sometimes this method may lead to a badly biased result, which is shown below. In other words, using a code observation to determine the travel time of a GPS signal can have the advantages of simplicity and efficiency in most cases but there is always the risk of being affected by gross errors in the code observation. In addition, this approach has another drawback, that is, the coefficients of linearized GPS observation equations are functions of code observations, which makes it difficult (if not

impossible) to correctly compute the covariance matrix of estimated unknowns.

Table 9.1 shows five sequential epochs of observation data in the RINEX format along with a header, which was extracted from a real data set. The information about the types of receiver and antenna, the version of RINEX software used, and the like, is given at the upper part of the table. Columns 1, 2 and 4 of the data in Table 9.1 are L1 code, L1 carrier and L2 carrier observations, respectively. Columns 3 and 5 are the signal strength of L1 and L2 carrier observations. The first row of each epoch record contains the observation time (year, month, day, hour, minute, and second), the information whether there was a power failure since the last epoch or not, the number of satellites tracked, and the tracked satellite numbers. The first row of each epoch record is followed by row(s) of observations, each row corresponds to one satellite and they have the same sequence as the tracked satellite numbers in the first row. For more details on the RINEX format, see [Gurtner 1994].

As can be seen from Table 9.1, during the listed first two epochs the code observation of satellite 20 decreased about 13470 meters, while during the listed second and third epochs it suddenly increased about 286320 meters. From then on the code observation returned to decreasing in the rate of about 13470 meters per epoch again. It can be seen from the record shown in the table that during the listed five epochs, no correction to the receiver clock was performed. With respect to the change of the corresponding L1 carrier observation, it appears reasonably stable. No strange behaviour can be found. In the whole period of the listed five epochs, the rate of the L1 carrier observation is about -70800 cycles per epoch, and moreover it can be verified that the L1 carrier observations shown in the table change linearly. Based on these phenomena, what we may conclude for the data is that the sudden change of the code observation of satellite 20 at the epoch 91 12 8 20 49 14.977 did not come from the change of the satellite-receiver distance. Instead one gross error as large as about 300 kilometres (corresponding to 1 millisecond) was included in the code observation. From this example we can see that a gross error as large as hundreds of kilometres may occur in a code observation, but the code-observation related carrier observation is still good.

Suppose in the processing of this data set one uses code observations to determine the travel time of GPS signals. As can be easily seen, the travel time of satellite 20 at the epoch 91 12 8 20 49 14.977 will be very badly distorted, so are the satellite position and in turn the computed satellite-receiver distance. In the case that there is no quality control in the data reduction, the final results will certainly be seriously biased. Whereas if there is quality control in the data reduction, then the actually 'good' carrier observation would likely be considered to contain a gross error along with the actually 'bad' code observation, because the gross error contained in the code observation will be transferred to the difference between the computed and observed carrier observations.

#### 9.4 Taylor expansion of observation equations

As has been made clear in the previous section, using iterations or code observations to determine the travel time of a GPS signal should not be recommended, particularly in real time high precision GPS applications. To overcome the difficulties in determining the travel time, this section expands GPS observation equations into Taylor series so that they can be

1 OBSERVATION DATA										RINEX VERSION / TYPE				
TRRINEXO V1.7 AIUB 09-DEC-91 12:59										PGM / RUN BY / DATE				
SA-test 24 hours 1-st session										COMMENT				
DE18										MARKER NAME				
										OBSERVER / AGENCY				
761	TRIMBLE 4000 SST								4.53	REC # / TYPE / VERS				
163	TRIMBLE 4000 SST									ANT # / TYPE				
3924657.3031	301166.7873		5001866.8972						APPROX POSITION XYZ					
	.1630	.0000		.0000				ANTENNA: DELTA H/E/N						
1	2							WAVELENGTH FACT L1/2						
3	C1	L1	L2					# / TYPES OF OBSERV						
15									INTERVAL					
1991	12	8	10	46	30.000000			TIME OF FIRST OBS						
91	12	8	20	48	44.9770000	0	7	6	2	12	21	23	13	20
					17835260.521	-23950502.894	5	-18229562.022	5					
					17601283.388	-22277821.047	6							
					14071693.521	-28919769.623	7	-22321439.685	9					
					16556729.216	-13505107.855	5	-8733940.868	5					
					16111506.763	-22066154.741	6	-16934272.357	6					
					15937410.614	-15851628.573	6	-10563524.298	5					
					18157028.724	-141667.975	3							
91	12	8	20	48	59.9770000	0	7	6	2	12	21	23	13	20
					17842071.357	-23914736.143	5	-18201691.912	2					
					17608230.458	-22241299.676	5							
					14065605.802	-28951757.091	7	-22346364.982	8					
					16552165.208	-13529080.691	5	-8752621.007	4					
					16113126.872	-22057626.568	6	-16927627.031	6					
					15926445.435	-15909259.855	6	-10608431.767	5					
					18143552.427	-212477.551	3							
91	12	8	20	49	14.9770000	0	7	6	2	12	21	23	13	20
					17848877.529	-23878961.112	5	-18173815.204	5					
					17615173.935	-22204760.929	4							
					14059534.310	-28983666.571	7	-22371229.508	9					
					16547632.779	-13552898.112	5	-8771180.026	3					
					16114771.654	-22048982.152	6	-16920891.142	6					
					15915500.552	-15966782.933	6	-10653254.922	5					
					→ 18429874.654	-283275.373	3							
91	12	8	20	49	29.9770000	0	7	6	2	12	21	23	13	20
					17855686.888	-23843174.173	5	-18145929.395	4					
					17622140.880	-22168201.270	5							
					14053478.841	-29015494.659	7	-22396030.608	8					
					16543131.091	-13576556.844	5	-8789615.403	4					
					16116441.607	-22040215.966	6	-16914060.351	6					
					15904573.575	-16024193.930	6	-10697990.753	5					
					18416402.591	-354059.290	3							
91	12	8	20	49	44.9770000	0	7	6	2	12	21	23	13	20
					17862495.318	-23807376.177	5	-18118034.790	3					
					17629099.263	-22131618.032	4							
					14047435.247	-29047241.976	7	-22420768.777	8					
					16538657.755	-13600057.249	5	-8807927.396	4					
					16118131.021	-22031323.806	6	-16907131.408	6					
					15893670.161	-16081492.957	6	-10742639.331	5					
					18402937.904	-424827.216	3	-	41712					

**Table 9.1:** An example of RINEX data with a gross error in the code observation of satellite 20 at epoch 91 12 8 20 49 14.977



solved without computing the travel time.

This section discusses first the expansion of satellite-receiver distances and next that of satellite clock biases. Finally it gives the expansion of observation equations.

**9.4.1 Expansion of satellite-receiver distances**

The distance between a satellite at the GPS time  $t-\tau$  and a receiver at the GPS time  $t$ , can be written as

$$\rho(t) = \|r^s(t-\tau) - r^r(t)\| = \sqrt{\langle r^s(t-\tau) - r^r(t), r^s(t-\tau) - r^r(t) \rangle} \tag{9.32}$$

where

- $r^s$ : position vector of the satellite in an inertial coordinate system
- $r^r$ : position vector of the receiver in an inertial coordinate system

Note that the travel time  $\tau$  is a function of  $t$  and for a receiver-satellite pair, it will be fixed when the reception time  $t$  of the GPS signal is fixed. Therefore, if the reception time  $t$  is used as a variable of the satellite-receiver distance,  $\tau$  has only one variable. But for convenience, let us define

$$\rho(t_1, t_2) = \|r^s(t_2) - r^r(t_1)\| \tag{9.33}$$

In order to eliminate the travel time  $\tau$  in the expression of the satellite-receiver distance, we expand  $\rho(t_1, t_2)$  into Taylor series as follows

$$\rho(t_1, t_2) = \rho(t_1^0, t_2^0) + \left[ (t_1 - t_1^0) \frac{\partial}{\partial t_1} + (t_2 - t_2^0) \frac{\partial}{\partial t_2} \right] \rho(t_1^0, t_2^0) + \frac{1}{2} \left[ (t_1 - t_1^0) \frac{\partial}{\partial t_1} + (t_2 - t_2^0) \frac{\partial}{\partial t_2} \right]^2 \rho(\xi_1, \xi_2) \tag{9.34}$$

with  $|\xi_1 - t_1^0| \leq |t_1 - t_1^0|, |\xi_2 - t_2^0| \leq |t_2 - t_2^0|$

which is equivalent to

$$\rho(t_1, t_2) = \rho(t_1^0, t_2^0) + \frac{\partial \rho(t_1^0, t_2^0)}{\partial t_1} \Delta t_1 + \frac{\partial \rho(t_1^0, t_2^0)}{\partial t_2} \Delta t_2 + \frac{1}{2} \frac{\partial^2 \rho(\xi_1, \xi_2)}{\partial t_1^2} \Delta t_1^2 + \frac{1}{2} \frac{\partial^2 \rho(\xi_1, \xi_2)}{\partial t_2^2} \Delta t_2^2 + \frac{\partial^2 \rho(\xi_1, \xi_2)}{\partial t_1 \partial t_2} \Delta t_1 \Delta t_2 \tag{9.35}$$

with  $\Delta t_1 = (t_1 - t_1^0), \Delta t_2 = (t_2 - t_2^0)$

Since

$$\rho^2(t_1, t_2) = \langle r^s(t_2) - r^r(t_1), r^s(t_2) - r^r(t_1) \rangle \quad (9.36)$$

we have

$$2\rho(t_1, t_2) \frac{\partial \rho(t_1, t_2)}{\partial t_1} = -2 \langle \dot{r}^r(t_1), r^s(t_2) - r^r(t_1) \rangle \quad (9.37)$$

The partial derivatives of (9.37) with respect to  $t_1$  and  $t_2$  read,

$$\left[ \frac{\partial \rho(t_1, t_2)}{\partial t_1} \right]^2 + \rho(t_1, t_2) \frac{\partial^2 \rho(t_1, t_2)}{\partial t_1^2} = -\langle \ddot{r}^r(t_1), r^s(t_2) - r^r(t_1) \rangle - \langle \dot{r}^r(t_1), \dot{r}^r(t_1) \rangle \quad (9.38)$$

$$\frac{\partial \rho(t_1, t_2)}{\partial t_1} \frac{\partial \rho(t_1, t_2)}{\partial t_2} + \rho(t_1, t_2) \frac{\partial^2 \rho(t_1, t_2)}{\partial t_1 \partial t_2} = -\langle \dot{r}^r(t_1), \dot{r}^s(t_2) \rangle \quad (9.39)$$

It follows from (9.37) that

$$\frac{\partial \rho(t_1, t_2)}{\partial t_1} = -\frac{1}{\rho(t_1, t_2)} \langle \dot{r}^r(t_1), r^s(t_2) - r^r(t_1) \rangle \quad (9.40)$$

and from (9.38) and (9.40) that

$$\frac{\partial^2 \rho(t_1, t_2)}{\partial t_1^2} = \frac{-1}{\rho(t_1, t_2)} \left( \langle \ddot{r}^r(t_1), r^s(t_2) - r^r(t_1) \rangle - \langle \dot{r}^r(t_1), \dot{r}^r(t_1) \rangle + \frac{\langle \dot{r}^r(t_1), r^s(t_2) - r^r(t_1) \rangle^2}{\rho(t_1, t_2)^2} \right) \quad (9.41)$$

As can be seen from (9.36), (9.40) and (9.41), replacing  $r^s(t_2)$  by  $(-r^r(t_1))$  and  $r^r(t_1)$  by  $(-r^s(t_2))$  along with  $t_1$  by  $t_2$  and  $t_2$  by  $t_1$  in (9.36), (9.40) and (9.41) gives

$$\frac{\partial \rho(t_1, t_2)}{\partial t_2} = \frac{1}{\rho(t_1, t_2)} \langle \dot{r}^s(t_2), r^s(t_2) - r^r(t_1) \rangle \quad (9.42)$$

$$\frac{\partial^2 \rho(t_1, t_2)}{\partial t_2^2} = \frac{1}{\rho(t_1, t_2)} \left( \langle \ddot{r}^s(t_2), r^s(t_2) - r^r(t_1) \rangle + \langle \dot{r}^s(t_2), \dot{r}^s(t_2) \rangle - \frac{\langle \dot{r}^s(t_2), r^s(t_2) - r^r(t_1) \rangle^2}{\rho(t_1, t_2)^2} \right) \quad (9.43)$$

Substituting (9.40) and (9.42) into (9.39) yields

$$\frac{\partial^2 \rho(t_1, t_2)}{\partial t_1 \partial t_2} = \frac{-1}{\rho(t_1, t_2)} \left( \langle \dot{r}^r(t_1), \dot{r}^s(t_2) \rangle - \frac{\langle \dot{r}^r(t_1), r^s(t_2) - r^r(t_1) \rangle \langle \dot{r}^s(t_2), r^s(t_2) - r^r(t_1) \rangle}{\rho(t_1, t_2)^2} \right) \quad (9.44)$$

Before we continue our derivations, let us first have a look at the magnitudes of the above derivatives. Using Cauchy-Schwarz' inequality it follows from (9.40) to (9.44) that

$$\left| \frac{\partial \rho(t_1, t_2)}{\partial t_1} \right| \leq \frac{1}{\rho(t_1, t_2)} \|\dot{r}^r(t_1)\| \cdot \|r^s(t_2) - r^r(t_1)\| = \|\dot{r}^r(t_1)\| \quad (9.45)$$

$$\begin{aligned} \left| \frac{\partial^2 \rho(t_1, t_2)}{\partial t_1^2} \right| &\leq \frac{1}{\rho(t_1, t_2)} \left( \|\ddot{r}^r(t_1)\| \cdot \|r^s(t_2) - r^r(t_1)\| + \left| \|\dot{r}^r(t_1)\|^2 - \frac{\|\dot{r}^r(t_1)\|^2 \|r^s(t_2) - r^r(t_1)\|^2 \cos^2 \theta}{\rho(t_1, t_2)^2} \right| \right) \\ &\leq \|\ddot{r}^r(t_1)\| + \frac{\|\dot{r}^r(t_1)\|^2}{\rho(t_1, t_2)} \end{aligned} \quad (9.46)$$

where  $\theta$  is the angle between the vectors  $\dot{r}^r(t_1)$  and  $r^s(t_2) - r^r(t_1)$ .

$$\left| \frac{\partial \rho(t_1, t_2)}{\partial t_2} \right| \leq \frac{1}{\rho(t_1, t_2)} \|\dot{r}^s(t_2)\| \cdot \|r^s(t_2) - r^r(t_1)\| = \|\dot{r}^s(t_2)\| \quad (9.47)$$

$$\begin{aligned} \left| \frac{\partial^2 \rho(t_1, t_2)}{\partial t_2^2} \right| &\leq \frac{1}{\rho(t_1, t_2)} \left( \|\dot{r}^s(t_2)\| \cdot \|r^s(t_2) - r^r(t_1)\| + \left| \|\dot{r}^s(t_2)\|^2 - \frac{\|\dot{r}^s(t_2)\|^2 \|r^s(t_2) - r^r(t_1)\|^2 \cos^2 \theta}{\rho(t_1, t_2)^2} \right| \right) \\ &\leq \|\ddot{r}^s(t_2)\| + \frac{\|\dot{r}^s(t_2)\|^2}{\rho(t_1, t_2)} \end{aligned} \quad (9.48)$$

where  $\theta$  is the angle between the vectors  $\dot{r}^s(t_2)$  and  $r^s(t_2) - r^r(t_1)$ .

$$\begin{aligned} \left| \frac{\partial^2 \rho(t_1, t_2)}{\partial t_1 \partial t_2} \right| &\leq \frac{1}{\rho(t_1, t_2)} (\|\dot{r}^r(t_1)\| \cdot \|\dot{r}^s(t_2)\| + \|\dot{r}^r(t_1)\| \cdot \|\dot{r}^s(t_2)\|) \\ &= \frac{2\|\dot{r}^r(t_1)\| \cdot \|\dot{r}^s(t_2)\|}{\rho(t_1, t_2)} \end{aligned} \quad (9.49)$$

Denoting the approximate value of the receiver-clock bias by  $dt^{r^0}(t)$  and its correction by  $\delta(dt^r(t))$ , then

$$dt^r(t) = dt^{r^0}(t) + \delta(dt^r(t)) \quad (9.50)$$

With varying satellite elevation, the travel time of a GPS signal will change. But it can be verified that it is in the range of 0.067 to 0.086 seconds, i.e.

$$0.067 \text{ s} < \tau < 0.086 \text{ s} \quad (9.51)$$

Let us assume that the size of the correction to the approximate value of the receiver-clock bias is less than one millisecond

$$|\delta(dt^r(t))| < 10^{-3} \text{ s} \quad (9.52)$$

and choose

$$\left. \begin{aligned} t_1 &= t, & t_2 &= t - \tau \\ t_1^0 &= t^0 = t^r - dt^r, & t_2^0 &= (t^r - dt^r) - \tau^0, \tau^0 = 0.077 \text{ s} \end{aligned} \right\} \quad (9.53)$$

then from (9.35), (9.53), (9.50), (9.52), and the definition of the clock bias we arrive at:

$$|\Delta t_1| = |t_1 - t_1^0| = |t - t^r + dt^r| = |-dt^r(t) + dt^r(t)| = |-\delta(dt^r(t))| < 10^{-3} \text{ s} \quad (9.54)$$

$$\begin{aligned} |\Delta t_2| &= |t_2 - t_2^0| = |t - \tau - (t^r - dt^r - \tau^0)| = |-\delta(dt^r(t)) - (\tau - \tau^0)| \\ &\leq |\delta(dt^r(t))| + |\tau - \tau^0| < 10^{-3} + 0.01 = 0.011 \text{ s} \end{aligned} \quad (9.55)$$

Taking the following values in an inertial coordinate system ([GPS-WG 1992], [NATO 1991a])

$$\left. \begin{aligned} \|\ddot{r}^r(t_1)\| &\approx 470 \frac{m}{s}, & \|\ddot{r}^r(t_1)\| &= 0.034 \frac{m}{s^2} \\ \|\ddot{r}^s(t_2)\| &\approx 4 \cdot 10^3 \frac{m}{s}, & \|\ddot{r}^s(t_2)\| &\approx 0.6 \frac{m}{s^2} \\ \rho(t_1, t_2) &> 2 \cdot 10^7 \text{ m} \end{aligned} \right\} \quad (9.56)$$

then we have:

$$\left| \frac{\partial \rho(t_1^0, t_2^0)}{\partial t_1} \right| |\Delta t_1| \leq 470 \cdot 10^{-3} = 0.47 \text{ m} \quad (9.57)$$

$$\left| \frac{\partial \rho(t_1^0, t_2^0)}{\partial t_2} \right| |\Delta t_2| \leq 4 \cdot 10^3 \cdot 0.011 = 44 \text{ m} \quad (9.58)$$

$$\frac{1}{2} \left| \frac{\partial^2 \rho(\xi_1, \xi_2)}{\partial t_1^2} \right| \Delta t_1^2 \leq \frac{1}{2} \left( 0.034 + \frac{470^2}{2 \cdot 10^7} \right) \cdot (10^{-3})^2 = 2.2 \cdot 10^{-8} \text{ m} \quad (9.59)$$

$$\frac{1}{2} \left| \frac{\partial^2 \rho(\xi_1, \xi_2)}{\partial t_2^2} \right| \Delta t_2^2 \leq \frac{1}{2} \left( 0.6 + \frac{(4 \cdot 10^3)^2}{2 \cdot 10^7} \right) \cdot 0.011^2 < 8.5 \cdot 10^{-5} \text{ m} \quad (9.60)$$

$$\left| \frac{\partial^2 \rho(\xi_1, \xi_2)}{\partial t_1 \partial t_2} \right| |\Delta t_1| |\Delta t_2| \leq \frac{2 \cdot 470 \cdot 4 \cdot 10^3}{2 \cdot 10^7} 10^{-3} \cdot 0.011 = 2 \cdot 10^{-5} \text{ m} \quad (9.61)$$

Noises of carrier observations are much less than those of code observations, they are usually in the order of millimetres. In order to replace the original term of the satellite-receiver distance in a GPS (code or carrier) observation equation by another one without introducing any errors greater than GPS observation noises, an expression for the distance should be accurate at the level of a few millimetres. On the other hand, this also means that any errors less than one millimetre in such an expression can be ignored.

Substituting (9.53) into (9.35) and then neglecting all second-order derivative quantities which are less than  $8.5 \cdot 10^{-5}$  m gives

$$\rho(t, t-\tau) = \rho(t^0, t^0-\tau^0) - \frac{\partial \rho(t^0, t^0-\tau^0)}{\partial t_1} \delta(dt^1) - \frac{\partial \rho(t^0, t^0-\tau^0)}{\partial t_2} [\delta(dt^2) + (\tau-\tau^0)] \quad (9.62)$$

Since

$$\tau(t) = \frac{1}{c} (\rho(t, t-\tau(t)) + \nabla^{am}(t)) \quad (9.63)$$

where

$\nabla^{am}$ : atmospheric effect resulted from troposphere and ionosphere

inserting (9.63) into (9.62) yields

$$\begin{aligned} \rho(t, t-\tau) = \rho(t^0, t^0-\tau^0) - \delta(dt^1) \left( \frac{\partial}{\partial t_1} + \frac{\partial}{\partial t_2} \right) \rho(t^0, t^0-\tau^0) - \frac{1}{c} \frac{\partial \rho(t^0, t^0-\tau^0)}{\partial t_2} \rho(t, t-\tau) \\ - \frac{1}{c} \frac{\partial \rho(t^0, t^0-\tau^0)}{\partial t_2} \nabla^{am} + \frac{\partial \rho(t^0, t^0-\tau^0)}{\partial t_2} \tau^0 \end{aligned} \quad (9.64)$$

Let us assume that the sizes of tropospheric and ionospheric delays are less than 15 and 75

metres (cf. [Saastamoinen 1973] and [Klobuchar and Doherty 1990]), respectively. Then the size of the atmospheric delay is less than 90 metres for code observations and 60 metres for carrier observations, since the effects of troposphere and ionosphere on carrier observations have opposite signs. It follows from (9.58) that

$$\frac{1}{c} \frac{\partial \rho(t^0, t^0 - \tau^0)}{\partial t_2} \nabla_{atm} < \begin{cases} \frac{1}{2.9979 \cdot 10^8} 4 \cdot 10^3 \cdot 90 = 1.2 \cdot 10^{-3} \text{ m, for the code} \\ \frac{1}{2.9979 \cdot 10^8} 4 \cdot 10^3 \cdot 60 = 8 \cdot 10^{-4} \text{ m, for the carrier} \end{cases} \quad (9.65)$$

which is negligible. Therefore (9.64) can be rewritten as

$$\begin{aligned} \rho(t, t - \tau) &= \rho(t^0, t^0 - \tau^0) - \delta(dt^r) \left( \frac{\partial}{\partial t_1} + \frac{\partial}{\partial t_2} \right) \rho(t^0, t^0 - \tau^0) \\ &\quad - \frac{1}{c} \frac{\partial \rho(t^0, t^0 - \tau^0)}{\partial t_2} \rho(t, t - \tau) + \frac{\partial \rho(t^0, t^0 - \tau^0)}{\partial t_2} \tau^0 \end{aligned} \quad (9.66)$$

i.e.

$$\begin{aligned} \left[ 1 + \frac{1}{c} \frac{\partial \rho(t^0, t^0 - \tau^0)}{\partial t_2} \right] \rho(t, t - \tau) &= \rho(t^0, t^0 - \tau^0) - \delta(dt^r) \left( \frac{\partial}{\partial t_1} + \frac{\partial}{\partial t_2} \right) \rho(t^0, t^0 - \tau^0) \\ &\quad + \frac{\partial \rho(t^0, t^0 - \tau^0)}{\partial t_2} \tau^0 \end{aligned} \quad (9.67)$$

or

$$\rho(t, t - \tau) = \left( 1 + \frac{1}{c} \frac{\partial \rho(t^0, t^0 - \tau^0)}{\partial t_2} \right)^{-1} \left[ \rho(t^0, t^0 - \tau^0) - \delta(dt^r) \left( \frac{\partial}{\partial t_1} + \frac{\partial}{\partial t_2} \right) \rho(t^0, t^0 - \tau^0) + \frac{\partial \rho(t^0, t^0 - \tau^0)}{\partial t_2} \tau^0 \right] \quad (9.68)$$

Since

$$\left| \frac{1}{c} \frac{\partial \rho(t^0, t^0 - \tau^0)}{\partial t_2} \right| \leq \frac{1}{2.9979 \cdot 10^8} 4 \cdot 10^3 \approx 1.3 \cdot 10^{-5} < 1 \quad (9.69)$$

we have

$$\left( 1 + \frac{1}{c} \frac{\partial \rho(t^0, t^0 - \tau^0)}{\partial t_2} \right)^{-1} = 1 - \frac{1}{c} \frac{\partial \rho(t^0, t^0 - \tau^0)}{\partial t_2} + \left( \frac{1}{c} \frac{\partial \rho(t^0, t^0 - \tau^0)}{\partial t_2} \right)^2 - \dots \quad (9.70)$$

By using the following values

$$\left. \begin{aligned} \rho(t^0, t^0 - \tau^0) &< 2 \cdot 10^7 \text{ m} \\ \left| \delta(dt^r) \left( \frac{\partial}{\partial t_1} + \frac{\partial}{\partial t_2} \right) \rho(t^0, t^0 - \tau^0) \right| &< 10^{-3} \cdot (470 + 4 \cdot 10^3) = 4.47 \text{ m} \\ \left| \frac{\partial \rho(t^0, t^0 - \tau^0)}{\partial t_2} \tau^0 \right| &\leq 4 \cdot 10^3 \cdot 0.077 = 308 \text{ m} \end{aligned} \right\} \quad (9.71)$$

substituting (9.70) into (9.68) and omitting the terms less than  $5.8 \cdot 10^{-5}$  m finally result in the Taylor expansion of the satellite-receiver distance as

$$\begin{aligned} \rho(t, t - \tau) = & \left\{ 1 - \frac{1}{c} \frac{\partial \rho(t^0, t^0 - \tau^0)}{\partial t_2} + \left( \frac{1}{c} \frac{\partial \rho(t^0, t^0 - \tau^0)}{\partial t_2} \right)^2 \right\} \rho(t^0, t^0 - \tau^0) \\ & - \delta(dt^r) \left( \frac{\partial}{\partial t_1} + \frac{\partial}{\partial t_2} \right) \rho(t^0, t^0 - \tau^0) + \left( 1 - \frac{1}{c} \frac{\partial \rho(t^0, t^0 - \tau^0)}{\partial t_2} \right) \frac{\partial \rho(t^0, t^0 - \tau^0)}{\partial t_2} \tau^0 \end{aligned} \quad (9.72)$$

Note that

- equation (9.72) is valid within the order of  $8.5 \cdot 10^{-5}$  m under the assumption that the receiver clock bias correction  $\delta(dt^r)$  is less than one millisecond in size, i.e.,  $|\delta(dt^r)| < 10^{-3}$  s;
- for a receiver clock being accurate up to one millisecond, i.e.,  $|dt^r| < 0.001$  s, the approximation  $dt^r$  of the receiver clock bias can simply be chosen to be zero.

#### 9.4.2 Expansion of satellite clock biases

In addition to the satellite-receiver distance, the satellite clock bias in a GPS observation equation is also a function of the travel time of a GPS signal. This section derives the Taylor expansion of it.

Since the satellite clock bias reads

$$dt^s(t) = t^s(t) - t \quad (9.73)$$

we arrive at

$$\begin{aligned}
 dt^s(t) &= dt^s(t_0) + \left. \frac{d(dt^s(t))}{dt} \right|_{t=\xi} \cdot (t-t_0), & \text{with } |\xi - t_0| \leq |t - t_0| \\
 &= dt^s(t_0) + \left. \frac{d(dt^s(t) - t)}{dt} \right|_{t=\xi} \cdot (t-t_0) \\
 &= dt^s(t_0) + \left[ \left. \frac{dt^s(t)}{dt} - 1 \right]_{t=\xi} \cdot (t-t_0) \\
 &= dt^s(t_0) + \left[ \frac{dt^s(t)}{d\phi^s(t)} \frac{d\phi^s(t)}{dt} - 1 \right]_{t=\xi} \cdot (t-t_0)
 \end{aligned} \tag{9.74}$$

that is

$$dt^s(t) = dt^s(t_0) + \left[ \frac{1}{\frac{d\phi^s(t)}{dt^s(t)}} \frac{d\phi^s(t)}{dt} - 1 \right]_{t=\xi} \cdot (t-t_0) \tag{9.75}$$

The derivative of the phase  $\phi^s(t)$  generated by the satellite oscillator with respect to its own time  $t^s(t)$  is the nominal frequency, denoted by  $f$ , i.e.,

$$\frac{d\phi^s(t)}{dt^s(t)} = f \tag{9.76}$$

which is a constant. The derivative of  $\phi^s(t)$  with respect to the GPS time  $t$  is the satellite frequency, denoted by  $f^s(t)$ , i.e.,

$$\frac{d\phi^s(t)}{dt} = f^s(t) \tag{9.77}$$

Inserting the above two expressions into (9.75) yields

$$\begin{aligned}
 dt^s(t) &= dt^s(t_0) + \left[ \frac{1}{f} f^s(t) - 1 \right]_{t=\xi} \cdot (t-t_0) \\
 &= dt^s(t_0) + \frac{f^s(\xi) - f}{f} (t-t_0)
 \end{aligned} \tag{9.78}$$

or

$$dt^s(t) = dt^s(t_0) + \frac{\delta f^s(\xi)}{f} \cdot (t-t_0), \quad |\xi - t_0| \leq |t - t_0| \tag{9.79}$$

where



$\delta f^s(t)$ : satellite-frequency bias

Replacing  $t$  by  $(t-\tau)$  and  $t_0$  by  $\left(t^0 - \frac{\rho(t^0, t^0 - \tau^0)}{c}\right)$  in (9.79) gives

$$dt^s(t-\tau) = dt^s\left(t^0 - \frac{\rho(t^0, t^0 - \tau^0)}{c}\right) + \frac{\delta f^s(\xi)}{f} \left( t - t^0 - \tau + \frac{\rho(t^0, t^0 - \tau^0)}{c} \right), \tag{9.80}$$

$$\left| \xi - t^0 - \tau + \frac{\rho(t^0, t^0 - \tau^0)}{c} \right| \leq \left| t - t^0 - \tau + \frac{\rho(t^0, t^0 - \tau^0)}{c} \right|$$

which reads after noticing (9.53) and (9.54) and the definition of the clock bias ( $dt^r = t^r - t$ )

$$dt^s(t-\tau) = dt^s\left(t^0 - \frac{\rho(t^0, t^0 - \tau^0)}{c}\right) + \frac{\delta f^s(\xi)}{f} \left( -\delta(dt^r) - \tau + \frac{\rho(t^0, t^0 - \tau^0)}{c} \right), \tag{9.81}$$

$$\left| \xi - t^0 - \tau + \frac{\rho(t^0, t^0 - \tau^0)}{c} \right| \leq \left| t - t^0 - \tau + \frac{\rho(t^0, t^0 - \tau^0)}{c} \right|$$

From (9.62), (9.57), (9.58), and (9.51) to (9.53), we arrive at

$$\tau - \frac{\rho(t^0, t^0 - \tau^0)}{c} = \frac{1}{c} (\rho(t, t-\tau) - \rho(t^0, t^0 - \tau^0))$$

$$\leq \frac{1}{c} \left\{ \left| \frac{\partial \rho(t^0, t^0 - \tau^0)}{\partial t_1} \right| |\delta(dt^r)| + \left| \frac{\partial \rho(t^0, t^0 - \tau^0)}{\partial t_2} \right| (|\delta(dt^r)| + |\tau - \tau^0|) \right\}$$

$$< \frac{1}{2.9979 \cdot 10^8} (470 \cdot 10^{-3} + 4 \cdot 10^3 (10^{-3} + 0.01))$$

$$< 1.5 \cdot 10^{-7} \text{ s} \tag{9.82}$$

It was reported in [Rocken and Meertens 1991] that

$$|\delta f^s(t)| \leq \begin{cases} 0.001 \text{ Hz, SA off} \\ 2 \text{ Hz, SA on} \end{cases} \tag{9.83}$$

Therefore, we obtain for the L1 observable

$$\left| \frac{c}{f_1} \delta f^s(\xi) \left( -\delta(dt^r) - \tau + \frac{\rho(t^0, t^0 - \tau^0)}{c} \right) \right| < \begin{cases} 0.19 \cdot 10^{-3} (10^{-3} + 1.5 \cdot 10^{-7}) \approx 1.9 \cdot 10^{-7} \text{ m, SA off} \\ 0.19 \cdot 2 (10^{-3} + 1.5 \cdot 10^{-7}) \approx 3.8 \cdot 10^{-4} \text{ m, SA on} \end{cases} \tag{9.84}$$

and for the L2 observable

$$\left| \frac{c}{f_2} \delta f^s(\xi) \left( -\delta(dt^r) - \tau + \frac{\rho(t^0, t^0 - \tau^0)}{c} \right) \right| < \begin{cases} 0.244 \cdot 10^{-3} (10^{-3} + 1.5 \cdot 10^{-7}) \approx 2.4 \cdot 10^{-7} \text{ m, SA off} \\ 0.244 \cdot 2 (10^{-3} + 1.5 \cdot 10^{-7}) \approx 4.9 \cdot 10^{-4} \text{ m, SA on} \end{cases} \quad (9.85)$$

As can be seen from (9.84) and (9.85), even in the case of SA on, the size (multiplied by the speed of light) of the second term on the right-hand side of (9.81) is less than the carrier observation noises. Thus we may neglect it and (9.81) is reduced to

$$dt^s(t - \tau) = dt^s \left( t^0 - \frac{\rho(t^0, t^0 - \tau^0)}{c} \right) \quad (9.86)$$

Note that

- in the case of SA off (or the size of satellite frequency bias less than 0.001 Hz), (9.86) is valid within the order of  $2.4 \cdot 10^{-7}$  m, after being multiplied by the speed of light;
- in the case of SA on (or the size of satellite frequency bias not greater than two Hz), (9.86) is valid within the order of  $4.9 \cdot 10^{-4}$  m, after being multiplied by the speed of light.

### 9.4.3 Expansion of observation equations

Based on the results derived in the previous two sub-sections, the Taylor expansion of GPS L1 and L2 code and carrier observation equations can be easily obtained as follow

$$P(t) = c_1 \cdot \rho(t^0, t^0 - \tau^0) + c_2 \cdot \delta(dt^r(t)) - c \cdot dt^s \left( t^0 - \frac{\rho(t^0, t^0 - \tau^0)}{c} \right) + \nabla^{p_0}(t) + I(t) + c_3 + e(t) \quad (9.87)$$

$$\bar{P}(t) = c_1 \cdot \rho(t^0, t^0 - \tau^0) + c_2 \cdot \delta(dt^r(t)) - c \cdot dt^s \left( t^0 - \frac{\rho(t^0, t^0 - \tau^0)}{c} \right) + \nabla^{p_0}(t) + r \cdot I(t) + c_3 + \bar{e}(t) \quad (9.88)$$

$$\lambda_1 \phi(t) = c_1 \cdot \rho(t^0, t^0 - \tau^0) + c_2 \cdot \delta(dt^r(t)) - c \cdot dt^s \left( t^0 - \frac{\rho(t^0, t^0 - \tau^0)}{c} \right) + \nabla^{p_0}(t) - I(t) + \lambda_1 \cdot A(t_0) + c_3 + \eta(t) \quad (9.89)$$

$$\lambda_2 \tilde{\Phi}(t) = c_1 \cdot \rho(t^0, t^0 - \tau^0) + c_2 \cdot \delta(dt^r(t)) - c \cdot dt^s(t^0 - \frac{\rho(t^0, t^0 - \tau^0)}{c}) + \nabla^{ro}(t) - r \cdot I(t) + \lambda_2 \cdot \tilde{A}(t_0) + c_3 + \tilde{\eta}(t) \tag{9.90}$$

where

$$\left. \begin{aligned} c_1 &= 1 - \frac{1}{c} \frac{\partial \rho(t^0, t^0 - \tau^0)}{\partial t_2} + \left( \frac{1}{c} \frac{\partial \rho(t^0, t^0 - \tau^0)}{\partial t_2} \right)^2 \\ c_2 &= c - \left( \frac{\partial}{\partial t_1} + \frac{\partial}{\partial t_2} \right) \rho(t^0, t^0 - \tau^0) \\ c_3 &= \left( 1 - \frac{1}{c} \frac{\partial \rho(t^0, t^0 - \tau^0)}{\partial t_2} \right) \frac{\partial \rho(t^0, t^0 - \tau^0)}{\partial t_2} \tau^0 \\ \tau^0 &= 0.077 \text{ s} \\ t^0 &= t^r - dt^r \\ \delta(dt^r(t)) &= dt^r(t) - dt^r \end{aligned} \right\} \tag{9.91}$$

As can be seen from the previous discussion, the above Taylor expansion of GPS observation equations has the following properties.

- It does not contain the travel time of a GPS signal, therefore, solving it does not need iterations or code observations for computing the satellite position and the satellite-clock bias. Because of this, we can save computing time and avoid the impact of any gross errors in code observations on determining satellite positions, satellite-clock biases, and consequently on the computed observations.
- It contains only up to first-order derivative terms, thus it is quite simple.
- The expansion makes it possible to determine the exact coefficients of linearized GPS observation equations.
- The assumptions underlying the expansion are
  - the size of the correction to receiver clock biases is less than one millisecond;
  - the size of satellite-frequency bias is not greater than two Hz.

### 9.5 A simplified expression for the partial derivative of satellite-receiver distances

In the previous section, the formulas were given to compute the partial derivatives of the satellite-receiver distance, which are included in the Taylor expansion of GPS observation equations. The details of the computation can be found in [Jin 1995b]. Although there is no problem using the formulas as they are, we will show below that for most GPS applications

the computation of the partial derivative of  $\rho(t_1, t_2)$  with respect to  $t_1$  can be further simplified.

Define

$r_b^r$ : position vector of a receiver at the WGS 84 system (body frame)

$\Omega$ : angle of the x-axis of the WGS 84 system with respect to the x-axis of the convention inertial system [King et al. 1985], [Seeber 1993]

$\dot{\Omega}_e$ : angular velocity with which the WGS 84 system rotates around the z-axis of the inertial system

Then the position of a receiver in the inertial system reads

$$r^r(t) = R_3(-\Omega(t)) r_b^r(t) \quad (9.92)$$

where

$$\Omega(t) = \dot{\Omega}_e \cdot t \quad (9.93)$$

$$R_3(-\Omega) = \begin{bmatrix} \cos \Omega & -\sin \Omega & 0 \\ \sin \Omega & \cos \Omega & 0 \\ 0 & 0 & 1 \end{bmatrix} \quad (9.94)$$

Since

$$\dot{r}^r(t) = \omega_e \times r^r(t) + R_3(-\Omega(t)) \dot{r}_b^r(t) \quad (9.95)$$

where

$$\omega_e = \begin{bmatrix} 0 & 0 & \dot{\Omega}_e \end{bmatrix}^* \quad (9.96)$$

(see [Jin 1995b]), substituting (9.95) into (9.40) gives

$$\begin{aligned} \frac{\partial \rho(t_1, t_2)}{\partial t_1} &= \frac{-1}{\rho(t_1, t_2)} \langle \omega_e \times r^r + R_3(-\Omega) \dot{r}_b^r, r^s - r^r \rangle \\ &= \frac{-1}{\rho(t_1, t_2)} (\langle \omega_e \times r^r, r^s \rangle - \langle \omega_e \times r^r, r^r \rangle + \langle R_3(-\Omega) \dot{r}_b^r, r^s - r^r \rangle) \end{aligned} \quad (9.97)$$

since  $\omega_e \times r^r$  is orthogonal to  $r^r$ , i.e.

$$\langle \omega_e \times r^r, r^r \rangle = 0 \quad (9.98)$$

As can be seen from (9.64), the partial derivative  $\frac{\partial \rho(t_1, t_2)}{\partial t_1}$  only appears in the coefficient

of the correction to the receiver clock bias in the Taylor expansion of GPS observation equations. For most GPS applications, a receiver is either static or moving with speed of less than 100 m/s in the WGS-84 coordinate system. As we know, for dynamic GPS applications the sampling interval is generally quite small (a few seconds), therefore in this case it may be possible to have an approximate value for the receiver clock bias that is accurate up to  $10^{-5}$  seconds. Based on these properties, we may assume

$$\left. \begin{aligned} \text{or} \quad & \|r_b^r\| = 0 \\ & \|r_b^r\| < 100 \frac{m}{s} \quad \text{and} \quad |\delta(dt^r)| < 10^{-5} s \end{aligned} \right\} \quad (9.99)$$

Thus

$$\left| \frac{\langle R_3(-\Omega)r_b^r, r^s - r^r \rangle}{\rho(t_1, t_2)} \right| |\delta(dt^r)| \leq \frac{\|R_3(-\Omega)r_b^r\| \|r^s - r^r\|}{\rho(t_1, t_2)} |\delta(dt^r)| = \|r_b^r\| |\delta(dt^r)| < 100 \cdot 10^{-5} = 10^{-3} m \quad (9.100)$$

which means that the last term in (9.97) is negligible when computing the partial derivative  $\frac{\partial \rho(t_1, t_2)}{\partial t_1}$  for the Taylor expansion of GPS observation equations. Therefore, using (9.98) we arrive at

$$\frac{\partial \rho(t_1, t_2)}{\partial t_1} = \frac{-1}{\rho(t_1, t_2)} \langle \omega_e \times r^r, r^s \rangle \quad (9.101)$$

Defining the satellite-position vector  $r^s$  and the receiver-position vector  $r^r$  in the inertial system as

$$\left. \begin{aligned} r^s &= [x^s \ y^s \ z^s]^* \\ r^r &= [x^r \ y^r \ z^r]^* \end{aligned} \right\} \quad (9.102)$$

it follows that

$$\omega_e \times r^r = \dot{\Omega}_e [-y^r \ x^r \ 0]^* \quad (9.103)$$

$$\langle \omega_e \times r^r, r^s \rangle = \dot{\Omega}_e (-y^r x^s + x^r y^s) \quad (9.104)$$

we finally arrive at

$$\frac{\partial \rho(t_1, t_2)}{\partial t_1} = \frac{\dot{\Omega}_e}{\rho(t_1, t_2)} (y^r x^s - x^r y^s) \quad (9.105)$$

There is one remark on the size of corrections to receiver clock biases. Based on some numerical results of Trimble 4000 SST receivers, it was found that the maximum rate of the receiver clock bias is less than  $5 \cdot 10^{-7}$ . In this case if the estimate of the receiver clock bias at epoch  $k-1$ , denoted by  $\hat{dt}^r(t_{k-1})$ , is used as the approximate value of the receiver clock bias at epoch  $k$ , i.e. choosing

$$\hat{dt}^{r^0}(t_k) = \hat{dt}^r(t_{k-1}) \quad (9.106)$$

then even for a sampling interval of 20 seconds, the correction to the receiver clock bias is less than  $10^{-5}$  seconds, because

$$\begin{aligned} |\delta(dt^r(t_k))| &= |dt^r(t_k) - \hat{dt}^{r^0}(t_k)| = |dt^r(t_k) - \hat{dt}^r(t_{k-1})| \\ &< 5 \cdot 10^{-7} \cdot 20 = 10^{-5} \text{ s} \end{aligned} \quad (9.107)$$

Of course, the size of  $\delta(dt^r(t_k))$  may vary from receiver to receiver and even from time to time, depending on the stability of the receiver clock. But for most dynamic GPS applications, the sampling intervals are certainly shorter than 20 seconds and moreover the approximate value of the receiver clock bias can be further improved by predicting it for the current epoch instead of choosing its estimate at the previous epoch. In short, inequality (9.100) will be valid in most GPS applications, therefore (9.105) can be used in general.

## 9.6 Concluding remarks

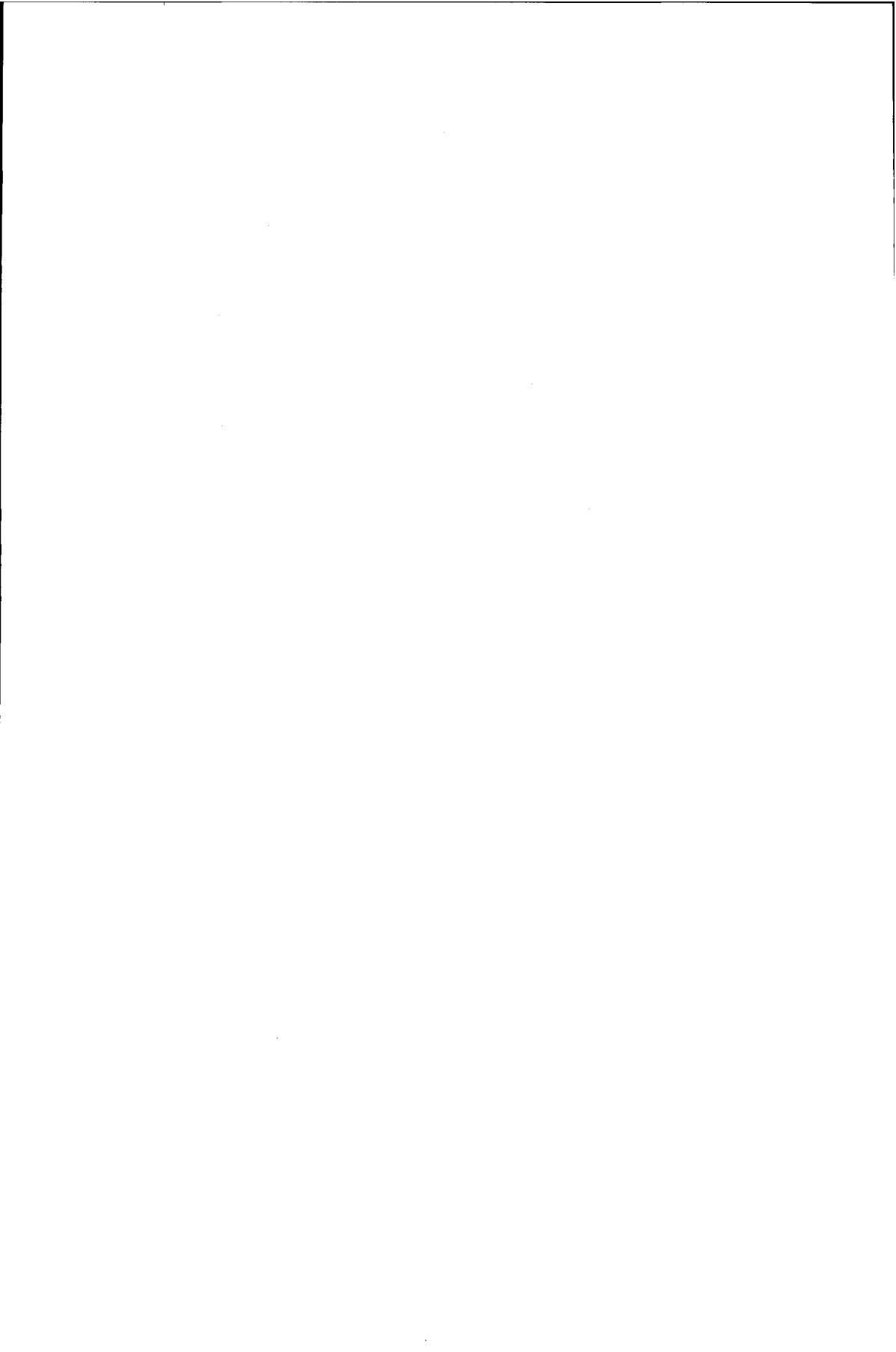
Based on the discussions and results in the previous sections, some important points are summarized below.

- An alternative derivation of carrier observation equations is given. The main difference between this derivation and many others is that no assumptions are made on the stability of satellite clocks. In addition, this derivation can clearly show what a carrier observable ambiguity consists of, so that one can exactly know what is cancelled in single, double or triple differences of carrier observations.
- It is proved that GPS observation equations can be expressed in the Taylor expansion which contains only up to first-order derivative quantities.
- Since the Taylor expansion does not contain the travel time of a GPS signal, solving it does not need iterations or code observations for the determination of the transmission time of the signal. As a result, the use of the Taylor expansion can save computing time and can avoid the impacts of any gross errors in code observations on determining satellite positions and satellite-clock biases, and consequently on the computed observations. In addition, it makes it possible to determine the exact coefficients of linearized GPS observation equations.
- The main assumptions underlying the Taylor expansion of GPS observation equations

are

- the size of the correction to receiver-clock biases is less than one millisecond;
- the size of satellite-frequency biases is less than two Hz.

Two remarks are worth making. First, the Taylor expansion of GPS observation equations has been used in a DGPS positioning system, which is based on the algorithms for carrier adjusted DCs and for carrier adjusted DGPS positioning. It has been shown that this approach works well. Second, many numerical checks have been carried out by computing satellite-receiver range using two different approaches. One is the above Taylor expansion algorithm and the other is the algorithm based on code observations. It was found that the differences between them were about  $10^9$  metres.





## Chapter 10

# Conclusions

This research has derived a new algorithm for the generation of carrier adjusted DCs. The new algorithm has some distinct features. First of all, this algorithm directly uses code and carrier observations in the measurement model of a Kalman filter, so that the measurements are not correlated in time if code and carrier observations can be assumed to have no time correlations. This makes it possible to use a simple stochastic observation model and to use the standard algorithm of the Kalman filter. Secondly, the algorithm accounts for biases like multipath errors and instrumental delays in code observations. It explicitly shows how code biases affect carrier adjusted DCs when dual or single frequency data is used. Thirdly, the algorithm can be easily integrated with the DIA quality control procedure, so that the quality of the estimated states can be guaranteed with a certain probability. Fourthly, in addition to generation of DCs, it also produces the change of ionospheric delays and that of code biases with time. It can, therefore, be used to investigate properties of ionospheric delays and code biases. Finally, all state estimates including DCs are not affected by the opposite influence of ionospheric delays on code and carrier observations.

By using dual-frequency data with a sampling interval of one second, the dynamic behaviour of SA clock errors and that of ionospheric delays can well be modelled by quadratic and linear functions, respectively. The modelling accuracy can be within a few millimetres.

Code biases were found and they may behave linearly and periodically with time. For the same receiver, code biases related to different satellites may have different behaviours and those related to the same satellite but observed at different frequencies (i.e. L1 and L2) may also behave differently.

Model testing experiments with simulated errors showed that cycle slips as small as one cycle can indeed successfully be detected and identified in real time. The DIA quality control procedure allows for detection and identification of single as well as multiple model errors. However the mean of the LOM test statistic is always smaller than its expectation, and the reasons need to be further investigated.

Based on carrier adjusted DCs, it has been shown that with increasing DC latencies, the accuracy of DC prediction decreases quadratically when SA clock errors are present and linearly when SA clock errors are absent. For latencies within 5, 10 and 15 seconds, the accuracies are usually within 0.05, 0.2 and 0.5 m, respectively. Using DC-acceleration estimates in the DC prediction can improve or worsen the accuracy when SA clock errors

are present or absent, respectively. But the deteriorated accuracies related to satellites without SA clock errors are still better than the improved ones related to satellites with SA clock errors. For latencies within 15 seconds, the accuracy of DC prediction based on DC-acceleration estimates can usually be reduced to below 0.2 metres.

By the use of code predicted residuals, the relationship between satellite elevation and the precision of GPS code observations was investigated, on the basis of data collected by TurboRogue SNR-8000, Trimble 4000 SSE and Trimble 4000 SST receivers. It turned out that the decrease of GPS code precision with decreasing elevation is very obvious at low elevations. When satellite elevation increases, the precision becomes more and more stable. The relationship between satellite elevation and the precision of code observations can quite well be modelled by an exponential function of the form  $y = a_0 + a_1 \cdot \exp\{-x/x_0\}$ , where  $y$  (the RMS error),  $a_0$  and  $a_1$  have units of metres, and  $x$  (elevation) and  $x_0$  are in degrees. For different types of receivers and different types of code observables, the parameters  $a_0$ ,  $a_1$  and  $x_0$  may be different.

An algorithm for carrier adjusted DGPS positioning has been developed. This algorithm can be applied at a mobile site when code and carrier observations are available. The algorithm directly uses code and carrier observations, rather than carrier filtered code observations, as input, therefore the stochastic model of observations can be easily specified. The algorithm can be applied in the case that the dynamic behaviour of mobile positions and receiver clock biases can or cannot be modelled. In the former case, the algorithm provides recursive estimates of mobile positions, whereas in the latter case, it provides instantaneous estimates of mobile positions. Since in the use of the algorithm there always exist redundancy, the algorithm can particularly well be integrated with a real time quality control procedure so as to ensure the quality of position estimates with a certain probability.

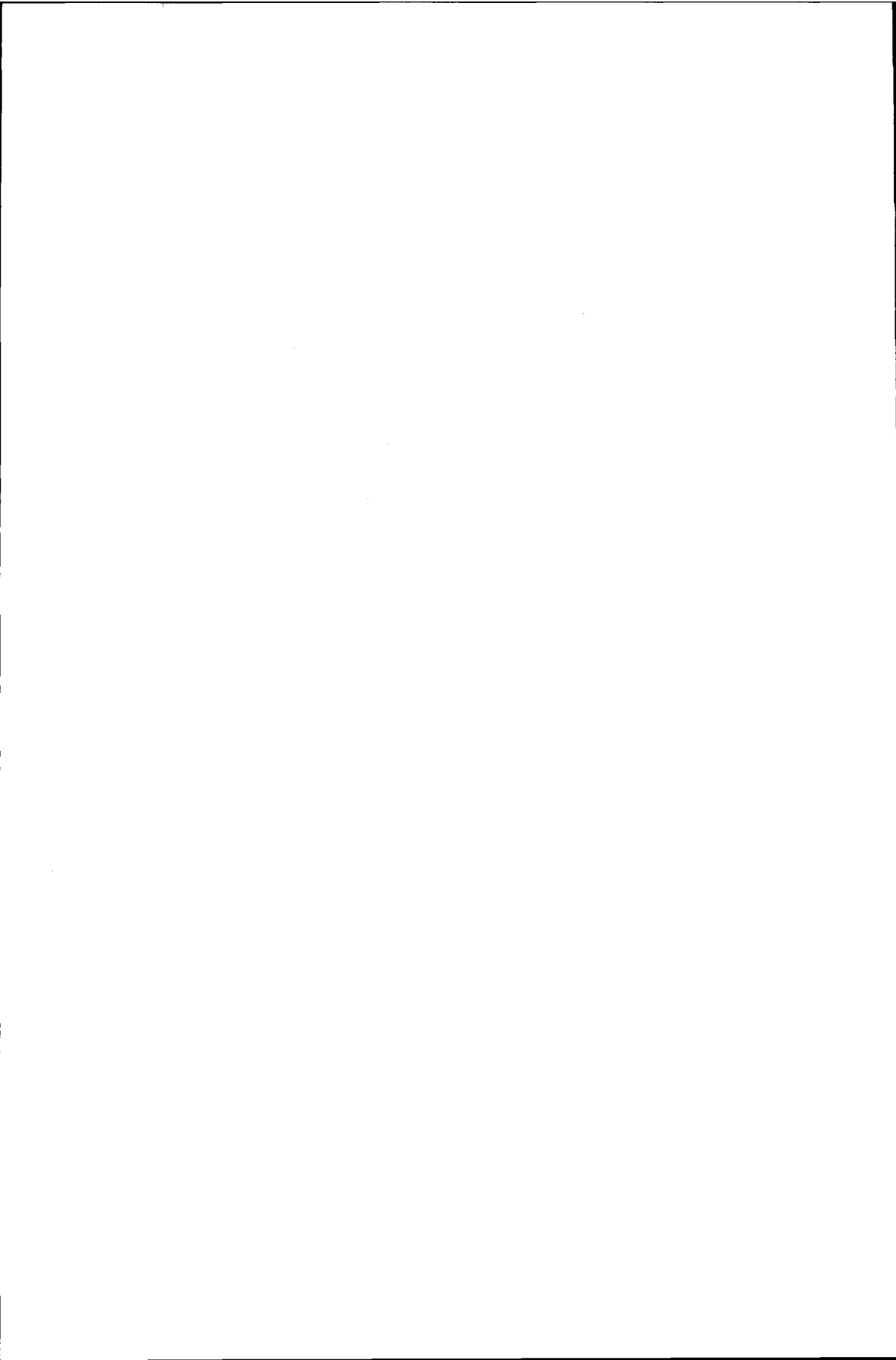
Based on data collected at two stations, which were 100 km apart, DGPS positioning experiments have been carried out by using the algorithms for carrier adjusted DCs and for carrier adjusted DGPS positioning. When dual-frequency data was used at both reference and mobile stations, half-metre instantaneous positioning accuracy was achieved. When the data used at the mobile station was replaced by single-frequency data (L1 code and carrier), the accuracy was still better than 7.5 decimeters. It was shown that the use of an elevation-dependent standard deviation for code observations can improve DGPS positioning accuracies and that it is more important to use dual-frequency data at a reference station than at a mobile station.

When ephemeris errors, vertical ionospheric delays, and vertical tropospheric delays are less than 10, 4.5, and 2.6 metres, respectively, using three reference stations in a 500×500 km<sup>2</sup> area can reduce the effect of ephemeris errors to one decimeter, ionospheric delays to less than two decimeters, and tropospheric delays to less than 2.5 decimeters. If a tropospheric delay model is used, the tropospheric delays can be further reduced to less than one decimeter.

GPS observation equations can be expanded into Taylor series which contain only up to

---

first-order derivative quantities. Since the Taylor expansion does not contain the travel time of a GPS signal, solving it does not need iterations or code observations for the determination of the transmission time of the GPS signal. As a result, the use of the Taylor expansion can save computing time and can avoid the impact of any gross errors in code observations on determining satellite positions and satellite-clock biases, and consequently on computed observations. In addition, it also makes it possible to determine the exact coefficients of linearized GPS observation equations.



# References

- Alsip DH, Butler JM, Radice JT (1992) *The Coast Guard's Differential GPS Program*. Navigation: Journal of The Institute of Navigation 39(4): 345-361
- Ashjaee J (1990) *Ashtech XII GPS Technology*. In: Proceedings of IEEE PLANS '90 Position Location and Navigation Symposium, Las Vegas, pp 184-190
- Ashkenazi V, Hill CJ, Ochieng WY (1993) *Wide-Area Differential GPS: A Performance Study*. Navigation: Journal of The Institute of Navigation 40(3): 297-319
- Ashkenazi V, Moore T, Hill CJ, Cross P, Roberts W, Hawksbee D, Mollon K, Winchester D, Jackson T (1994) *Standards for Benchmarking Differential GPS*. In: Proceedings of ION GPS-94, The Institute of Navigation, Alexandria, VA, pp 1285-1290
- Axelrad P, Brown RG (1996) *GPS Navigation Algorithms*. In: Parkinson BW, Spilker Jr JJ, Axelrad P, Enge P (eds), *Global Positioning System: Theory and Applications*, Vol. I, American Institute of Aeronautics and Astronautics, Inc., pp 409-433
- Baarda W (1968) *A Testing Procedure for Use in Geodetic Networks*. Netherlands Geodetic Commission, Publications on Geodesy, New Series, Vol. 2(5), Delft, The Netherlands
- Bakker R, Lapucha D (1994) *Performance Comparison of Two Methods of Multiple Reference Stations DGPS*. In: Proceedings of ION GPS-94, The Institute of Navigation, Alexandria, VA, pp 1035-1041
- Beser J, Parkinson BW (1982) *The Application of NAVSTAR Differential GPS in the Civilian Community*. Navigation: Journal of The Institute of Navigation 29(2): 107-136
- Blackwell EG (1985) *Overview of Differential GPS Methods*. Navigation: Journal of The Institute of Navigation 32(2): 114-125
- Breeuwer EJ, Moelker DJ, van Willigen D (1993) *The MSL Integrated Approach System: Hybrid Position Calculation and Initial Flight Results*. In: Proceedings of Workshop: Integrated Navigation, Netherlands Institute of Navigation, Amsterdam

- Brown A (1989) *Extended Differential GPS*. Navigation: Journal of The Institute of Navigation 36(3): 265-286
- Brown RG, Hwang PYC (1992) *Introduction to Random Signals and Applied Kalman Filtering*. John Wiley & Sons, New York Chichester Brisbane Toronto Singapore
- Brunner FK, Tregoning P (1994) *Tropospheric Propagation Effects in GPS Height Results Using Meteorological Observations*. Australian Journal of Geodesy, Photogrammetry and Surveying 60: 49-65
- Casewell I, Basker S, Johnson G, Håkegård O, Forssel B, Hein G, Oskam D (1994) *A European Wide Area DGPS Experiment: Final Results*. In: Proceedings of ION GPS-94, The Institute of Navigation, Alexandria, VA, pp 1547-1557
- de Cevins J, Ponsot P (1995) *A340-DGPS Landing Experiment*. In: Proceedings of ION GPS-95, The Institute of Navigation, Alexandria, VA, pp 763-772
- Chao YC, Tsai YJ, Walter T, Kee C, Enge P, Parkinson B (1995a) *The Ionospheric Model Improvement for the Stanford WAAS Network*. In: Proceedings of the 1995 National Technical Meeting, The Institute of Navigation, Alexandria, VA, pp 531-538
- Chao YC, Tsai YJ, Walter T, Kee C, Enge P, Parkinson B (1995b) *An Algorithm for Inter-frequency Bias Calibration and Application to WAAS Ionosphere Modelling*. In: Proceedings of ION GPS-95, The Institute of Navigation, Alexandria, VA, pp 639-646
- Clynch JR, Thurmond G, Rosenfeld L, Schramm R (1992) *Error Characteristics of GPS Differential Positions and Velocities*. In: Proceedings of ION GPS-92, The Institute of Navigation, Alexandria, VA, pp 969-978
- van Dierendonck AJ (1993) *Receiver Technology, Developments and Performance, and RTCM Data Link Standards for Precision Differential Operation*. In: Navtech Seminars Inc., Dynamic Real Time DSNS (Part I), Navtech Seminars Inc., USA
- van Dierendonck AJ, Enge P (1994) *The Wide Area Augmentation System (WAAS) Signal Specification*. In: Proceedings of ION GPS-94, The Institute of Navigation, Alexandria, VA, pp 985-994
- van Dierendonck AJ (1995) *Understanding GPS Receiver Technology: A Tutorial*. GPS World, 6(1): 34-44
- Euler H, Goad C (1991) *On Optimal Filtering of GPS Dual Frequency Observations without Using Orbit Information*, Bulletin Géodésique 65: 130-143

- Feess WA, Stephens SG (1987) *Evaluation of GPS Ionospheric Time-Delay Model*. IEEE Transactions on Aerospace and Electronic Systems 23(3): 332-338
- Forbes F, Ryan S, Wee S (1994) *The Canadian Coast Guard DGPS Project*. In: Proceedings of ION GPS-94, The Institute of Navigation, Alexandria, VA, pp 1451-1460
- Fruehauf H (editor) (1991) *Precision Time and Frequency Handbook*. Ball Corporation, Efratom Division, USA
- Gelb A (editor) (1974) *Applied Optimal Estimation*. The Massachusetts Institute of Technology Press, Cambridge, Massachusetts, and London, England
- Goad C (1990) *Optimal Filtering of Pseudorange and Phases from Single-Frequency GPS Receivers*. Navigation: Journal of The Institute of Navigation 37(3): 249-262
- Gouldman M, Hermann B, Weedon D (1989) *Evaluation of GPS Production Ephemeris and Clock Quality*. In: Proceedings of the Fifth International Geodetic Symposium on Satellite Positioning, Physical Science Laboratory, New Mexico State University, Vol. 1, pp 210-222
- GPS-WG (1992) *GPS Observation Equations (Continued)*. GPS Working Group Lecture 9, Delft Geodetic Computing Centre, Faculty of Geodetic Engineering, Delft University of Technology, The Netherlands
- GSD (1993) *GPS Positioning Guide*. Geodetic Survey Division, Energy, Mines and Resources, Canada
- Gurtner W (1994) *RINEX: The Receiver-Independent Exchange Format*. GPS World 5(7): 48-52
- Hatch R (1982) *The Synergism of GPS Code and Carrier Measurements*. In: Proceedings of the Third International Geodetic Symposium on Satellite Doppler Positioning, Las Cruces, New Mexico, February 8-12, pp 1213-1232
- Hofmann-Wellenhof B, Lichtenegger H, Collins J (1992) *Global Positioning System Theory and Practice*. Springer-Verlag, Wien New York
- Hwang PYC, Brown RG (1990) *GPS Navigation: Combining Pseudorange with Continuous Carrier Phase Using a Kalman Filter*. Navigation: Journal of The Institute of Navigation 37(2): 181-196
- Jin XX (1995a) *A Recursive Procedure for Computation and Quality Control of GPS Differential Corrections*. Publications of the Delft Geodetic Computing Centre, LGR-Series No. 8, Delft University of Technology, The Netherlands

- Jin XX (1995b) *Taylor Expansion of GPS Observation Equations*. Publications of the Delft Geodetic Computing Centre, LGR-Series No. 11, Delft University of Technology, The Netherlands
- Jin XX (1995c) *The Change of GPS Code Accuracy with Satellite Elevation*. In: Proceedings of The 4th International Conference on Differential Satellite Navigation Systems (DSNS), The Nordic Institute of Navigation
- Jin XX, van der Marel H, de Jong C (1995) *Computation and Quality Control of Differential GPS Corrections*. In: Proceedings of ION GPS-95, The Institute of Navigation, Alexandria, VA, pp 1071-1079
- Jin XX, de Jong C (1995) *Prediction Accuracy of Differential GPS Corrections and its Change with Latency*. GPS Nieuwsbrief, Netherlands Geodetic Commission, 10<sup>e</sup> jaargang No. 2, pp 1-6
- Jin XX, de Jong C (1996a) *Relationship between Satellite Elevation and Precision of GPS Code Observations*. The Journal of Navigation 49(2): 253-265
- Jin XX, de Jong C (1996b) *Improvement of DGPS Performance in Medium Areas by Using a Network of DGPS Reference Stations*. In: Proceedings of The 5th International Conference on Differential Satellite Navigation Systems (DSNS), The Russian Institute of Radionavigation and Time
- Jin XX (1996a) *A New Algorithm for Generating Carrier Adjusted Differential GPS Corrections*. Journal of Geodesy 70(11)
- Jin XX (1996b) *Algorithm for Carrier Adjusted DGPS Positioning*. In: Proceedings of ION GPS-96, The Institute of Navigation, Alexandria, VA
- de Jong C (1990) *GPSNav A PC Software Package for real-time Differential Positioning with GPS*. GPS Nieuwsbrief, Netherlands Geodetic Commission, 5<sup>e</sup> jaargang No. 1, pp 16-31
- Kalman RE (1960) *A New Approach to Linear Filtering and Prediction Problems*. ASME Journal of Basic Engineering 82: 34-45
- Kee C, Parkinson BW, Axelrad P (1991) *Wide Area Differential GPS*. Navigation: Journal of The Institute of Navigation 38(2): 123-146
- King RW, Masters EG, Rizos C, Stolz A, Collins J (1985) *Surveying with GPS*. School of Surveying, University of New South Wales, Kensington, Australia
- Klobuchar JA (1987) *Ionospheric Time-Delay Algorithm for Single-Frequency GPS Users*. IEEE Transactions on Aerospace and Electronic Systems 23(3): 325-331



- Klobuchar JA, Doherty PH (1990) *The Statistics of Ionospheric Time Delay for GPS Ranging on L1*. In: Proceedings of ION GPS-90, The Institute of Navigation, Alexandria, VA, pp 161-168
- Koch KR (1982) *Kalman Filter and Optimal Smoothing Derived by the Regression Model*. Manuscripta Geodaetica 7(2): 133-144
- Kremer GT, Kalafus RM, Loomis PVW, Reynolds JC (1990) *The Effect of Selective Availability on Differential GPS Corrections*. Navigation: Journal of The Institute of Navigation 37(1): 39-52
- Lachapelle G, Kielland P, Casey M (1992) *GPS for Marine Navigation and Hydrography*. International Hydrographic Review, Monaco, LXIX(1): 43-69
- Lachapelle G, Cannon ME, Lan H, Tang C, Wee S, Ryan S (1995) *DGPS Positioning Accuracy Performance Analysis with RTCM Message Types 1/9 and 18-21 Using Various Receiver Technologies*. In: Proceedings of ION GPS-95, The Institute of Navigation, Alexandria, VA, pp 899-906
- Landau H (1988) *On the Use of the Global Positioning System in Geodesy and Geodynamics: Model Formulation, Software Development, and Analysis*. PhD thesis, Civil Engineering and Surveying Faculty, University of the Federal Armed Forces, Munich, Germany
- Landau H (1993) *Differential System Design, Error Analysis and Performance*. In: Navtech Seminars Inc., Fundamentals of Differential Satellite Navigation Systems, Navtech Seminars Inc., USA
- Langley RB (1994) *RTCM SC-104 DGPS Standard*. GPS World 5(5): 48-53
- Leick A (1990) *GPS Satellite Surveying*. John Wiley & Sons, New York
- LGR (1982) *The Delft Approach for the design and Computation of Geodetic Networks*. In: Forty Years of Thought, Delft Geodetic Computing Centre (LGR), Faculty of Geodetic Engineering, Delft University of Technology, The Netherlands
- Loomis P (1986) *Design Document for Differential GPS Ground Reference Station Pseudorange Correction Generation Algorithm*. DOT-CG-N-03-86, US Department of Transportation
- Loomis P, Kremer G, Reynolds J (1989) *Correction Algorithm for Differential GPS Reference Stations*. Navigation: Journal of The Institute of Navigation, 36(2): 179-193
- Loomis P, Sheynblat L, Mueller T (1991) *Differential GPS Network Design*. In: Proceedings of ION GPS-91, The Institute of Navigation, Alexandria, VA, pp

511-520

- van der Marel H (1993) *Modelling of GPS Ionospheric Delays for Geodetic Applications*. Presented at URSI commission G meeting, Eindhoven, The Netherlands
- van der Marel H, Georgiadou Y (1994) *TEC-observations from GPS under Anti-Spoofing*. In: Kersley L (ed), *Proceedings of the International Beacon Satellite Symposium*, University of Wales, Aberystwyth UK, pp 5-8
- McNally BD, Warner DN, Hegarty DM, Schultz TA, Bronson R (1991) *Flight Evaluation of Precision Code Differential GPS for Terminal Area Positioning*. In: *Proceedings of ION GPS-91*, The Institute of Navigation, Alexandria, VA, pp 557-569
- Mikhail EM (1976) *Observations and Least Squares*. Harper & Row, New York
- Mueller II, Zerbini S (editors) (1989) *The Interdisciplinary Role of Space Geodesy*. Lecture Notes in Earth Sciences Vol. 22, Springer, Berlin
- Mueller T (1994a) *Minimum Variance Network DGPS Algorithm*. In: *Proceedings of IEEE PLANS '94 Position Location and Navigation Symposium*, pp 418-425
- Mueller T (1994b) *Wide Area Differential GPS*. *GPS World* 5(6): 36-44
- NATO (1991a) *NAVSTAR GPS User Equipment: introduction*. US Air Force Space Systems Division, NAVSTAR-GPS Joint Program Office at Los Angeles Air Force Base, California, USA
- NATO (1991b) *Technical Characteristics of the NAVSTAR GPS*. NATO NAVSTAR GPS Project Steering Committee
- NGS (1986) *Geodetic Glossary*. National Geodetic Survey, National Oceanic and Atmospheric Administration, USA
- Parkinson BW, Enge PK (1996) *Differential GPS*. In: Parkinson BW, Spilker Jr JJ, Axelrad P, Enge P (eds), *Global Positioning System: Theory and Applications*, Vol. II, American Institute of Aeronautics and Astronautics, Inc., pp 3-50
- Pietraszewski D, Spalding J, Viehweg L, Luft L (1988) *U.S. Coast Guard Differential GPS Navigation Field Test Findings*. *Navigation: Journal of The Institute of Navigation* 35(1): 55-72
- Remondi BW (1984) *Using the Global Positioning System (GPS) Phase Observable for Relative Geodesy: Modelling, Processing, and Results*. Doctoral Dissertation. Centre for Space Research, University of Texas at Austin, USA

- Remondi BW (1985) *Global Positioning System Carrier Phase: Description and Use*. Bulletin Géodésique 59: 361-377
- Roberts WDS, Cross PA (1993) *The Effect of DGPS Temporal Correlation within the Kalman Filter Applied to Offshore Positioning*. The Hydrographic Journal 67: 5-11
- Rocken C, Meertens C (1991) *Monitoring selective availability dither frequencies and their effect on GPS data*. Bulletin Géodésique 65: 162-169
- Rothacher M, Beutler G, Gurtner W, Brockmann E, Mervart L (1993) *Bernese GPS Software V3.4: Documentation*.
- RTCM SC-104 (1994) *RTCM Recommended Standards for Differential NAVSTAR GPS Service*. Radio Technical Commission for Maritime Services, Washington, D.C., USA
- Saastamoinen J (1972) *Atmospheric Correction for the Troposphere and Stratosphere in Radio Ranging of Satellites*. In: Henriksen SW, Mancini A, Chovitz BH (eds), *The Use of Artificial Satellites for Geodesy*, Geophysical Monograph 15, American Geophysical Union, Washington DC, pp 247-251
- Saastamoinen J (1973) *Contributions to the Theory of Atmospheric Refraction*. Bulletin Géodésique 107: 13-34
- Salzmann MA (1993) *Least Squares Filtering and Testing for Geodetic Navigation Applications*. PhD thesis, Faculty of Geodetic Engineering, Delft University of Technology, The Netherlands
- Seeber G (1993) *Satellite Geodesy: Foundations, Methods, and Applications*. Walter de Gruyter, Berlin New York
- Tang W, Johnson N, Graff J (1989) *Differential GPS Operation with Multiple Ground Reference Stations*. In: Proceedings of ION GPS-89, The Institute of Navigation, Alexandria, VA, pp 319-323
- Teunissen PJG (1984) *Quality Control in Geodetic Networks*. In: Grafarend E, Sansò F (eds), *Optimization and Design of Geodetic Networks*, Springer Verlag, Berlin, pp 526-547
- Teunissen PJG, Salzmann MA (1988) *Performance Analysis of Kalman Filters*. Report 88.2, Section of Mathematical and Physical Geodesy, Faculty of Geodetic Engineering, Delft University of Technology, The Netherlands
- Teunissen PJG (1989) *Inleiding Toetsingstheorie*. Lecture Notes, Faculty of Geodetic Engineering, Delft University of Technology, The Netherlands

- Teunissen PJG, Salzmann MA (1989) *A Recursive Slippage Test for Use in State-Space Filtering*. *Manuscripta Geodaetica* 14(6): 383-390
- Teunissen PJG (1990a) *Quality Control in Integrated Navigation Systems*. In: Proceedings of IEEE PLANS '90 Position Location and Navigation Symposium, Las Vegas, pp 158-165
- Teunissen PJG (1990b) *An Integrity and Quality Control Procedure for Use in Multi Sensor Integration*. In: Proceedings of ION GPS-90, The Institute of Navigation, Alexandria, VA, pp 513-522
- Teunissen PJG (1990c) *Dynamische Gegevensverwerking I, inleiding filtertheorie*, Lecture Notes, Faculty of Geodetic Engineering, Delft University of Technology, The Netherlands
- Teunissen PJG (1991) *The GPS Phase-Adjusted Pseudorange*. In: Proceedings of the Second International Workshop on High Precision Navigation, Stuttgart/Freudenstadt, November, pp 115-125
- Teunissen PJG (1994) *Mathematische Geodesie I: Inleiding vereffeningstheorie*. Lecture Notes, Faculty of Geodetic Engineering, Delft University of Technology, The Netherlands
- Wells DE, Beck N, Delikaraoglou D, Kleusberg A, Krakiwsky EJ, Lachapelle G, Langley RB, Nakiboglu M, Schwarz KP, Tranquilla JM, Vaníček P (1987) *Guide to GPS Positioning*. Canadian GPS Associates, Fredericton, New Brunswick, Canada

## Appendix A

# Dynamic model with a constant acceleration or velocity

This appendix derives the dynamic model with a constant acceleration and the dynamic model with a constant velocity.

### A.1 Dynamic model with a constant acceleration

Let  $S(t)$  be a random process and its third-order time derivative, denoted by  $\ddot{\bar{S}}(t)$ , be a zero-mean white noise process with constant spectral density  $q_{\ddot{\bar{S}}}$ . It follows that

$$E\{\ddot{\bar{S}}(t)\} = 0 \quad (\text{A.1})$$

$$E\{\ddot{\bar{S}}(t)\ddot{\bar{S}}(t+\tau)\} = \sigma_{\ddot{\bar{S}}}(\tau) = q_{\ddot{\bar{S}}}\delta(\tau) \quad (\text{A.2})$$

where  $q_{\ddot{\bar{S}}}$  has unit of  $\text{m}^2/\text{s}^5$  and  $\delta(\tau)$  is the delta function with the property

$$\int_{-\infty}^{\infty} G(x)\delta(x-x_0)dx = G(x_0) \quad (\text{A.3})$$

if  $G(x)$  is a finite-valued function which is continuous at  $x = x_0$  [Gelb 1974].

Obviously

$$\ddot{\bar{S}}(t) = \ddot{\bar{S}}(t_0) + \int_{t_0}^t \ddot{\bar{S}}(\tau) d\tau \quad (\text{A.4})$$

thus it follows that

$$\begin{aligned} \dot{S}(t) &= \dot{S}(t_0) + \int_{t_0}^t \ddot{\bar{S}}(\tau_1) d\tau_1 \\ &= \dot{S}(t_0) + \ddot{\bar{S}}(t_0)(t-t_0) + \int_{t_0}^t \int_{t_0}^{\tau_1} \ddot{\bar{S}}(\tau) d\tau d\tau_1 \end{aligned} \quad (\text{A.5})$$

which in turn results in

$$\begin{aligned}
 S(t) &= S(t_0) + \int_{t_0}^t \dot{S}(\tau_2) d\tau_2 \\
 &= S(t_0) + \dot{S}(t_0)(t-t_0) + \frac{1}{2} \ddot{S}(t_0)(t-t_0)^2 + \int_{t_0}^t \int_{t_0}^{\tau_2} \int_{t_0}^{\tau_1} \ddot{S}(\tau) d\tau d\tau_1 d\tau_2 \quad (\text{A.6})
 \end{aligned}$$

Before continuing the derivation, a formula of transforming a double integral to a single integral is introduced [Teunissen 1990c].

For any continuous functions  $f'(x)$  and  $h(x)$ , with  $f'(x)$  the derivative of  $f(x)$  with respect to  $x$ , we have:

$$\int_{t_0}^t f'(x) h(x) dx = [f(x) h(x)]_{t_0}^t - \int_{t_0}^t f(x) h'(x) dx \quad (\text{A.7})$$

It follows then by substituting

$$f(x) = x, \quad h(x) = \int_{t_0}^x u(y) dy \quad (\text{A.8})$$

into (A.7) that

$$\int_{t_0}^t \int_{t_0}^x u(y) dy dx = t \int_{t_0}^t u(y) dy - \int_{t_0}^t x u(x) dx \quad (\text{A.9})$$

or

$$\int_{t_0}^t \int_{t_0}^x u(y) dy dx = \int_{t_0}^t (t-x) u(x) dx \quad (\text{A.10})$$

Applying (A.10) to (A.5) and (A.6) gives

$$\dot{S}(t) = \dot{S}(t_0) + \ddot{S}(t_0)(t-t_0) + \int_{t_0}^t (t-\tau) \ddot{S}(\tau) d\tau \quad (\text{A.11})$$

$$S(t) = S(t_0) + \dot{S}(t_0)(t-t_0) + \frac{1}{2} \ddot{S}(t_0)(t-t_0)^2 + \int_{t_0}^t \int_{t_0}^{\tau_2} (\tau_2 - \tau_1) \ddot{S}(\tau_1) d\tau_1 d\tau_2 \quad (\text{A.12})$$

The double integral in (A.12) can be transformed into a single integral as follows. Since

$$\int_{t_0}^t \int_{t_0}^{\tau_2} (\tau_2 - \tau_1) \ddot{S}(\tau_1) d\tau_1 d\tau_2 = \int_{t_0}^t \tau_2 \int_{t_0}^{\tau_2} \ddot{S}(\tau_1) d\tau_1 d\tau_2 - \int_{t_0}^t \int_{t_0}^{\tau_2} \tau_1 \ddot{S}(\tau_1) d\tau_1 d\tau_2 \quad (\text{A.13})$$

it follows with (A.10) that

$$\int_{t_0}^t \int_{t_0}^{\tau_2} \tau_1 \ddot{S}(\tau_1) d\tau_1 d\tau_2 = \int_{t_0}^t (t-\tau) \tau \ddot{S}(\tau) d\tau \tag{A.14}$$

and with integration by parts that

$$\begin{aligned} \int_{t_0}^t \tau_2 \int_{t_0}^{\tau_2} \ddot{S}(\tau_1) d\tau_1 d\tau_2 &= \left[ \frac{\tau_2^2}{2} \int_{t_0}^{\tau_2} \ddot{S}(\tau_1) d\tau_1 \right]_{t_0}^t - \int_{t_0}^t \frac{\tau_2^2}{2} \ddot{S}(\tau_2) d\tau_2 \\ &= \frac{t^2}{2} \int_{t_0}^t \ddot{S}(\tau) d\tau - \int_{t_0}^t \frac{\tau^2}{2} \ddot{S}(\tau) d\tau \\ &= \frac{1}{2} \int_{t_0}^t (t^2 - \tau^2) \ddot{S}(\tau) d\tau \end{aligned} \tag{A.15}$$

Substituting (A.13) together with (A.14) and (A.15) into (A.12) yields

$$S(t) = S(t_0) + \dot{S}(t_0)(t-t_0) + \frac{1}{2} \ddot{S}(t_0)(t-t_0)^2 + \frac{1}{2} \int_{t_0}^t (t-\tau)^2 \ddot{S}(\tau) d\tau \tag{A.16}$$

Usually people are interested in the state transition equations from time  $t_{k-1}$  to  $t_k$  and the corresponding covariance matrix of system dynamic noises,  $t_0$  and  $t$  in the above expressions are replaced by  $t_{k-1}$  and  $t_k$ , respectively. From the results of (A.16), (A.11) and (A.4), we arrive at

$$\underbrace{\begin{bmatrix} S_k \\ \dot{S}_k \\ \ddot{S}_k \end{bmatrix}}_{x_k} = \underbrace{\begin{bmatrix} 1 & \Delta t_k & \frac{1}{2} \Delta t_k^2 \\ & 1 & \Delta t_k \\ & & 1 \end{bmatrix}}_{\Phi_{k,k-1}} \underbrace{\begin{bmatrix} S_{k-1} \\ \dot{S}_{k-1} \\ \ddot{S}_{k-1} \end{bmatrix}}_{x_{k-1}} + \underbrace{\int_{t_{k-1}}^{t_k} \begin{bmatrix} \frac{1}{2} (t_k-t)^2 \ddot{S}(t) \\ (t_k-t) \ddot{S}(t) \\ \ddot{S}(t) \end{bmatrix} dt}_{d_k} \tag{A.17}$$

It follows with (A.1) that

$$E\{d_k\} = 0 \tag{A.18}$$

and with (A.2) that

$$E\{d_k d_k^*\} = \int_{t_{k-1}}^{t_k} \int_{t_{k-1}}^{t_k} Q_{11} d\tau_2 d\tau_1 \tag{A.19}$$

where

$$Q_{11} = \begin{bmatrix} \frac{1}{4}(t_k - \tau_1)^2(t_k - \tau_2)^2 q_S \delta(\tau_2 - \tau_1) & & SYM. \\ \frac{1}{2}(t_k - \tau_1)^2(t_k - \tau_2) q_S \delta(\delta_2 - \delta_1) & (t_k - \tau_1)(t_k - \tau_2) q_S \delta(\tau_2 - \tau_1) & \\ \frac{1}{2}(t_k - \tau_1)^2 q_S \delta(\tau_2 - \tau_1) & (t_k - \tau_1) q_S \delta(\tau_2 - \tau_1) & q_S \delta(\tau_2 - \tau_1) \end{bmatrix} \quad (A.20)$$

By using (A.3) it follows that

$$\begin{aligned} \int_{t_{k-1}}^{t_k} \int_{t_{k-1}}^{t_k} Q_{11} d\tau_2 d\tau_1 &= \int_{t_{k-1}}^{t_k} \int_{-\infty}^{\infty} Q_{11} d\tau_2 d\tau_1 \\ &= \int_{t_{k-1}}^{t_k} \begin{bmatrix} \frac{1}{4}(t_k - \tau_1)^2(t_k - \tau_2)^2 q_S & & SYM. \\ \frac{1}{2}(t_k - \tau_1)^2(t_k - \tau_2) q_S & (t_k - \tau_1)(t_k - \tau_2) q_S & \\ \frac{1}{2}(t_k - \tau_1)^2 q_S & (t_k - \tau_1) q_S & q_S \end{bmatrix} d\tau_1 \\ &= \begin{bmatrix} \frac{1}{20}(t_k - t_{k-1})^5 q_S & & SYM. \\ \frac{1}{8}(t_k - t_{k-1})^4 q_S & \frac{1}{3}(t_k - t_{k-1})^3 q_S & \\ \frac{1}{6}(t_k - t_{k-1})^3 q_S & \frac{1}{2}(t_k - t_{k-1})^2 q_S & (t_k - t_{k-1}) q_S \end{bmatrix} \end{aligned} \quad (A.21)$$

Inserting (A.21) into (A.19) then yields

$$E\{d_k d_k^*\} = \begin{bmatrix} \frac{1}{20} \Delta t_k^5 q_S & & SYM. \\ \frac{1}{8} \Delta t_k^4 q_S & \frac{1}{3} \Delta t_k^3 q_S & \\ \frac{1}{6} \Delta t_k^3 q_S & \frac{1}{2} \Delta t_k^2 q_S & \Delta t_k q_S \end{bmatrix} \quad (A.22)$$

In addition, it can be seen from (A.2) and (A.3) that

$$E\{d_k d_l^*\} = 0, \quad k \neq l \quad (A.23)$$



## A.2 Dynamic model with a constant velocity

Assume  $S(t)$  is a random process and its second-order time derivative, denoted by  $\ddot{S}(t)$ , is a zero-mean white noise process with constant spectral density  $q_{\ddot{S}}$ , i.e.

$$E\{\ddot{S}(t)\} = 0 \quad (\text{A.24})$$

$$E\{\ddot{S}(t)\ddot{S}(t+\tau)\} = \sigma_{\ddot{S}\ddot{S}}(\tau) = q_{\ddot{S}}\delta(\tau) \quad (\text{A.25})$$

where  $q_{\ddot{S}}$  has unit of  $\text{m}^2/\text{s}^3$ .

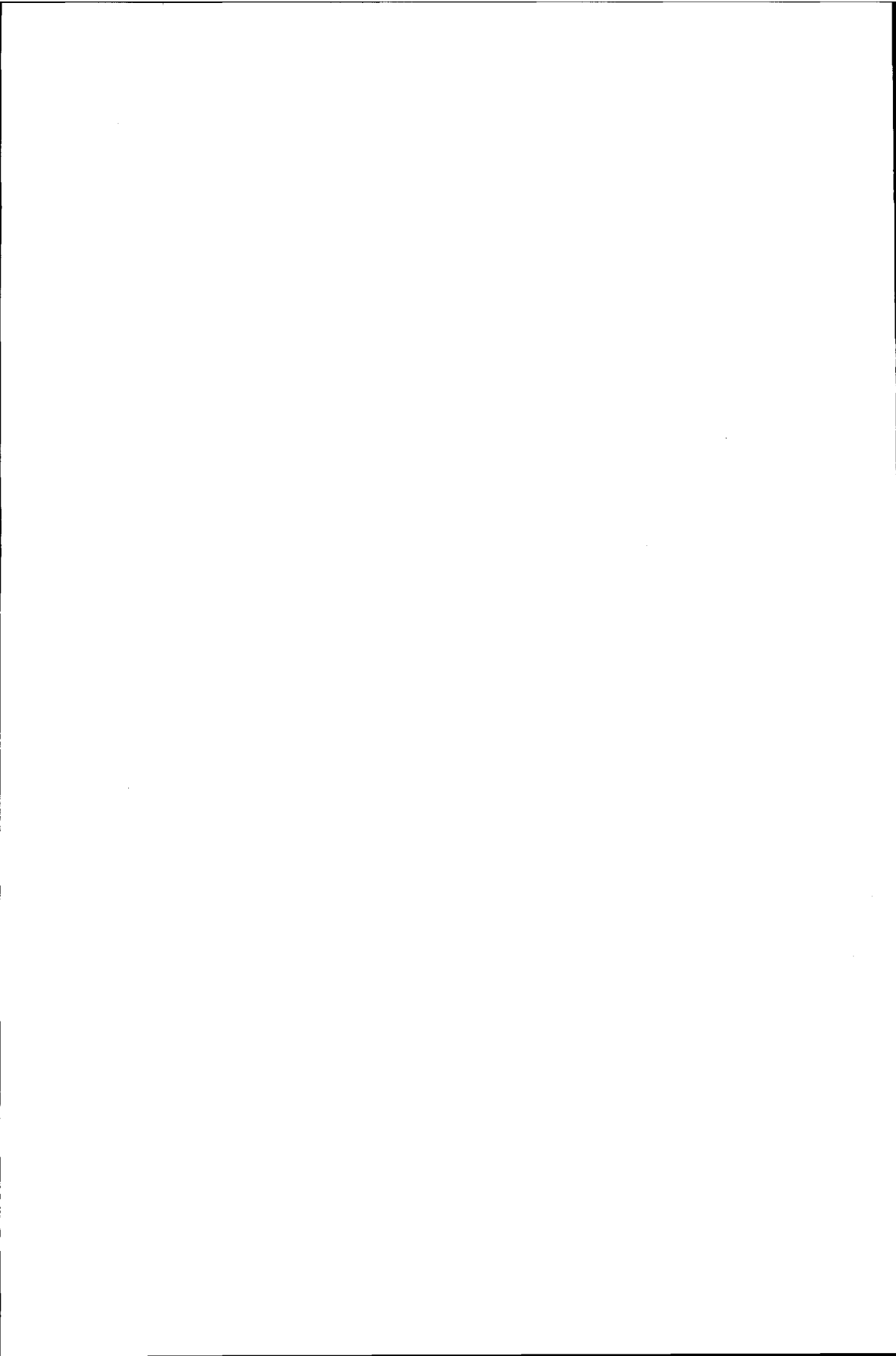
Based on the above derivation, it can be easily seen that the dynamic model with a constant velocity reads

$$\underbrace{\begin{bmatrix} S_k \\ \dot{S}_k \end{bmatrix}}_{x_k} = \underbrace{\begin{bmatrix} 1 & \Delta t_k \\ & 1 \end{bmatrix}}_{\Phi_{k,k-1}} \underbrace{\begin{bmatrix} S_{k-1} \\ \dot{S}_{k-1} \end{bmatrix}}_{x_{k-1}} + \underbrace{\int_{t_{k-1}}^{t_k} \begin{bmatrix} (t_k - t) \ddot{S}(t) \\ \ddot{S}(t) \end{bmatrix} dt}_{d_k} \quad (\text{A.26})$$

$$E\{d_k\} = 0 \quad (\text{A.27})$$

$$E\{d_k d_k^*\} = \begin{bmatrix} \frac{1}{3} \Delta t_k^3 q_{\ddot{S}} & \text{SYM.} \\ \frac{1}{2} \Delta t_k^2 q_{\ddot{S}} & \Delta t_k q_{\ddot{S}} \end{bmatrix} \quad (\text{A.28})$$

$$E\{d_k d_l^*\} = 0, \quad k \neq l \quad (\text{A.29})$$



## Appendix B

# Zero correlations between dynamic noises and estimate errors of differential corrections

According to (7.8), the dynamic noise  $w^i(t_k)$  of DCs is a function of dynamic noises of DCs from time  $t_{DC}$  to  $t_k$ . It follows from (7.5) that  $\mu_1^i(t_{DC})$  is the error of the estimated DC at time  $t_{DC}$  and is, therefore, a function of measurement noises and dynamic noises of DCs from the initial time of the filter to the time  $t_{DC}$ . Since measurement noises are assumed to be uncorrelated with the dynamic noises, any correlation between  $w^i(t_k)$  and  $\mu_1^i(t_{DC})$  can only result from the correlation between the dynamic noises in them. As we know, a DC is the sum of an ionosphere-free DC and an ionospheric delay. Thus, a dynamic noise of a DC consists of a dynamic noise of an ionosphere-free DC and that of an ionospheric delay. In the generation of DCs, we assume that the dynamic noises of both ionosphere-free DCs and ionospheric delays are white noises, which means the noises are uncorrelated, if they are not related to the same time interval. Since the dynamic noises contained in  $w^i(t_k)$  is related to the time interval from  $t_{DC}$  to  $t_k$  and those in  $\mu_1^i(t_{DC})$  is related to the time interval from the initial time of the filter to  $t_{DC}$ , thus there is no correlation between  $w^i(t_k)$  and  $\mu_1^i(t_{DC})$ . In the same way we can proof the zero correlation between  $w^i(t_k)$  and  $\mu_2^i(t_{DC})$ .



## Appendix C

# Carrier adjusted DGPS positioning models based on dual frequency data

Chapter 7 derived the carrier adjusted DGPS positioning models based on L1 code and carrier observations. This appendix shows how to adapt the positioning models when L2 carrier and code observations are also available.

### C.1 The case of L1 code and carrier plus L2 carrier observations

Let us define the combination of the ionospheric delay and the L2 carrier ambiguity as

$$\tilde{I}^i(t_k) = I^i(t_k) + \frac{1}{2}\lambda_2\tilde{N}^i \quad (\text{C.1})$$

and denote

$$y^i(t_k) = \begin{bmatrix} P^i(t_k) - c dt^{i^0}(t_k) - \hat{V}_r^i(t_k) - \rho^{i^0}(t_k) \\ \lambda_1 \phi^i(t_k) - c dt^{i^0}(t_k) - \hat{V}_r^i(t_k) - \rho^{i^0}(t_k) \\ \lambda_2 \tilde{\Phi}^i(t_k) - c dt^{i^0}(t_k) - \hat{V}_r^i(t_k) - \rho^{i^0}(t_k) \end{bmatrix}, \quad e^i(t_k) = \begin{bmatrix} \epsilon^i(t_k) - \mu^i(t_k) \\ \eta^i(t_k) - \mu^i(t_k) \\ \tilde{\eta}^i(t_k) - \mu^i(t_k) \end{bmatrix} \quad (\text{C.2})$$

$$A^i(t_k) = \begin{bmatrix} \frac{\partial \rho^{i^0}(t_k)}{\partial x_1} & 0 & \frac{\partial \rho^{i^0}(t_k)}{\partial x_2} & 0 & \frac{\partial \rho^{i^0}(t_k)}{\partial x_3} & 0 & 1 & 0 \\ \frac{\partial \rho^{i^0}(t_k)}{\partial x_1} & 0 & \frac{\partial \rho^{i^0}(t_k)}{\partial x_2} & 0 & \frac{\partial \rho^{i^0}(t_k)}{\partial x_3} & 0 & 1 & 0 \\ \frac{\partial \rho^{i^0}(t_k)}{\partial x_1} & 0 & \frac{\partial \rho^{i^0}(t_k)}{\partial x_2} & 0 & \frac{\partial \rho^{i^0}(t_k)}{\partial x_3} & 0 & 1 & 0 \end{bmatrix} \quad (\text{C.3})$$

Then the measurement model reads

$$\underbrace{\begin{bmatrix} y^1(t_k) \\ \vdots \\ y^m(t_k) \end{bmatrix}}_{y_k} = \underbrace{\begin{bmatrix} A^1(t_k) & \begin{bmatrix} 0 & 0 & 0 \\ -2 & 0 & 0 \\ 0 & 0 & -(1+r) \end{bmatrix} \\ \vdots & \ddots \\ A^m(t_k) & \begin{bmatrix} 0 & 0 & 0 \\ -2 & 0 & 0 \\ 0 & 0 & -(1+r) \end{bmatrix} \end{bmatrix}}_{A_k} \underbrace{\begin{bmatrix} \Delta x_1(t_k) \\ \Delta \dot{x}_1(t_k) \\ \Delta x_2(t_k) \\ \Delta \dot{x}_2(t_k) \\ \Delta x_3(t_k) \\ \Delta \dot{x}_3(t_k) \\ c \cdot \delta T(t_k) \\ c \cdot \delta \dot{T}(t_k) \\ \vdots \\ \bar{I}^1(t_k) \\ \bar{I}^1(t_k) \\ \vdots \\ \bar{I}^m(t_k) \\ \bar{I}^m(t_k) \\ \bar{I}^m(t_k) \end{bmatrix}}_{x_k} + \underbrace{\begin{bmatrix} e^1(t_k) \\ \vdots \\ e^m(t_k) \end{bmatrix}}_{e_k} \tag{C.4}$$

with

$$E\{e_k\} = 0 \tag{C.5}$$

$$E\{e_k e_l^*\} = \delta_{kl} \left[ \begin{array}{ccc} \sigma_e^2 + \sigma_{\bar{\varphi}_r}^2(t_k) & & SYM. \\ \sigma_{\bar{\varphi}_r}^2(t_k) & \sigma_{\bar{\eta}}^2 + \sigma_{\bar{\varphi}_r}^2(t_k) & \\ \sigma_{\bar{\varphi}_r}^2(t_k) & \sigma_{\bar{\varphi}_r}^2(t_k) & \sigma_{\bar{\eta}}^2 + \sigma_{\bar{\varphi}_r}^2(t_k) \end{array} \right] \tag{C.6}$$

$$\left[ \begin{array}{ccc} \sigma_e^2 + \sigma_{\bar{\varphi}_r}^2(t_k) & & SYM. \\ \sigma_{\bar{\varphi}_r}^2(t_k) & \sigma_{\bar{\eta}}^2 + \sigma_{\bar{\varphi}_r}^2(t_k) & \\ \sigma_{\bar{\varphi}_r}^2(t_k) & \sigma_{\bar{\varphi}_r}^2(t_k) & \sigma_{\bar{\eta}}^2 + \sigma_{\bar{\varphi}_r}^2(t_k) \end{array} \right]$$

and the dynamic model reads

$$x_k = \underbrace{\begin{bmatrix} F_k & & & & & \\ & F_k & & & & \\ & & F_k & & & \\ & & & F_k & & \\ & & & & \tilde{F}_k & \\ & & & & & \ddots \\ & & & & & & \tilde{F}_k \end{bmatrix}}_{\Phi_{k,k-1}} x_{k-1} + \underbrace{\begin{bmatrix} \tilde{d}(t_k) \\ \tilde{d}(t_k) \\ d^1(t_k) \\ \vdots \\ d^m(t_k) \end{bmatrix}}_{d_k} \quad (C.7)$$

where

$$\tilde{F}_k = \begin{bmatrix} 1 & \Delta t_k & 0 \\ 0 & 1 & 0 \\ 0 & \Delta t_k & 1 \end{bmatrix} \quad (C.8)$$

with

$$E\{d_k\} = 0 \quad (C.9)$$

$$E\{d_k d_l^*\} = \delta_{kl} \begin{bmatrix} \begin{bmatrix} S_k \\ q_x \begin{bmatrix} S_k \\ S_k \\ S_k \end{bmatrix} \end{bmatrix} & & & & \\ & q_c S_k & & & \\ & & q_r \tilde{S}_k & & \\ & & & \ddots & \\ & & & & q_r \tilde{S}_k \end{bmatrix} \quad (C.10)$$

where





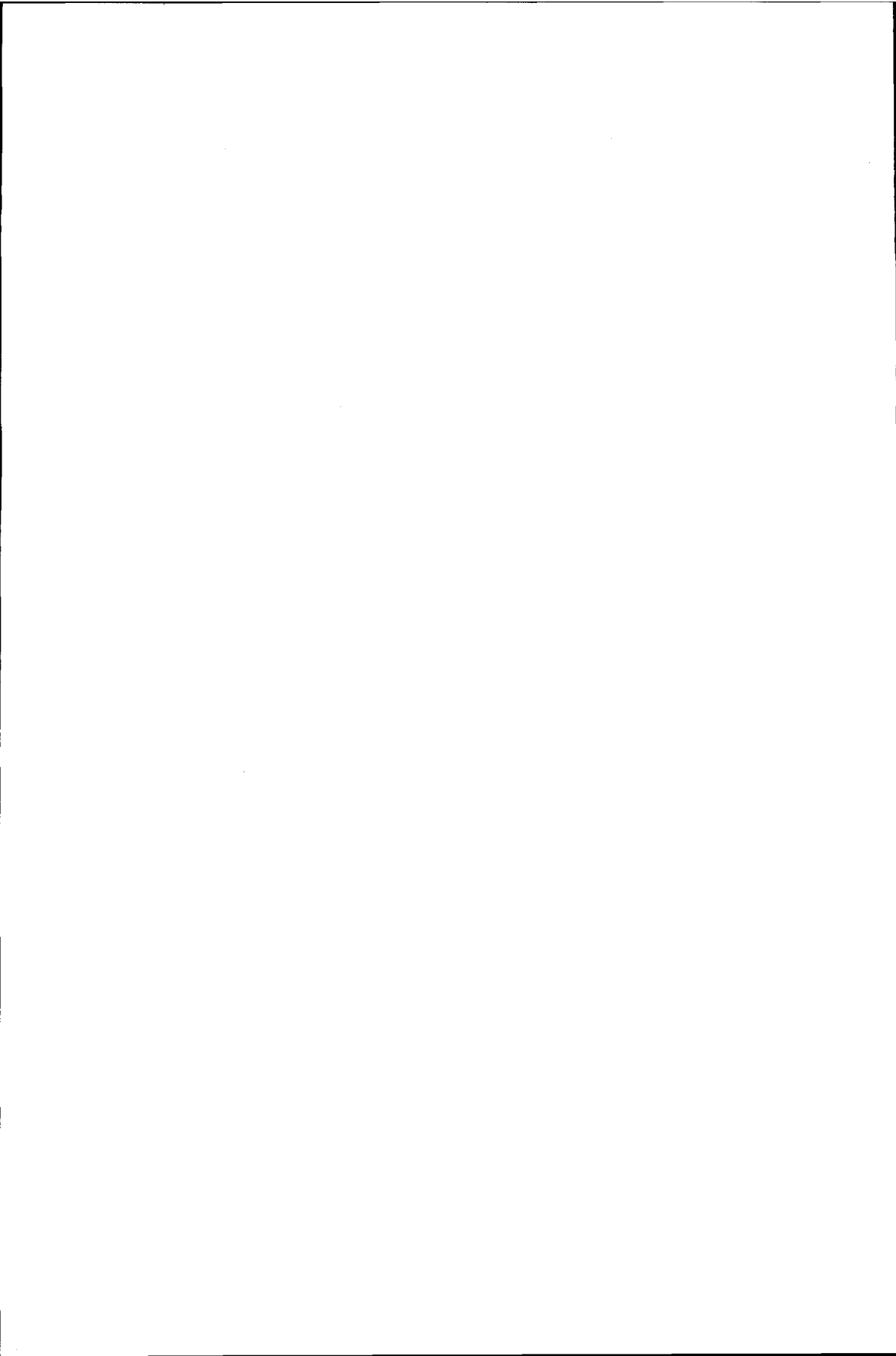
$$\underbrace{\begin{bmatrix} y^1(t_k) \\ \vdots \\ y^m(t_k) \end{bmatrix}}_{y_k} = \underbrace{\begin{bmatrix} A^1(t_k) & \begin{bmatrix} 0 & 0 & 0 & 0 \\ -2 & 0 & 0 & 0 \\ 0 & 0 & -(1+r) & 0 \\ 0 & 0 & 0 & r-1 \end{bmatrix} \\ \vdots & \ddots \\ A^m(t_k) & \begin{bmatrix} 0 & 0 & 0 & 0 \\ -2 & 0 & 0 & 0 \\ 0 & 0 & -(1+r) & 0 \\ 0 & 0 & 0 & r-1 \end{bmatrix} \end{bmatrix}}_{A_k} \underbrace{\begin{bmatrix} \Delta x_1(t_k) \\ \Delta \dot{x}_1(t_k) \\ \Delta x_2(t_k) \\ \Delta \dot{x}_2(t_k) \\ \Delta x_3(t_k) \\ \Delta \dot{x}_3(t_k) \\ c \cdot \delta T(t_k) \\ c \cdot \delta \dot{T}(t_k) \\ \text{---} \\ \bar{I}^1(t_k) \\ \dot{I}^1(t_k) \\ \bar{I}^1(t_k) \\ I^1(t_k) \\ \vdots \\ \bar{I}^m(t_k) \\ \dot{I}^m(t_k) \\ \bar{I}^m(t_k) \\ I^m(t_k) \end{bmatrix}}_{x_k} + \underbrace{\begin{bmatrix} e^1(t_k) \\ \vdots \\ e^m(t_k) \end{bmatrix}}_{e_k}$$

(C.14)

with



$$\bar{S}_k = \begin{bmatrix} \frac{1}{3}\Delta t_k^3 & & & & \text{SYM.} \\ \frac{1}{2}\Delta t_k^2 & \Delta t_k & & & \\ \frac{1}{3}\Delta t_k^3 & \frac{1}{2}\Delta t_k^2 & \frac{1}{3}\Delta t_k^3 & & \\ \frac{1}{3}\Delta t_k^3 & \frac{1}{2}\Delta t_k^2 & \frac{1}{3}\Delta t_k^3 & \frac{1}{3}\Delta t_k^3 & \\ \frac{1}{3}\Delta t_k^3 & \frac{1}{2}\Delta t_k^2 & \frac{1}{3}\Delta t_k^3 & \frac{1}{3}\Delta t_k^3 & \end{bmatrix} \quad (\text{C.17})$$



## Appendix D

# Four identities and variation of $\frac{\Delta Ip}{\cos z'}$ with zenith distances

### D.1 Proof of

$$\mu = \arcsin\{\cos\theta \cos E\} \quad 0 \leq \theta \leq \pi \quad \text{and} \quad 0 \leq E \leq \frac{\pi}{2}$$

(D.1)

Figure D.1 illustrates the geometric relationships among a reference station, a user station, and a satellite, where

- S*: Satellite
- P*<sub>1</sub>: reference station
- P*: user station
- E*: satellite elevation
- $\theta$ : horizontal angle of the line *PS* with respect to the line *P*<sub>1</sub>*P*
- $\delta$ : distance between user station *P* and reference station *P*<sub>1</sub>
- $\mu$ : angle between the line *P*<sub>1</sub>*P* and the line orthogonal to the line *PS* through *P*<sub>1</sub>
- S'*: projection of *S* on the horizontal plane through *P*
- $\delta_1$ : projection of  $\delta$  on the direction *P* to *S*
- $\delta_2$ : projection of  $\delta$  on the direction *P* to *S'*

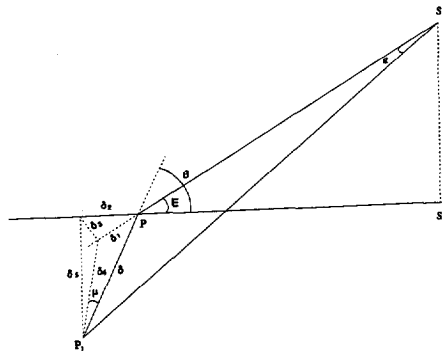


**Figure D.1:** Geometric relationship among two stations and a satellite.

It follows from the figure that

$$\left. \begin{aligned} \delta_1 &= \delta \sin \mu & 0 \leq \mu \leq \frac{\pi}{2} \\ \delta_2 &= \delta \cos \theta & 0 \leq \theta \leq \pi \end{aligned} \right\} \quad (\text{D.2})$$

Since  $\delta_3$  is in the vertical plane consisting of the three points  $S$ ,  $S'$  and  $P$ , it is orthogonal to the horizontal line  $\delta_5$ . Thus we arrive at

$$\begin{aligned} \delta_3^2 &= \delta_4^2 - \delta_5^2 \\ &= (\delta \cos \mu)^2 - (\delta \sin \theta)^2 \\ &= \delta^2 [(1 - \sin^2 \mu) - (1 - \cos^2 \theta)] \\ &= \delta^2 \cos^2 \theta - \delta^2 \sin^2 \mu \\ &= \delta_2^2 - \delta_1^2 \end{aligned} \quad (\text{D.3})$$

which means that  $\delta_1$  is the projection of  $\delta_2$  on the direction  $P$  to  $S$ , i.e.

$$\delta_1 = \delta_2 \cos E \quad (\text{D.4})$$

Inserting (D.4) into (D.2) yields

$$\sin \mu = \cos \theta \cos E \quad 0 \leq \theta \leq \pi \quad \text{and} \quad 0 \leq E \leq \frac{\pi}{2} \quad (\text{D.5})$$

from which (D.1) follows.

## D.2 Proof of

$$\boxed{\Delta \hat{r}_j - \Delta r_j = 0} \quad (\text{D.6})$$

As can be seen from Figure D.1, when  $E=0$ , we have  $\mu = \frac{\pi}{2} - \theta$ . This results in

$$\cos \mu = \sin \theta \quad (\text{D.7})$$

Without loss of generality, let us assume the x-axis of the local coordinate system directs the satellite from reference station 1 (i.e. the master station). Then, we have

$$\left. \begin{aligned} \delta_{1,j} \cos \mu_{1,j} &= \Delta y_j \\ \delta_{1,2} \cos \mu_{1,2} &= \Delta y_2 \\ \delta_{1,3} \cos \mu_{1,3} &= \Delta y_3 \end{aligned} \right\} \quad (D.8)$$

Since

$$\begin{bmatrix} \Delta x_2 & \Delta y_2 \\ \Delta x_3 & \Delta y_3 \end{bmatrix}^{-1} = \frac{1}{\Delta x_2 \Delta y_3 - \Delta y_2 \Delta x_3} \begin{bmatrix} \Delta y_3 & -\Delta y_2 \\ -\Delta x_3 & \Delta x_2 \end{bmatrix} \quad (D.9)$$

we have

$$\begin{aligned} \Delta \hat{r}_j - \Delta r_j &= \frac{d \cos \alpha_1}{r_1} \left\{ -\delta_{1,j} \cos \mu_{1,j} + [\Delta x_j \ \Delta y_j] \begin{bmatrix} \Delta x_2 & \Delta y_2 \\ \Delta x_3 & \Delta y_3 \end{bmatrix}^{-1} \begin{bmatrix} \delta_{1,2} \cos \mu_{1,2} \\ \delta_{1,3} \cos \mu_{1,3} \end{bmatrix} \right\} \\ &= \frac{d \cos \alpha_1}{r_1} \left\{ -\Delta y_j + \frac{[\Delta x_j \ \Delta y_j]}{\Delta x_2 \Delta y_3 - \Delta y_2 \Delta x_3} \begin{bmatrix} \Delta y_3 & -\Delta y_2 \\ -\Delta x_3 & \Delta x_2 \end{bmatrix} \begin{bmatrix} \Delta y_2 \\ \Delta y_3 \end{bmatrix} \right\} \\ &= \frac{d \cos \alpha_1}{r_1} \left\{ -\Delta y_j + \frac{[\Delta x_j \ \Delta y_j]}{\Delta x_2 \Delta y_3 - \Delta y_2 \Delta x_3} \begin{bmatrix} 0 \\ -\Delta x_3 \Delta y_2 + \Delta x_2 \Delta y_3 \end{bmatrix} \right\} \\ &= \frac{d \cos \alpha_1}{r_1} \left\{ -\Delta y_j + [\Delta x_j \ \Delta y_j] \begin{bmatrix} 0 \\ 1 \end{bmatrix} \right\} \\ &= 0 \end{aligned} \quad (D.10)$$

### D.3 Proof of

$$\boxed{l_p = R \left( \arcsin \left\{ \frac{R}{R+h} \sin z \right\} - \arcsin \left\{ \frac{R}{R+r} \sin z \right\} \right)} \quad (D.11)$$

It can be seen from Figure D.2 that

$$\angle P_1SO = \arcsin \left\{ \frac{R}{R+r} \sin z \right\} \quad (D.12)$$

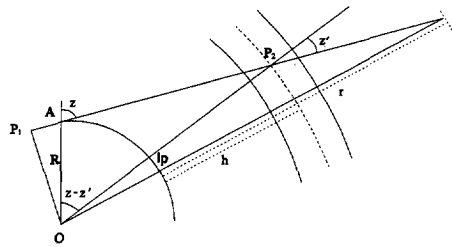


Figure D.2: Zenith distance at the ionospheric point.

$$\begin{aligned} \angle P_2OS &= z' - \angle P_1SO \\ &= z' - \arcsin\left\{\frac{R}{R+r} \sin z\right\} \end{aligned} \tag{D.13}$$

Since

$$\sin z' = \frac{R}{R+h} \sin z \tag{D.14}$$

(see, e.g., [Hofmann-Wellenhof 1992]), we arrive at

$$\begin{aligned} Ip &= R \cdot \angle P_2OS \\ &= R \left( z' - \arcsin\left\{\frac{R}{R+r} \sin z\right\} \right) \\ &= R \left( \arcsin\left\{\frac{R}{R+h} \sin z\right\} - \arcsin\left\{\frac{R}{R+r} \sin z\right\} \right) \end{aligned} \tag{D.15}$$

#### D.4 Proof of

$$\Delta Ip = R \cdot \overline{AB} \cdot \cos z_b \left( \frac{1}{((R+h)^2 - R^2 \sin^2 z_b)^{1/2}} - \frac{1}{((R+r)^2 - R^2 \sin^2 z_b)^{1/2}} \right) \tag{D.16}$$

It follows from (D.11) that



$$\begin{aligned} \Delta Ip &= Ip_a - Ip_b \\ &= R \left( \arcsin \left\{ \frac{R}{R+h} \sin z_a \right\} - \arcsin \left\{ \frac{R}{R+r} \sin z_a \right\} - \arcsin \left\{ \frac{R}{R+h} \sin z_b \right\} + \arcsin \left\{ \frac{R}{R+r} \sin z_b \right\} \right) \end{aligned} \tag{D.17}$$

As can be seen from Figure D.3, AS and BS can be considered parallel lines, due to the great heights of GPS satellites. Therefore we have

$$z_a \approx z_b + \frac{\overline{AB}}{R} \tag{D.18}$$

Thus

$$\begin{aligned} \Delta Ip &= R \left( \arcsin \left\{ \frac{R}{R+h} \sin \left\{ z_b + \frac{\overline{AB}}{R} \right\} \right\} - \arcsin \left\{ \frac{R}{R+h} \sin z_b \right\} \right. \\ &\quad \left. - \arcsin \left\{ \frac{R}{R+r} \sin \left\{ z_b + \frac{\overline{AB}}{R} \right\} \right\} + \arcsin \left\{ \frac{R}{R+r} \sin z_b \right\} \right) \end{aligned} \tag{D.19}$$

Assume

$$y = \arcsin \{ a \sin x \} \tag{D.20}$$

then

$$\begin{aligned} \arcsin \{ a \sin \{ x_0 + \Delta x \} \} &\approx \arcsin \{ a \sin x_0 \} + \left. \frac{dy}{dx} \right|_{x=x_0} \cdot \Delta x \quad \text{for small } \Delta x \\ &= \arcsin \{ a \sin x_0 \} + \frac{a \cos x_0}{(1 - a^2 \sin^2 x_0)^{1/2}} \Delta x \end{aligned} \tag{D.21}$$

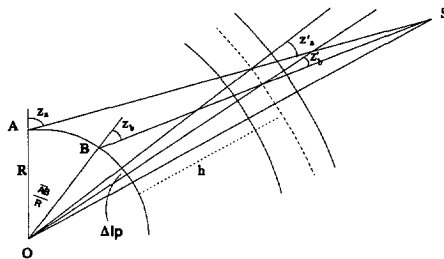


**Figure D.3:** Difference of zenith distance at the ionospheric point between two stations, after [van der Marel 1993].

By using the above result, it is easy to see (D.16) is valid.

### D.5 Variation of $\frac{\Delta I_p}{\cos z'}$ with the zenith distance

Figure D.4 shows the variation of  $\frac{\Delta I_p}{\cos z'}$  with the zenith distance, on the assumption that the distance between stations A and B (see Figure D.3) is 1 km. As can be seen from (D.18), when the distance is not 1 km, then  $\frac{\Delta I_p}{\cos z'}$  can be simply obtained by multiplying the corresponding value in the figure by the distance with units of kilometres. From the figure we can see that  $\frac{\Delta I_p}{\cos z'}$  reaches its maximum at the zenith distance of about  $70^\circ$ .

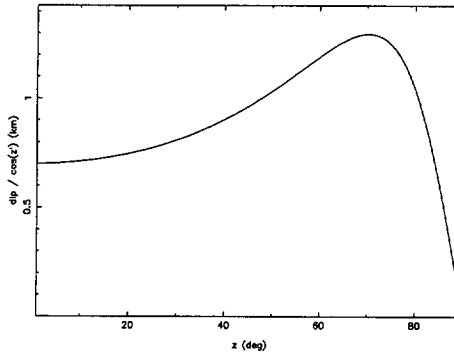


**Figure D.4:** Variation of  $\Delta I_p / \cos z'$ , where the distance between stations A and B is 1 km.

# Samenvatting

## Met fasemetingen ondersteunde DGPS plaatsbepaling: theorie en experimentele resultaten

Door het gebruik van DGPS worden systematische fouten in GPS waarnemingen aanzienlijk gereduceerd of zelfs geëlimineerd, resulterend in nauwkeurige relatieve posities. Er is daarom veel aandacht besteed aan DGPS in tal van real-time toepassingen. De prestaties van een DGPS plaatsbepalingssysteem hangen af van de volgende factoren: 1) het genereren van differentiële GPS correcties op een bekend DGPS referentiestation; 2) het versturen van de correcties naar een mobiel station; 3) het berekenen van de posities van het mobiele station.

In deze dissertatie wordt een nieuw algoritme ontwikkeld voor het genereren van differentiële correcties. Het algoritme heeft enkele specifieke eigenschappen. Ten eerste gebruikt het de oorspronkelijke code- en fasewaarnemingen als invoer voor het waarnemingsmodel van een Kalman filter. Indien de oorspronkelijke waarnemingen niet gecorreleerd zijn in de tijd, zoals algemeen wordt aangenomen, kan van een eenvoudig stochastisch model voor de waarnemingen worden uitgegaan en kan gebruik worden gemaakt van de standaarduitdrukkingen voor het Kalman filter. Ten tweede brengt het algoritme de effecten in rekening van systematische fouten, veroorzaakt door multipath en instrumentele vertragingen, in de codewaarnemingen. Deze effecten kunnen expliciet worden aangetoond in de differentiële correcties, gegenereerd met een- of twee-frequentie data. Ten derde kan het algoritme eenvoudig worden geïntegreerd met een procedure voor het waarborgen van de kwaliteit van de geschatte grootheden. Ten vierde worden naast differentiële correcties ook de veranderingen in ionosfeer en de systematische fouten in de codewaarnemingen geschat als functie van de tijd. Het algoritme kan daardoor ook worden gebruikt voor nader onderzoek naar de eigenschappen van deze grootheden. Ten vijfde worden alle geschatte grootheden niet beïnvloed door het tegengestelde effect van de ionosfeer op code- en fasewaarnemingen.

Gebruik makend van data van TurboRogue SNR-8000, Trimble 4000 SSE en Trimble 4000 SST ontvangers is de relatie onderzocht tussen de elevatie van de satellieten en de precisie van de codewaarnemingen. De verslechtering van de precisie blijkt het duidelijkst bij lage elevaties. Wanneer de elevatie toeneemt, wordt de precisie steeds stabiel. De precisie van de codewaarnemingen als functie van de elevatie kan worden beschreven door de exponentiële functie  $y = a_0 + a_1 \exp\{-x/x_0\}$ , met  $y$  (de precisie),  $a_0$  en  $a_1$  in meters en  $x$  (de elevatie) en  $x_0$  in graden. De parameters  $a_0$ ,  $a_1$  en  $x_0$  zijn afhankelijk van het type ontvanger en de gebruikte codewaarnemingen.

Voor code- en fasewaarnemingen, verzameld met een waarnemingsinterval van een seconde, kan het dynamisch gedrag van de satellietklokfouten (behept met de effecten ten gevolge van Selective Availability) en de ionosfeer worden beschreven door respectievelijk een kwadratische en een lineaire functie. De nauwkeurigheid van deze modellen is in de orde van

grootte van enkele millimeters.

Behalve voor het genereren van differentiële correcties op een referentiestation, is ook een alternatief algoritme ontwikkeld voor de bepaling van de posities van een mobiel station. Dit algoritme kan worden gebruikt indien zowel code- als fasewaarnemingen beschikbaar zijn. Ook hier worden de oorspronkelijke waarnemingen gebruikt in plaats van bijvoorbeeld enkel de met de fasewaarnemingen gladgestreken codewaarnemingen, zodat een eenvoudig stochastisch model kan worden gebruikt. Het algoritme kan zowel worden gebruikt voor het geval dat het dynamisch gedrag van positie en klok van de ontvanger kan worden gemodelleerd, als voor het geval dat dit niet zo is. In het eerste geval levert het algoritme gefilterde schattingen van positie en ontvangerklofout, in het tweede is het resultaat een schatting van de instantane waarden van deze grootheden. Het algoritme kan worden geïntegreerd met een real-time procedure voor kwaliteitscontrole. Doordat in dit algoritme altijd overtalligheid aanwezig is zodra een positie kan worden bepaald, kan de kwaliteitscontrole zelfs worden uitgevoerd wanneer slechts vier satellieten worden waargenomen.

Met behulp van de data, verzameld op twee stations op 100 kilometer afstand van elkaar, wordt aangetoond dat een positienuwkeurigheid van een halve meter kan worden gerealiseerd, wanneer zowel op het referentie- als op het mobiele station L1 en L2 code- en fasewaarnemingen worden gebruikt. De nauwkeurigheid neemt af tot 0,75 meter indien op het mobiele station slechts L1 waarnemingen aanwezig zijn. Het gebruik van een stochastisch model voor de codewaarnemingen dat afhankelijk is van de elevatie van de satellieten draagt bij tot een verbetering van de positienuwkeurigheid. Verder is het gebruik van twee-frequentiewaarnemingen belangrijker voor het referentiestation dan voor het mobiele.

Indien een netwerk van referentiestations beschikbaar is, is het mogelijk een correctievector te berekenen, waarmee de effecten in GPS waarnemingen ten gevolge van baanfouten, de ionosfeer en de troposfeer kunnen worden gereduceerd. Voor een gebied van 500x500 km<sup>2</sup> met drie referentiestations bedragen de restfouten respectievelijk minder dan een decimeter, twee decimeter en 2,5 decimeter.

De waarnemingsvergelijkingen voor GPS code- en fasemetingen kunnen worden ontwikkeld in een Taylorreeks met ten hoogste eerste orde afgeleiden. Doordat in de Taylorreeks de reistijd van het GPS signaal niet voorkomt, is het niet nodig gebruik te maken van iteraties of codewaarnemingen voor de bepaling van het tijdstip van uitzenden van het signaal. Ontwikkeling in een Taylorreeks resulteert daarom in een vermindering van de benodigde rekentijd en vermijdt de invloed van blunders in de codewaarnemingen op de bepaling van satellietposities en -klofouten en dus ook op de berekende waarnemingen.

# Acknowledgements

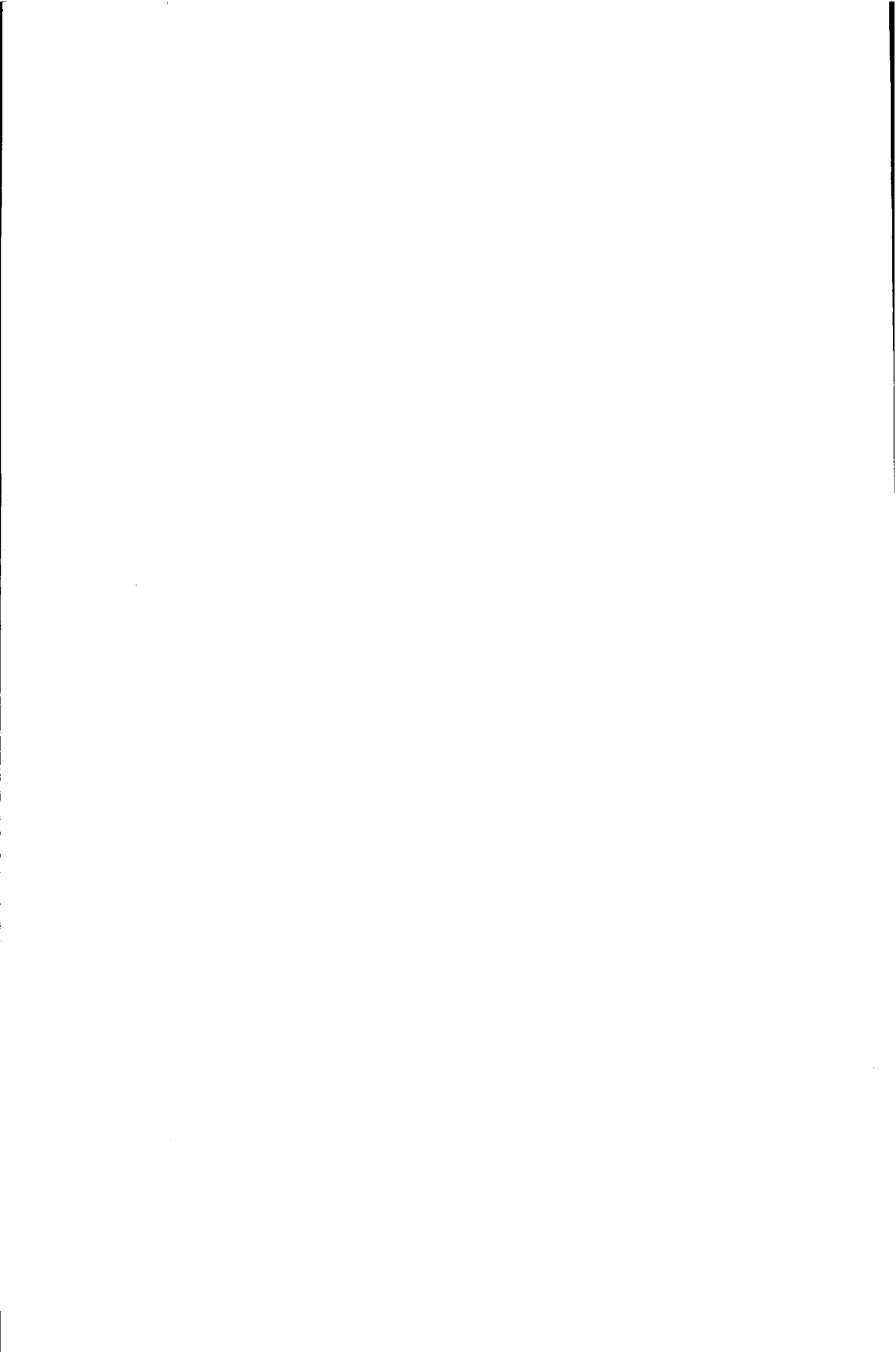
The author appreciates his promoters Prof. P. Cross, Prof. R. Klees and Prof. M. Vosselman for their support. He is grateful to Prof. P. Teunissen, Mr. C. de Jong and Dr. H. van der Marel for many beneficial discussions with them. Mr C. de Jong made valuable improvement on the draft dissertation and translated the abstract into Dutch (the title was translated by Christian Tiberius). Ms R. van Akkeren Sciarone did excellent job for having the dissertation finished. Thanks also go to Henk de Heus, Paul de Jonge, Peter Joosten, Martin Salzmann, Christian Tiberius, and all other colleagues for their direct or indirect helps in many aspects. He is indebted to his wife Suqin and his son Boming for their understanding and support.

# Curriculum Vitae

9 Sep. 1956	born in Wuhan, China
Jan. 1982	obtained BSc degree in geodesy from Wuhan Technical University of Surveying and Mapping (WTUSM)
July 1987	obtained MSc degree in geodesy from WTUSM
Jan. 1982 - Sep. 1984	graduated teaching assistant at Department of Geodesy of WTUSM
Sep. 1987 - Mar. 1990	lecturer at Department of Geodesy of WTUSM
Mar. 1990 - Oct. 1996	research associate at Faculty of Geodetic Engineering of Delft University of Technology, The Netherlands









## Propositions

Xin-Xiang JIN

- 1) Compared with other existing algorithms, the new algorithm for carrier adjusted differential corrections, which is introduced by this thesis, has the property to provide optimal solutions under certain conditions. (this thesis)
- 2) The real-time DIA quality control procedure can be well used at a DGPS reference station to monitor GPS performance and to detect model errors in GPS observations. When a good external clock is used at the reference station, cycle slips as small as one cycle in carrier observations can be detected and identified. (this thesis)
- 3) The algorithm for carrier adjusted DGPS positioning can be used at a DGPS mobile station when the dynamic behaviour of receiver clock biases and mobile positions can or cannot be modelled. In the former case, the algorithm provides recursive solutions of the positions. In the latter case, the algorithm provides single-epoch solutions. (this thesis)
- 4) When ephemeris errors, vertical ionospheric delays, and vertical tropospheric delays are less than 10, 4.5, and 2.6 metres, respectively, using three reference stations in a  $500 \times 500$  km<sup>2</sup> area can reduce the effect of ephemeris errors to one decimeter, ionospheric delays to less than two decimeters, and tropospheric delays to less than 2.5 decimeters. If a tropospheric delay model is used, the tropospheric delays can be further reduced to less than one decimeter. (this thesis)
- 5) GPS observation equations can be expanded into Taylor series which contain only up to first-order derivative quantities. Since this Taylor expansion does not contain the travel time of a GPS signal, solving it needs neither iterations nor code measurements for the determination of the transmission time of the GPS signal. (this thesis)
- 6) Assumptions like normal distribution and uncorrelation are sometimes incorrectly interpreted as facts in data processing.
- 7) Success often depends on both one's effort and good luck. One should first do his/her best for his/her ambition and then wait for the chance to come.
- 8) The more one learns, the less one may find he/she knows.
- 9) Quite often, the more simple a word or a concept, the more difficult to explain and to define.
- 10) Having happy life may only mean that one is satisfied with his/her life and does not necessarily mean the possession of a beautiful house, a luxurious car, and etc. It may be correct to say people have better life now than tens of years ago, but it may not be correct to say people have more happy life now than tens of years ago, since it seems nowadays people have more to complain.
- 11) That one needs a job is not only for earning money but also for making life joyful.

1. The first part of the report deals with the general situation in the country during the year 1950-1951. It is noted that the economy has shown a marked improvement over the previous year, with a steady increase in production and a corresponding rise in the standard of living.

2. The second part of the report discusses the progress made in the various sectors of the economy. It is noted that the agricultural sector has shown a significant increase in output, while the industrial sector has also made considerable gains.

3. The third part of the report deals with the social and cultural aspects of the country. It is noted that there has been a steady improvement in the educational system, and that the cultural life of the people has become more vibrant and active.

4. The fourth part of the report discusses the foreign relations of the country. It is noted that the country has maintained a policy of peaceful coexistence with all nations, and that it has established friendly relations with a number of important countries.

5. The fifth part of the report deals with the internal security of the country. It is noted that the country has maintained a high level of internal security, and that there has been no major disturbance during the year.

6. The sixth part of the report discusses the financial position of the country. It is noted that the country has maintained a balanced budget, and that the financial position is generally sound.

7. The seventh part of the report deals with the progress made in the various fields of science and technology. It is noted that there has been a steady increase in research and development, and that the country has made significant progress in several key areas.

8. The eighth part of the report discusses the progress made in the various fields of art and literature. It is noted that there has been a steady increase in the production of art and literature, and that the country has made significant progress in several key areas.

9. The ninth part of the report deals with the progress made in the various fields of sports and recreation. It is noted that there has been a steady increase in the participation in sports and recreation, and that the country has made significant progress in several key areas.

10. The tenth part of the report discusses the progress made in the various fields of health and medicine. It is noted that there has been a steady increase in the number of hospitals and clinics, and that the country has made significant progress in several key areas.

11. The eleventh part of the report deals with the progress made in the various fields of education. It is noted that there has been a steady increase in the number of schools and colleges, and that the country has made significant progress in several key areas.

12. The twelfth part of the report discusses the progress made in the various fields of social work and welfare. It is noted that there has been a steady increase in the number of social workers and welfare workers, and that the country has made significant progress in several key areas.